2011

Derivation of the eruption history of the prehistoric Ring Creek lava flow, Southern British Columbia

Samuel Bruno
Western Washington University

DERIVATION OF THE ERUPTION HISTORY OF THE PREHISTORIC RING CREEK LAVA FLOW, SOUTHERN BRITISH COLUMBIA

BY

Samuel Bruno

Accepted in Partial Completion

of the Requirements for the Degree

Master of Science

Moheb A. Ghali, Dean of Graduate School

ADVISORY COMMITTEE

Chair, Dr. Scott Babcock

Dr. Pete Stelling

Dr. Cathie Hickson

Dr. Scott Linneman

MASTER'S THESIS

In presenting this thesis in partial fulfillment of the requirements for a master's degree at Western Washington University, I grant to Western Washington University the non-exclusive royalty-free right to archive, reproduce, distribute, and display the thesis in any and all forms, including electronic format, via any digital library mechanisms maintained by WWU.

I represent and warrant this is my original work, and does not infringe or violate any rights of others. I warrant that I have obtained written permissions from the owner of any third party copyrighted material included in these files.

I acknowledge that I retain ownership rights to the copyright of this work, including but not limited to the right to use all or part of this work in future works, such as articles or books.

Library users are granted permission for individual, research, and non-commercial reproduction of this work for educational purposes only. Any further digital posting of this document requires specific permission from the author.

Any copying or publication of this thesis for commercial purposes, for for financial gain, is not allowed without my written permission.

Samuel Bruno
5/16/11

DERIVATION OF THE ERUPTION HISTORY OF THE PREHISTORIC RING CREEK LAVA FLOW, SOUTHERN BRITISH COLUMBIA

A Thesis
Presented to
The Faculty of
Western Washington University

In Partial Fulfillment
of the Requirements for the Degree
Master of Science

By
Samuel John Bruno
May, 2011

ABSTRACT

The Ring Creek lava flow is a 10,000 year old, post-glacial dacitic lava flow that originated from Opal Cone, a small cinder cone on the south east flank of Mt. Garibaldi, British Columbia. Disequilibrium texture of amphibole combined with clotting in plagioclase suggests that the Ring Creek magma stalled beneath Opal Cone for at least 440 days before the eruption of the Ring Creek lava flow. Use of an igneous plagioclase-liquid thermo barometer and hygrometer indicate shallow storage conditions of 818 - 868^{o} C, 2.4 – 3.6 kbar, and 0.2 - 2.0 wt% H_2O. Surge in plagioclase growth, evidenced by complex zonation and clotting, in conjunction with amphibole reaction, indicates substantial degassing prior to the emplacement of the Ring Creek lava flow. A possible reason for stalling of the Ring Creek magma, as well as eruption mechanism for Opal Cone, is glacial ice. Glacial studies suggest the Mamquam River Valley, which the Ring Creek lava flow currently occupies, was completely deglaciated just prior to the emplacement of the Ring Creek lava flow in approximately 900 years or less. Deglaciation of the Mamquam River Valley corresponds to a deduction of at least 4.5 MPa of overburdening pressure, which could have initiated a positive feedback loop of degassing and upwelling of the Ring Creek magma. This scenario is supported by progressive amphibole reaction observed in samples associated with three morphologically distinct (yet chemically identical) flow units which include a torta (or potentially a tuya), a lava flow underlying the Ring Creek lava flow, and the Ring Creek lava flow.

Because of the prehistoric nature of the Ring Creek lava flow and the lack of ideal phases such as magnetite and stable amphibole, multiple assumptions were made to use

mathematical and chemical models. The igneous plagioclase-liquid thermo barometer and hygrometer shows poor correlation (R^2) when calculating temperature (0.55), pressure (0.012), and water content (0.4) of hydrous dacite. Estimation of heat loss parameters used to calculate extrusion rate, eruption duration, and emplacement duration required the assumption of exact consistency between the Ring Creek and analogue lavas, which is not likely. Other mathematical models used to calculate eruption duration and flow velocity make simplifying assumptions of constant slope of underlying topography, flow velocity, morphology, and vent radius. In an effort to compensate for the high degree of uncertainty of applied models, several approaches were used to create a most likely scenario for the evolution of the Ring Creek magma and emplacement of the Ring Creek lava flow.

Using flow morphology and the Gratz number, emplacement of the Ring Creek lava flow was estimated to range from 1 – 20 years. From this estimate, an average flow front velocity of $1x10^{-4}$ m/s is estimated assuming constant flow front advance. Flow length, measured in the field and using ArcGIS, and flow velocity were used to calculate lava core cooling rate of $3.5x10^{-3}$ C/hr. Viscosity estimates of 10^{10} – 10^{11} Pas were calculated using morphology and flow velocity as inputs for the Jeffrey's equation. Viscosity, core cooling rate, and flow front velocity estimates suggest that the Ring Creek lava flow was well insulated by thick lava armor, which would have accommodated slow core cooling and prolong advancement. Insulation by lava armor is supported by estimates of 65 m for the combined thickness of flow plug and lava armor.

ACKNOWLEDGEMENTS

I could not have obtained an eruption history for the Ring Creek lava flow without the support and guidance of my advisor Dr. Pete Stelling, whose patience and kind-heartedness often gave me strength and insight to deal with the many difficulties that occurred during the project. I am very thankful and appreciative of the efforts and input of the thesis committee. Dr. Cathie Hickson provided invaluable field support, an excellent critical eye, and most importantly, the funding for all field work completed. Without her support, there would not have been a project. Dr. Scott Linneman provided several crucial texts that gave me the understanding I needed to mathematically describe the evolution of the lava flow. From the wealth of information provided by Dr. Linneman, I have greatly increased my understanding of physical volcanology. Dr. Scott Babcock has also provided invaluable support and input throughout the project and I owe him many thanks.

Due to the complexity of the project, many people outside of the thesis committee were involved, and without their support some pieces of the eruption history of the Ring Creek lava flow would remain undetermined. Dr. Scott Kuehner of the University of Washington provided much help during the use of electron microprobe facility. Dr. Scott Rowland, of the University of Hawaii, was extremely helpful with troubleshooting of the lava flow modeling software, FLOWGO, which was much appreciated. Dr. Andy Harris, of the University of Hawaii, was also extremely helpful during the process of applying his work to the Ring Creek lava flow to derive important parameters. His help is greatly appreciated. Dr. John Clague, of Simon Frasier University in British Columbia, provided

valuable information on glaciers within the area of Opal Cone, which proved to be an important aspect of the eruptive history of the Ring Creek lava flow. Dr. Keith Putirka, of California State University Fresno, provided crucial support during the application of his plagioclase based thermo-barometer to the Ring Creek lava flow. Without his support, intensive parameters of the Ring Creek lava flow would remain poorly constrained.

I would also like to give thanks to Dave Carlin and Elspeth Miller of the EPCOR dam facility. Without their help and cooperation, many important hypotheses would not have been reached, and crucial samples would not have been collected. The staff of the Canadian Hydro facility were also very accommodating and thanks to their cooperation, several key outcrops were analyzed. Finally, I would like to thank my field assistants Malika Ulmi and Courtney Jermyn, of the Geological Survey of Canada for their wonderful support during the field work portion of the project. Analyses conducted during the project were funded by the graduate research fund of Western Washington University, as well as the Geology department.

TABLE OF CONTENTS

LIST OF FIGURES

LIST OF TABLES

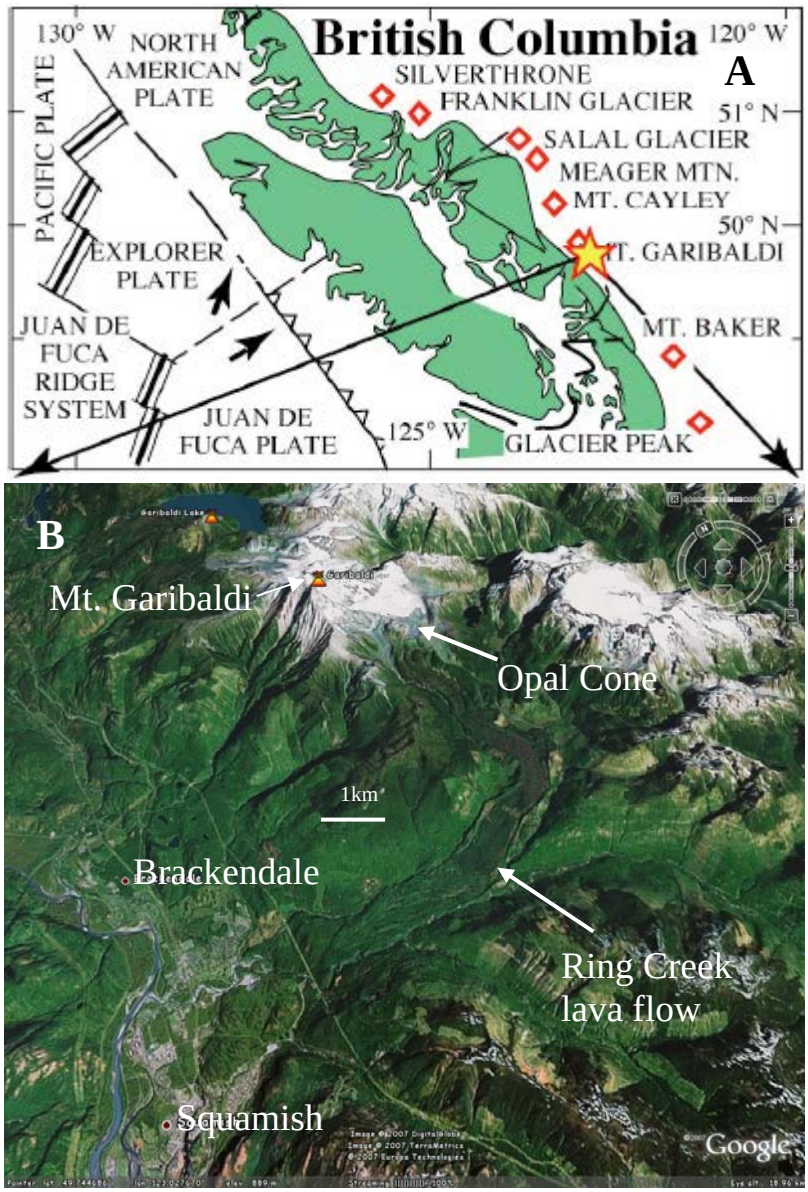

Figure 1) (A) Mt. Garibaldi within the Garibaldi Volcanic Belt (GVB), Southern B.C. (B) Opal Cone and the Ring Creek lava flow. Image modified from Powell (2005; Fig. 1) using Google Earth.

Statement of Problem

To shed light on the emplacement of a lava flow, values for flow properties such as extrusion rate, eruption duration, and flow velocity must be estimated. Typically, methods used to estimate flow properties require parameters such as flow front temperature, lava core temperature, and post-eruptive viscosity which can only be directly measured while the lava is still active. Thus, estimating these properties for pre-historic lavas is challenging. A solution to this problem is to employ models that re-establish properties of active lavas (e.g. viscosity, flow front temperature, and lava crust thickness) in terms of final flow morphology (flow length, width, and height). This process essentially back calculates a likely scenario for the evolution of a pre-historic lava flow. However, these relationships are associated with significant error (deSilva et al., 1994; Carrasco-Nunez, 1997). With such expected error in mind, multiple relationships were applied to the Ring Creek lava flow with the hopes of producing several ranges whose values overlap to yield a more narrowly defined data set that describes the eruption and emplacement of the Ring Creek lava flow.

GEOLOGY OF THE MAMQUAM RIVER VALLEY

The basement material in the greater Mt. Garibaldi area consists of metavolcanic and minor metasedimentary rocks which have been intruded broadly by the quartz diorite Squamish batholith (Mathews, 1958a). Stratigraphically above Cretaceous material is a 6.5 km-thick sequence of bedded, fossiliferous clastic sediments containing Upper Cretaceous fossils, which was later intruded by quartz diorite dikes, and subsequently

faulted (Mathews 1958a). Mapping efforts made by Mathews (1958a) have been updated and expanded upon by Price and Monger (2003). These basement rocks were again deformed during Tertiary subduction of the Juan de Fuca and Explorer plates along the Cascadia Subduction Zone (CSZ) (Powell, 2005). Modern volcanism is caused by the oblique subduction of the Juan de Fuca plate beneath North America.

Glaciation

Following Tertiary subduction, extensive glaciation occurred accompanied by Pleistocene-Holocene volcanism. Recent glaciation occurred in two glacial stades approximately 50 ka and 26-13.5 ka (Powell, 2005). These glacial advances created many U-shaped valleys which would become relatively smooth channels in which lava could flow (Mathews 1958; Green et. al, 1988). After the peak of the Fraser stade at approximately 14.5 ka, multiple stages of deglaciation, followed by a readvance, occurred in the Mt. Garibaldi-Howe Sound area (Kelman et al., 2002; Friele and Clague, 2002; Figure 2).

Firele and Clague (2002) suggest that deglaciation of the Frasier lowland as well as the upper regions of Mt. Garibaldi occurred between the 15 ka and 10.6 ka (^{14}C years). Radiocarbon dating of charcoal rich sediments (Brooks and Friele, 1992) and whole pieces in situ (Friele and Clague, 2002) suggests a complete deglaciation of the Squamish river valley and greater Howe Sound area by 11.3 ka-10.6 ka (^{14}C years; Figure 3). The final glacial event to occur was the Little Ice Age readvance which resulted in several morainal deposits around the Opal Cone area.

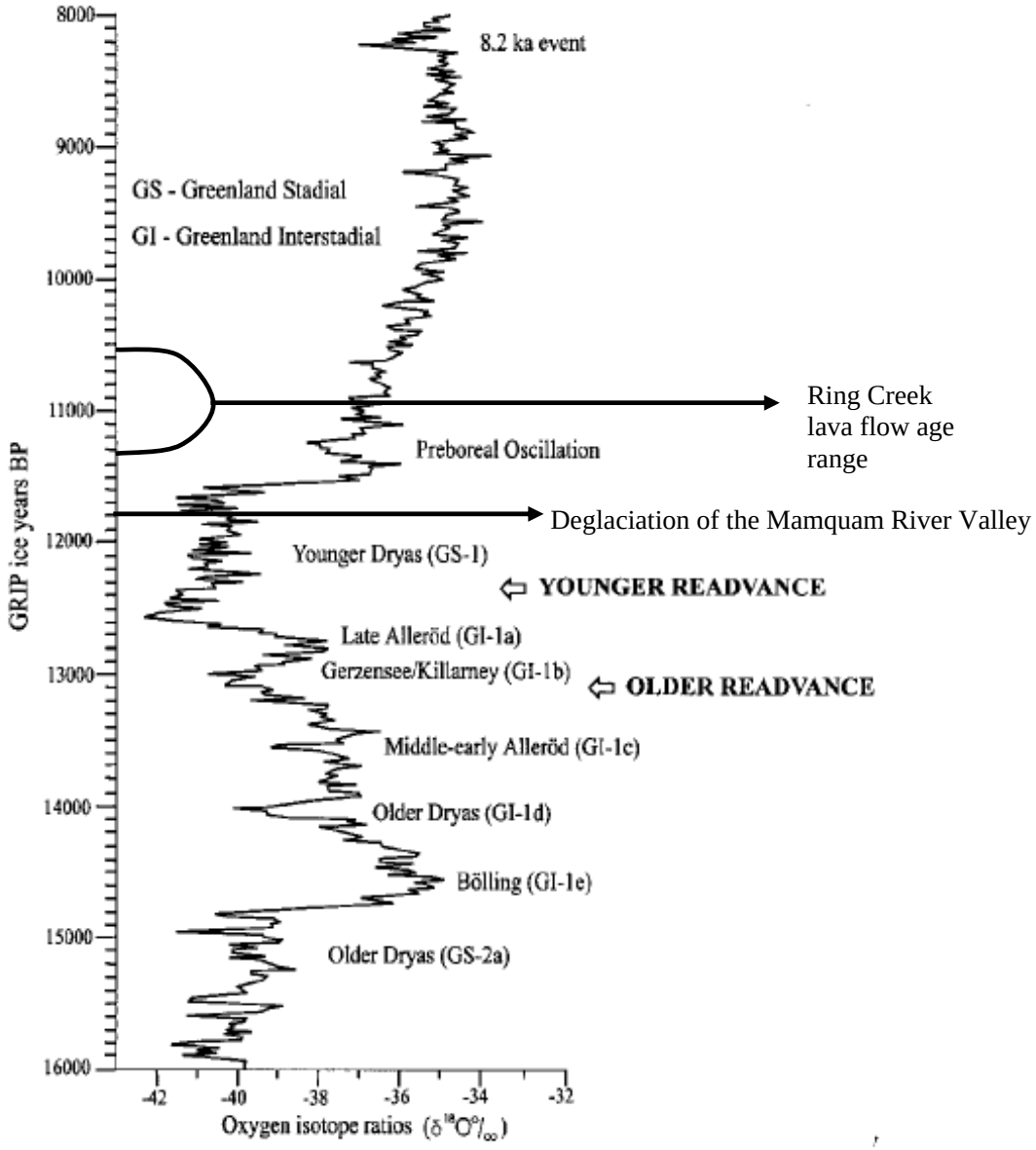

Figure 2) Comparison of glacial readvances observed in the greater Squamish area and δ^{18} O records from GRIP ice cores. Note the rapid increase in δ^{18}O after approximately 11.7 ka which suggests rapid deglaciation in the area. Figure modified from Björk et al., (1998; Fig. 1).

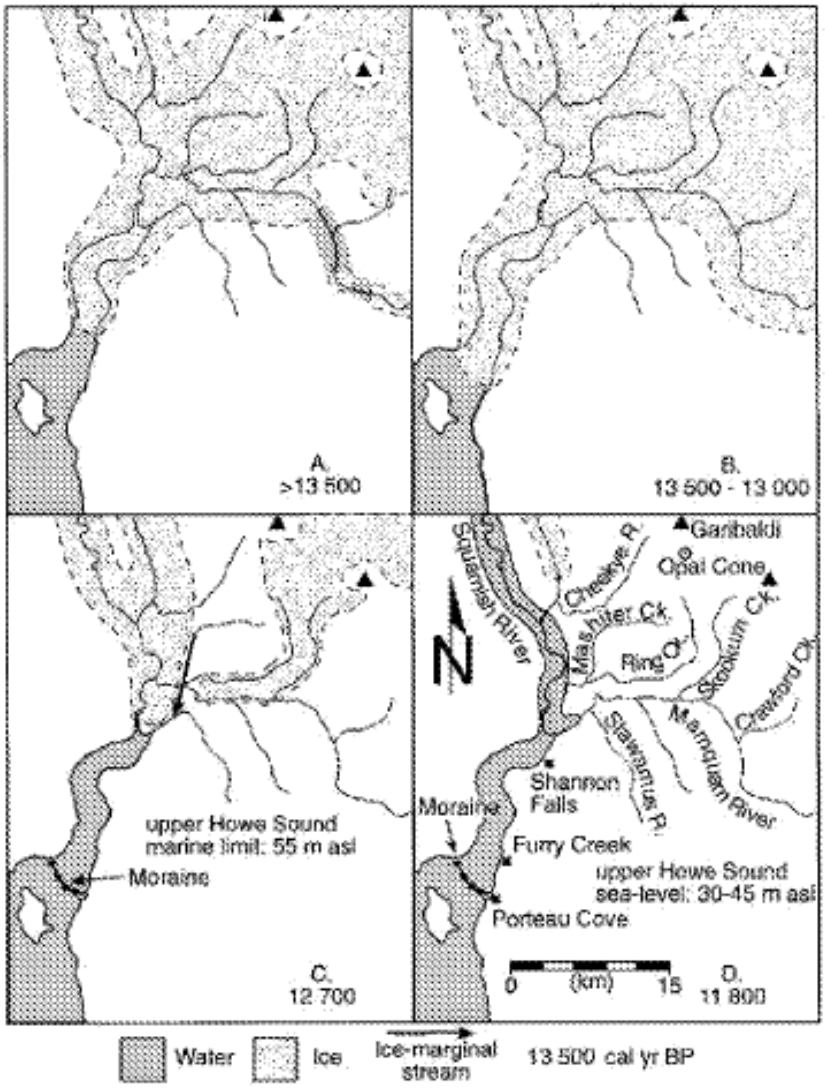

Figure 3) Evolution of glaciers in the greater Squamish area. Dates progress to modern day from top left to bottom right. Note the complete deglaciation that occurred between 12.7 and 11.8 ka. Figure taken from Friele and Clague, (2002; Fig. 9).

Quaternary Volcanism

Evidence of lava-ice interaction has been observed in many of the volcanic suites throughout British Columbia in the form of domes, tuyas, steeply sloped cooling margins, complex jointing patterns and many other features typical of sub-glacial to ice-marginal features (Kelman et al., 2002).

Quaternary Volcanism in the Mt. Garibaldi area has been divided into six eruptive units: The Mulligan Mountain, Mamquam Mountain, Mamquam River, Paul Ridge, Skookum Creek, and Ring Creek volcanics. These are collectively referred to as the Raffuse Creek-Mamquam River Suite (Powell, 2005; Figure 4). The domes within the Raffuse Creek-Mamquam River suite range in composition from basaltic andesite to dacite (54 – 64 wt% SiO_2) and appear to be relatively low volume, high viscosity dome structures, consistent with sub-glacial eruptions.

The Ring Creek lava flow represents the final, most siliceous, and most voluminous member of the Raffuse Creek-Mamquam River suite. When the Ring Creek flow was erupted it filled the Mamquam River Valley floor, separating Ring Creek and Skookum Creek which resulted in the current drainage pattern observed in Figure 1. As the youngest member of the Raffuse Creek-Mamquam River volcanic suite, the Ring Creek unit is thought to be the only known post-glacial lava in the region (Mathews, 1958a). Brooks and Friele (1992) have dated charcoal-rich sediments directly underlying the toe of the Ring Creek lava flow to 9.7 ka (± 160 years).

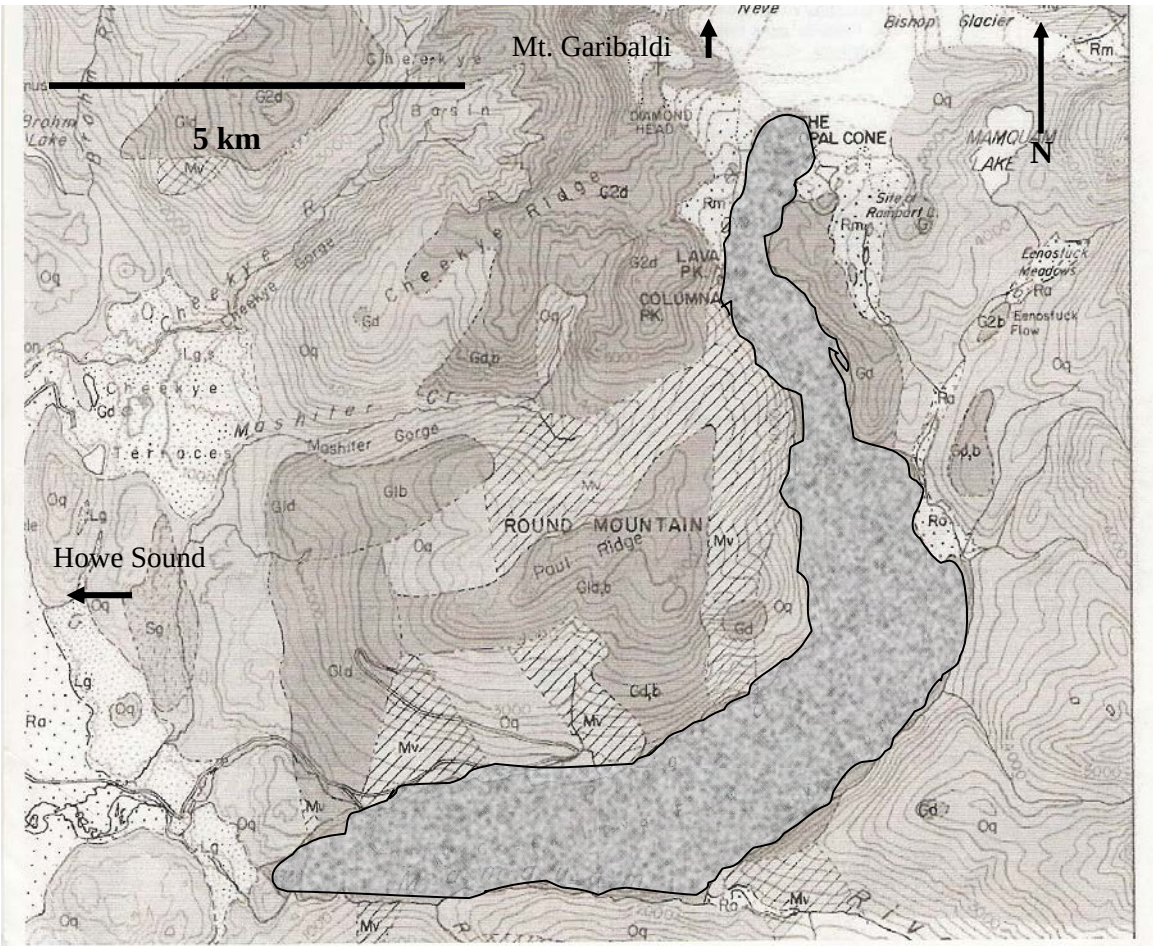

Figure 4) Geologic map of the Mamquam river valley and surrounding Squamish area. The Ring Creek lava flow is shaded. Figure modified from Mathews (1958b). Other Quaternary volcanic products are represented by dark grey shaded polygons.

Modeling of the Ring Creek lava flow

The problem of modeling the eruptive history of pre-historic lava flows has been encountered by previous workers (deSilva et al., 1994; Carrasco-Nunez, 1997), and has been circumvented by relating morphology to rheology and time dependent variables. deSilva et al. (1994) study of the Chao dacite (in northern Chile) provides an excellent example of the application of such relationships to a prehistoric lava flow. Using morphological estimates (length, width, and thickness) and the Grätz number (which relates viscous, gravitational, and thermal properties), deSilva et al. (1994) estimated extrusion rate and subsequent eruption duration of the Chao. In an effort to test the internal consistency of their data, deSilva et al. (1994) also employed a relationship, developed by Kilburn and Lopes (1991), to estimate eruption duration and subsequent extrusion rate.

Recent work on modeling emplacement of dacitic lavas has been conducted on the active Santiaguito block flow in Guatemala. Harris et al. (2002); Harris et al. (2003); Harris et al. (2004) made empirical observations and used Enhanced Thematic Mapping (ETM+, thermal satellite imagery) to examine the emplacement process of three lavas emplaced in 2000, 2001, and 2002. Each of these lavas are referred to as the Santiaguito block lava flow by Harris et al. (2002), Harris et al. (2003), and Harris et al. (2004). From their analyses, thermal properties (lava core temperature, flow front temperature, and radiative heat loss) were estimated and used to determine time dependent variables (e.g. extrusion rate, cooling rate, and emplacement duration). Rheological parameters such as lava armor were also estimated using thermal data. Lava armor typically refers to the

brittle surface crust portion of a lava flow. Previous workers have observed that thick lava armor prolongs crust survival time (the time lava armor exists until being fractured and transported away or beneath the lava flow) and facilitates lava flow growth (Kilburn and Lopes, 1991; Harris et al., 2004). These relationships produce more constrained data than methods employed by deSilva et al. (1994) to model the Chao dacite.

METHODOLOGY

To constrain the eruptive history of the Ring Creek lava flow, physical, chemical and mineralogical data were gathered and input into a series of rheological equations. Physical data was gathered by field observations and digital analysis (ArcGIS), chemical data was obtained through the use of an electron microprobe and X-Ray Fluorescence (XRF), and mineralogical data was obtained using a petrographic microscope. The equations employed by this study characterize the storage conditions of the Ring Creek magma and estimate post-eruptive properties of viscosity, cooling times and lengths (where cooling length reflects length reached as a result of a specific cooling rate), extrusion rate, flow velocity, and duration of both eruption and emplacement. Independent evaluation of the equations and assumptions used on the Ring Creek lava flow was conducted on the compositionally analogous dacites of the Chao flow (Northern Chile) and the Santiaguito flow (Guatemala).

Field Investigations

Field investigations of the Ring Creek lava flow were conducted over the summers of 2007 and 2008, during which time approximately 70 samples were collected.

Figure 5 shows the location of 13 representative samples; for GPS sample location data see Appendix I. Dimensional and textural observations of the flow were also made, and mapping was conducted to refine the spatial extent of the Ring Creek lava flow, specifically near the vent and the flow toe. Mapping efforts also included characterizing two large outcrops bordering the flow front (Figure 6), and locating morainal material at and around Opal Cone (Figure 7). At three outcrops along the southern margin of the Ring Creek lava flow, joint patterns and dimensions were documented. A concerted effort was made to locate any explosive pyroclastic deposits that may be associated with the early stages of this eruption.

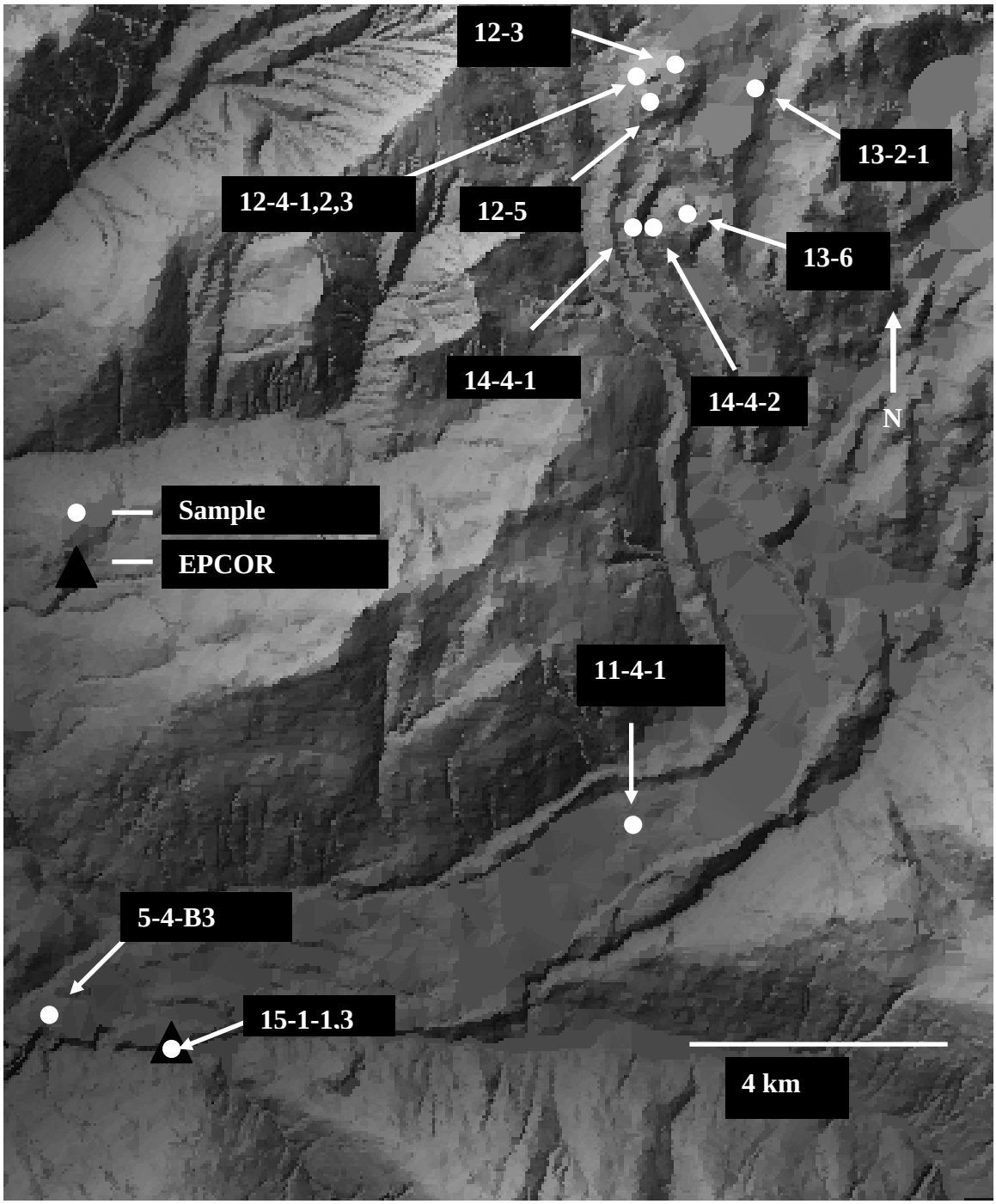

Figure 5) Location map for samples collected for thin section, whole rock, and hand sample analyses. Samples 15-1-1 and 15-1-3 were collected at different stratigraphic locations (top to bottom) from the same outcrop at the EPCOR dam facility.

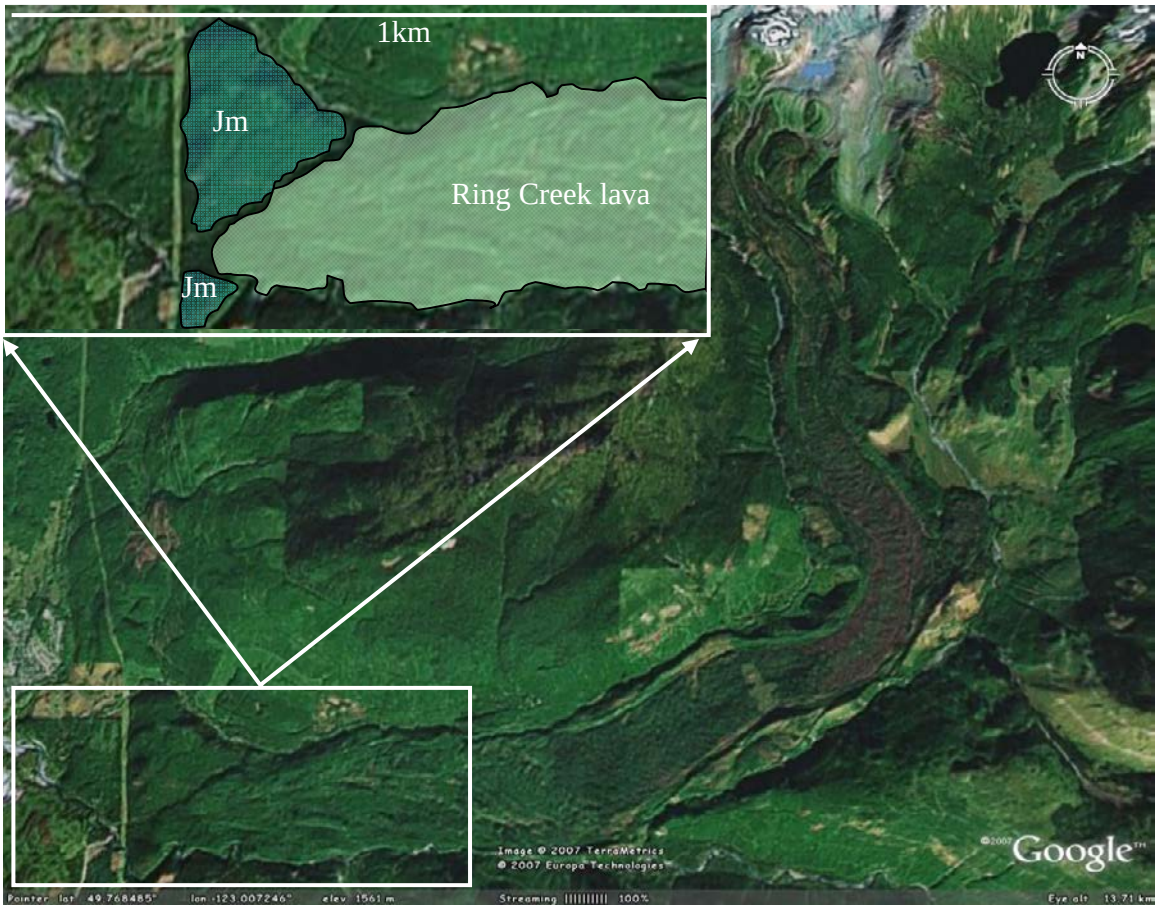

Figure 6) Terminus of the Ring Creek lava flow dammed by two outcrops of Jurassic metasedimentary and metavolcanic (Jm) rocks. Image collected using Google Earth.

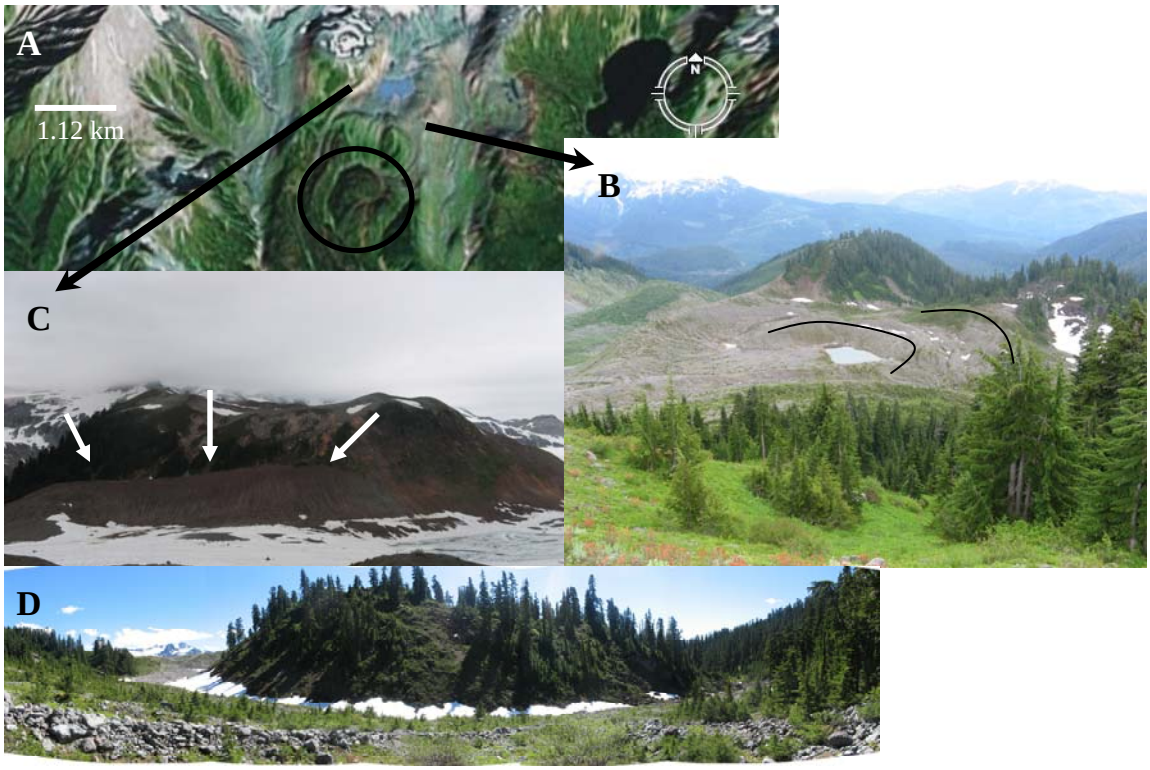

Figure 7) Field observations of the Opal Cone area: (A) Map view of the Opal Cone area. (B) Terminal moraines south-east of Opal Cone; bold lines mark the ridges of the moraines. (C) White arrows denote a medial moraine nestled against the side of Opal Cone. (D) A dome structure south of Opal Cone (denoted by the circle in A); the image faces south.

Chemistry

Whole rock XRF analyses of 11 samples (Table 1) were conducted at Geosciences Lab in British Columbia through the Geologic Survey of Canada. These data, combined with previous compositional data published by Mathews (1958b) and Powell (2005), were used as input parameters for the several rheological equations. Additionally, these data were used to examine compositional variation throughout the lava flow. For minor element chemistry see Appendix II

Electron Microprobe analyses of plagioclase phenocrysts and groundmass glass (Table 2) were conducted at the University of Washington under the supervision of Dr. Scott Keuhner. All analyses used a 1 micron diameter, 15-21 nA, and 15 keV beam. Plagioclase rims and micro-phenocrysts and adjacent groundmass glass were analyzed with a Na-loss compensation algorithm. A total of 60 point analyses were made for plagioclase (rims and microphenocrysts in the groundmass) and 30 point analyses for groundmass glass near the plagioclase. For complete microprobe data, see Appendix III.

Sample	Al2O3	CaO	Fe2O3	K2O	SiO2	MgO	MnO	Na2O	P2O5	TiO2	LOI	Total
12-3^{C}	16.83	5.54	4.9	1.64	62.31	2.46	0.09	4.37	0.27	0.59	0.74	99.74
12-5^{C}	16.92	5.66	4.87	1.71	62.17	2.47	0.09	4.33	0.28	0.6	1.05	100.17
13-2-1^{P}	17.43	5.77	5.02	1.4	62.62	2.51	0.09	4.56	0.26	0.61	-0.15	100.12
13-6^{D}	16.32	5.54	4.44	2.18	63.95	2.23	0.08	4.61	0.34	0.73	0.3	100.71
14-4-1	17.26	5.7	4.82	1.38	62.35	2.47	0.09	4.49	0.26	0.58	0.41	99.82
14-4-2	17.05	5.58	4.76	1.43	62.67	2.45	0.09	4.56	0.28	0.61	1.1	100.58
11-4-1	16.76	5.59	4.92	1.76	62.09	2.48	0.09	4.35	0.28	0.59	0.68	99.6
15-1-1	17.14	5.54	4.87	1.48	62.5	2.4	0.09	4.49	0.25	0.57	0.66	99.98
15-1-3	17.07	5.51	4.8	1.47	63.55	2.39	0.09	4.46	0.25	0.56	0.7	100.87
5-15-B3	17.2	5.59	4.76	1.45	62.7	2.44	0.09	4.49	0.26	0.56	0.37	99.91
*RM-02-10-1	17.71	5.52	1.49	1.76	62.15	2.58	0.09	4.35	0.28	0.62	NA	101.32
*RM-02-11-1	17.47	5.54	1.51	1.78	62.2	2.62	0.09	4.38	0.28	0.63	NA	100.83

Table 1) Whole rock chemistry for the Ring Creek lava flow. Samples with an asterisk represent data taken from Powell (2005), NA denotes unavailable data. Superscripts C, P, and D for samples 12-3, 12-5. 13-2-1, and 13-6 represent locations cone, plateau, and dome respectively. For sample locations, see Figure 5. Numbers reported are in oxide wt% format. LOI is loss on ignition.

Sample	Position	SiO2	TiO2	Al2O3	FeO	MgO	CaO	Na2O	K2O	Total	An	Ab	Or
12-4-1	Ph	54.7	NA	28.58	0.66	0.07	11.27	4.67	0.22	100.17	0.55	0.44	0.01
12-4-1	Ph	58.69	NA	25.64	0.73	0.04	8.03	6.38	0.53	100.04	0.52	0.46	0.02
12-4-2	Ph	54.1	NA	28.73	0.7	0.06	12.01	4.62	0.21	100.43	0.58	0.41	0.01
12-4-2	Ph	56.47	NA	27.49	0.75	0.06	10.05	5.7	0.28	100.80	0.49	0.5	0.02
12-4-3	Ph	53.69	NA	29.18	0.65	0.09	12.36	4.37	0.14	100.47	0.6	0.39	0.01
12-4-3	Ph	55.49	NA	28.72	0.69	0.08	11.34	4.77	0.21	101.29	0.56	0.43	0.01
15-1-1	Ph	53.86	NA	29.45	0.65	0.03	12.53	4.39	0.2	101.12	0.6	0.38	0.01
15-1-1	Ph	55.43	NA	28.55	0.63	0.04	11.29	4.84	0.21	101.00	0.56	0.43	0.01
15-1-3	Ph	52.95	NA	29.47	0.59	0.04	12.27	4.42	0.16	99.91	0.6	0.39	0.01
15-1-3	Ph	54.8	NA	28.69	0.57	0.04	11.4	5.19	0.31	101.01	0.54	0.44	0.02
*RM-11	Ph - rim	54.13	NA	29.92	0.31	0.01	10.14	5.25	0.22	99.98	0.51	0.47	0.01
*RM-11	Ph - rim	57.25	NA	27.6	0.22	0	8.53	6.03	0.21	99.84	0.43	0.55	0.01
*RM-11	Ph - int.	55.18	NA	28.8	0.21	0.01	10	5.45	0.16	99.81	0.5	0.49	0.01
*RM-11	Ph - int.	54.85	NA	29.1	0.22	0.04	10.2	5.41	0.15	99.97	0.51	0.48	0.01
12-4-1	Glass	62.33	0.24	20.16	1.11	0.58	5.20	6.46	1.23	97.30	NA	NA	NA
12-4-1	Glass	79.17	0.73	10.30	1.58	0.09	0.23	1.73	4.17	97.99	NA	NA	NA
12-4-2	Glass	75.5	0.62	11.47	1.25	0.06	0.49	2.83	4.24	96.46	NA	NA	NA
12-4-2	Glass	77.58	0.62	10.64	1.44	0.09	0.27	2.77	4.66	98.07	NA	NA	NA
12-4-3	Glass	71.97	0.44	14.88	1.23	0.28	2.32	4.91	3.21	99.24	NA	NA	NA
12-4-3	Glass	77.33	0.62	10.71	1.67	0.12	0.25	2.63	4.70	98.02	NA	NA	NA
15-1-1	Glass	61.57	0.00	22.97	0.77	0.03	5.09	7.87	1.04	99.34	NA	NA	NA
15-1-1	Glass	76.84	0.33	12.08	1.16	0.05	1.33	3.61	3.00	98.41	NA	NA	NA
15-1-3	Glass	70.24	0.55	15.55	1.36	0.16	2.22	5.09	3.50	98.66	NA	NA	NA
15-1-3	Glass	75.79	0.59	11.43	1.49	0.13	0.29	1.64	5.04	96.39	NA	NA	NA

Table 2) Electron Microprobe composition data (Ph = plagioclase under the position column) and glass. Samples with an asterisk represent plagioclase data taken from Powell (2005). NA represents data not obtained for the given analysis.

Microscopy

Thirteen thin sections were commercially prepared by Vancouver Petrographics for transmitted and reflected light microscopy and electron microprobe analysis. Locations of the samples collected for thin section analysis can be seen in Figure 5. All thin sections were digitally scanned and 100-spot point counts were conducted using a 10x10 grid placed over the digital image. Reflected light microscopy and SEM analyses were used to identify magnetite-ilmenite pairs for Fe-Ti thermometry, but no equilibrium pairs were found.

Digital Analysis

ArcGIS software by ESRI was used to estimate area, volume, and depth of the Ring Creek lava flow. Digital Elevation Models of the area were created from a custom made 7.5’ quadrangle prepared and provided by the Geologic Survey of Canada. The DEM was modified to remove the lava flow in order to estimate the pre-eruptive topography of the area and improve thickness estimates for the flow (Figure 8). Several cross sectional profiles were created along the length of the flow to examine flow structures and levee width.

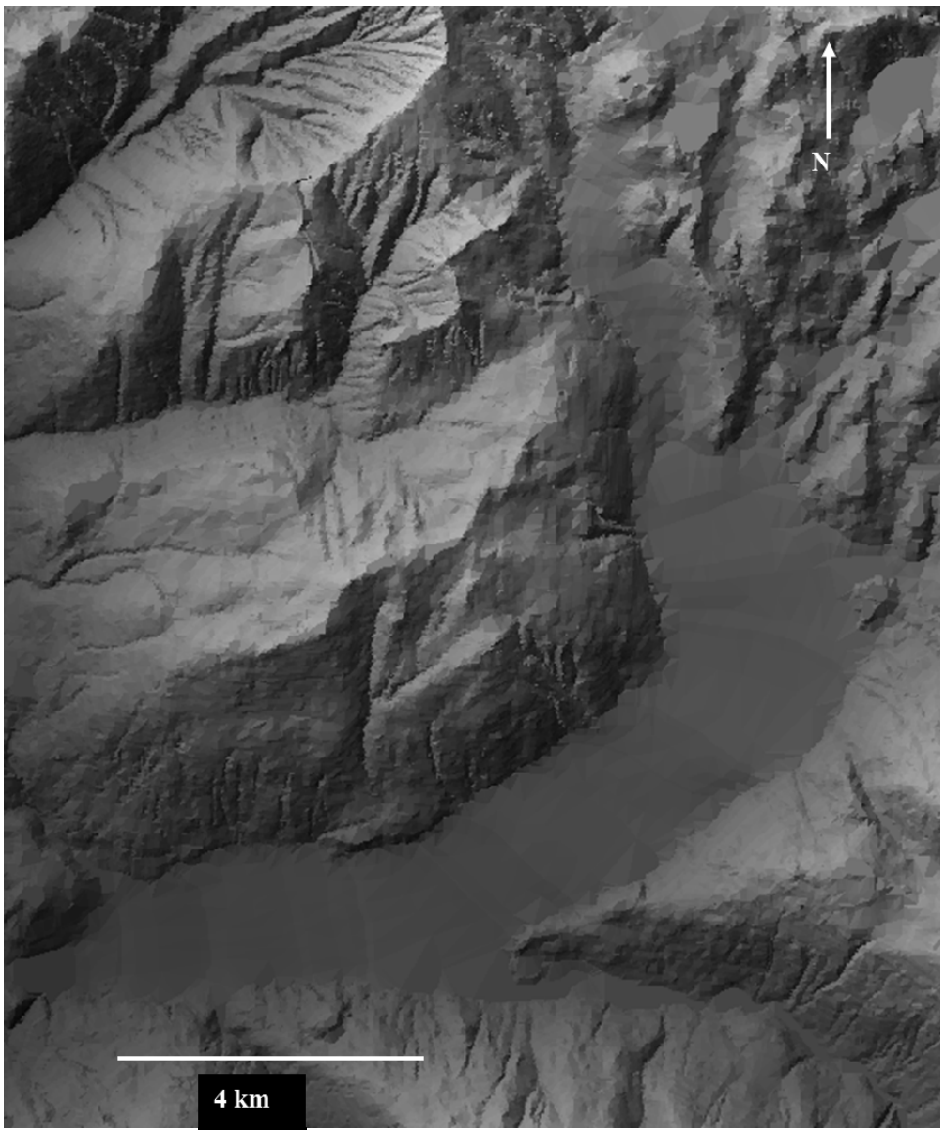

Figure 8) DEM of the Mamquam river valley excluding the Ring Creek lava flow. DEM does not exclude Opal Cone and the dome structure, both emplaced prior to the Ring Creek lava flow.

Calculation of intensive parameters

Because the mineral phase assemblage in the Ring Creek lava lacks magnetite-ilmenite pairs, a plagioclase-liquid thermometer was used to create a probable P-T-X_{H2O} range for the Ring Creek magma. Pre-eruptive temperature was calculated following the methods of Putirka (2005). Total pressure (lithostatic and fluid pressure) on the magma was estimated using a geothermo-barometer from Putirka (2005). Finally volatile (H_2O) content was calculated using the plagioclase-melt hygrometer developed by Putirka (2005). These equations are summarized below.

Temperature, pressure, and water content

In Putirka's (2005) study, estimates of temperature and pressure are determined using melt equilibrium between end-member plagioclase components, anorthite (An) and albite (Ab), and liquid (glass) in a volcanic rock using the following equations:

$$\frac{10^4}{T} = 6.12 + 0.257Ln\left(\frac{An^{Pl}}{Ca^{Liq}\left(Al^{Liq}\right)^2\left(Si^{Liq}\right)^2}\right) - 3.166\left[Ca^{Liq}\right] + 0.2166\left[H_2O^{Liq}\right] \quad (1)$$

$$- 3.137\left[\frac{Al^{Liq}}{Al^{Liq} + Si^{Liq}}\right] + 1.216\left[Ab^{Pl}\right]^2 - 2.475\times10^2\left(P\right)$$

$$\left(P\right) = -42.2 + 4.94\times10^{-2}\left[T\right] + 1.16\times10^{-2}\left(T\right)Ln\left(\frac{Ab^{Pl}Al^{Liq}Ca^{Liq}}{An^{Pl}Na^{Liq}Si^{Liq}}\right) \quad (2)$$

$$- 382.3\left[Si^{Liq}\right]^2 + 514.2\left[Si^{Liq}\right]^3 - 19.6Ln\left[Ab^{Pl}\right] - 139.8\left[Ca^{Liq}\right]$$

$$+ 287.2\left[Na^{Liq}\right] + 163.9\left[K^{Liq}\right]$$

$$H_2O(wt\%) = 24.757 - 2.26\times10^{-3}TLn\left(\frac{An^{Pl}}{Ca^{Liq}\left(Al^{Liq}\right)^2\left(Si^{Liq}\right)^2}\right) - 3.487\left[Ab^{Pl}\right] \qquad (3)$$

$$+1.927\left[\frac{An^{Pl}}{\frac{Ca^{Liq}}{\left(Ca^{Liq}+Na^{Liq}\right)}}\right]$$

Where Pl and Liq represent plagioclase or liquid components. Liquid components (Ca, Na, and Al) are calculated as cation fractions, and plagioclase components (An and Ab) are calculated from cation fractions (e.g. An = CaO/[CaO + $NaO_{0.5}$ + $KO_{0.5}$]). Si^{Liq} is defined as the anhydrous cation fraction of SiO_2 in the liquid. Equations (1) – (3) were derived from regression analysis of partial melting experiments, in which plagioclase crystals were grown at a range of pressures and temperatures, and varying liquid composition. Equations 1 and 2 above were simultaneously solved to produce a temperature estimate without the use of pressure data. This temperature estimate was then input into equation (2) to determine a pressure estimate. Finally, this pressure estimate was then input back into equation (1) in order to check internal consistency. Once magmatic pressure and temperature values were calculated, equation (3) was used to estimate pre-eruptive water content.

Viscosity

Using the temperature and pressure estimates from equations (1) – (3; Table 3), viscosity was calculated using an equation proposed by Whittington (2009). Through empirical analysis of the change in viscosity of synthetic dacitic liquid with varying

Temperature (^{o}C)	836	±76	Putirka (2005) eqn (1&2)
Pressure (kbar)	3.3	±2.9	Putirka (2005) eqn (3&2)
Water content (wt %)	0.6	±1.6	Putirka (2005) eqn (4&2)
Log viscosity (Pas)	8.31	±0.58	Whittington* (2009) eqn (5)

Table 3) Intensive parameters calculated for Ring Creek magma. Standard deviations listed were determined during calculations. Eqn (#) = equation in text.

temperature, pressure and water content, Whittington (2009) developed the following relationship:

$$Log_{10}\eta = \frac{-4.43 + \left[7618.3 - 17.25 Log_{10}\left(w + 0.26\right)\right]}{\left[T - \left\{406.1 - 292 Log_{10}\left(w + 0.26\right)\right\}\right]} \quad (4)$$

where η is viscosity (Pas), w is wt% water respectively, and T is temperature (^{o}K).

CALCULATION OF FLOW PROPERTIES

Dimensional data gathered during field investigations and using ArcGIS were input into rheological equations used by Kilburn and Lopes (1991), deSilva et al. (1994), Moore et al. (1978), and Parfitt and Wilson (2008). Dimensional data was also used with intensive parameter estimates from equations 1 – 4 in models developed by Harris et al. (2002) Harris et al. (2003) and Harris et al. (2004). Because a variety of models were used to estimate active flow properties, minimum, maximum, and mean values of flow properties (e.g. yield strength, eruption duration, and emplacement duration) were used to quantify error during calculations. Equations (5) – (12) are summarized in Table 4 at the end of this section.

Extrusion rate and eruption duration – Thermal and Satellite

Using a combination of ground based measurements and long term (4 years) satellite imagery, Harris et al. (2002), Harris et al. (2003), and Harris et al. (2004) produced a model that relates extrusion rate to thermal, heat loss, and rheological properties of a lava flow. This is done with the following relationship:

$$E_r = \frac{Q_{tot}}{\rho\left(C_p \Delta T + C_L \Delta\varphi\right)} \quad (5)$$

Where E_r is extrusion rate (m^3/s), Q_{tot} is total heat lost from the lava flow (W/m^2) (See Appendix IV for calculation of Q_{tot}), ρ is lava density (kg/m^3), C_p is the specific heat capacity of lava (J/kgK), ΔT is the liquidus-solidus temperature difference (^oK), C_L is the latent heat of crystallization (J/kg), and Δφ is the post-eruption crystallization (dimensionless). Because the Ring Creek flow occurred prior to the development of satellite imagery, the values for variables ΔT and C_L are assumed to be similar to those of the 2000 Santiaguito flow. The heat capacity, C_p, of the Ring Creek flow was calculated following Kays and Crawford (1980), and all other variables were either directly measured for the Ring Creek lava or calculated as described in sections 3.6.1, 3.6.2 and Appendix IV. The assumption of similarity (for ΔT and C_L) is justified based on the similarity of composition, morphology, phase assemblage, and calculated viscosity between the Ring Creek and Santiaguito lavas. Models proposed by Harris et al. (2002), Harris et al. (2003), and Harris et al. (2004) are also used as a comparison standard, for the Ring Creek lava flow, because thermal, morphometric, and time dependent parameters (e.g. flow velocity) for the Santiaguito lava were all directly observed in the field or using ETM (Enhanced Thematic mapping) satellite imagery.

Eruption duration and Extrusion rate – Morphometric – Santiaguito Analogue

Using morphometric parameters (length, width, and height) Kilburn and Lopes (1991) established the following mathematical relationship to describe eruption duration:

$$\left(\frac{W_m}{L_m}\right)H^2 \sin\alpha = bkt \quad (6)$$

Where W_m is the maximum flow width (m), L_m is the maximum flow length, H is the flow thickness, α is the slope angle of the underlying topography, b is a dimensionless proportionality constant with a value of 3 for flows with an aspect ratio larger than 1, k is the thermal diffusivity of the flow (m^2/day), and t is time (days).

Extrusion rate and eruption duration – Morphometric – Chao Analogue

deSilva et al. (1994) calculated eruption duration using a slightly different approach from Kilburn and Lopes (1991). They first examined extrusion rate using the Grätz number as done by Hulme and Fielder (1977) and Wilson and Head (1983), in order to determine eruption duration. The following relationship expresses extrusion rate as a function of both physical and thermal parameters:

$$V_f = \frac{Gz\kappa WL}{H} \quad (7)$$

Where V_f is the extrusion rate (m^3/s), G_z is the dimensionless Grätz number, κ is thermal diffusivity (m^2/s), W is flow width (m), L is flow length (m), and H is flow thickness (depth; m). The Grätz number relates thermal diffusivity (m^2/s) to the equivalent flow diameter, which describes the time necessary for a lava flow of given diameter to cool. Experimental analysis of the Grätz number (of flows of varying composition) has revealed that when flows stop advancing, the Grätz number is typically 320.

Yield strength – Morphometric

Yield strength was initially calculated following the methods of Moore et al. (1978), who determined that yield strength can be related to topography and levee width (distance from the outside to inside boundary of a levee) by the following relationship:

$$\tau_y = \rho g\left(\sin^2 \alpha\right) 2w_b \quad (8)$$

where τ_y is yield strength (Pa), ρ is lava density (kg/m^3), g is the acceleration due to gravity (m/s^2), sinα is the slope of underlying topography, and w_b is the levee width (m).

In a similar approach, Parfitt and Wilson (2008) present an expression that relates yield strength to depth of the lava flow as opposed to width of the levees:

$$S = \rho g d\left(\sin \alpha\right) \quad (9)$$

Where S is yield strength (Pa), ρ is lava density (kg/m^3), d is lava flow depth (m), and sinα is slope of underlying topography.

Core cooling and cooling limited length – Thermal and Morphometric

Core cooling of a lava flow reflects the amount of heat lost (^{o} C/m) within the Newtonian core. By establishing a relationship to describe core cooling, other parameters such as limiting length and cooling duration (^{o} C/hr) of a lava flow can be calculated. Harris et al. (2004) propose the following relationship to describe core cooling:

$$L_{cool} = \frac{\Delta T}{\left(\frac{\delta T}{\delta x}\right)} \quad (10)$$

Here L_{cool} is the cooling limited length (m), ΔT represents the liquidus-solidus temperature difference (^{o}K; from equation 5) and $\delta T/\delta x$ is the core cooling (^{o}K/m). To apply the equation to the Ring Creek lava flow, ΔT was converted from ^{o}K to ^{o}C. Assuming the modern length of the Ring Creek lava flow was the cooling limited length and taking ΔT from Harris et al. (2002), equation (10) was rearranged to solve for core cooling. Multiplying core cooling by flow velocity, obtained from emplacement duration from equation (11), core cooling rate of the Ring Creek lava flow was calculated. Assuming the core cooling rate value represents constant cooling of the core of the Ring Creek lava flow, an alternate emplacement duration value was estimated.

Emplacement duration and flow velocity - Morphometric

Emplacement duration of a lava flow describes the amount of time needed for total eruptive volume to cool to the point at which advance halts. This differs from eruption duration; in that eruption duration describes the time necessary for a source (e.g. Opal Cone) to erupt lava of a given volume. Emplacement duration for the Ring Creek lava flow was calculated following Parfitt and Wilson's (2008) use of the Grätz number. Mathematically, the Grätz (G_z) number is described as:

$$Gz = \frac{d_e^{\,2}}{\kappa t} \qquad (11)$$

Where G_z is the Grätz number (320 for emplaced lavas), d^2_e is the cross sectional area of the channel through which the fluid flows (m^2), k is thermal diffusivity (m^2/s), and t is time in seconds. Assuming a constant flow front velocity during emplacement,

the flow velocity can be used to estimate post-eruptive viscosity. In their study, Harris et al. (2004) use flow velocity to estimate post-eruptive viscosity through the Jeffrey's equation:

$$\eta = \frac{g\rho \sin\theta d^2}{3V} \tag{12}$$

where η is viscosity (Pa s), ρ is lava density (kg/m^3), sinθ is slope of underlying topography, d is flow depth (m), and V is flow front velocity (m/s).

Parameter	Definition	Value	Source (Equation listed)
E_r	Effusion rate (m^3/s)	Calculated Table 7	Harris et al. (2004)
Q_{tot}	Total heat loss	Calculated Table 7	eqn (5)
ρ	Lava density (kg/m^3)	2591	
Cp	Specific heat capacity (J/kgK)	1150	
ΔT	Liquidus-solidus difference (K)	448	
Cl	Latent heat of crystallization (J/kg)	$3.5x10^{-5}$	
Δφ	Post-eruption crystallinity	0.45	
W_m	Maximum flow width (m)	Measured Table 6	Kilburn and Lopez
L_m	Maximum flow length (m)	Measured Table 6	(1991) eqn (6)
H	Flow depth	Measured Table 6	
α	Slope of underlying topography	Measured Table 6	
b	Dimensionless constant	3	
k	Thermal diffusivity (m^2/s)	$9.83x10^{-7}$	
T	Eruption duration (days[4], s[5,7])	Calculated Table 7	
V_f	Effusion rate (m^3/s)	Calculated Table 7	deSilva et al. (1994)
Gz	Grätz number	320	eqn (7)
κ	Thermal diffusivity (m^2/s)	$9.83x10^{-7}$	
W	Lava flow width (m)	Measured Table 6	
L	Flow length (m)	Measured Table 6	
H	Flow depth (m)	Measured Table 6	
τ_y	Yield strength (Pa)	Calculated Table 7	Moore et al. (1978)
ρ	Lava density (kg/m^3)	2591	eqn (8)
g	Acceleration due to gravity (m^2/s)	9.82	
θ	Slope of underlying topography	Measured Table 6	
w_b	Levee width (m)	Measured Table 6	
S	Yield strength (Pa)	Calculated Table 7	Parfitt &
ρ	Lava density (kg/m^3)	2591	Wilson (2008)
g	Acceleration due to gravity (m^2/s)	9.82	eqn (9)
d	Flow depth (m)	Measured Table 6	
α	Slope of underlying topography	Measured Table 6	
L_{cool}	Cooling limited length (m)	18000	Harris et al. (2004)
ΔT	Liquidus-solidus difference (K)	448	eqn (10)
δT/δx	Core cooling ($^oC/m$)	Calculated Table 7	
Gz	Grazt number	320	Parfitt
d_e	Lava channel width and depth (m)	Measured Table 6	& Wilson (2008)
κ	Thermal diffusivity (m^2/s)	$9.83x10^{-7}$	eqn (11)
t	Emplacement duration (s)	Calculated Table 7	
η	Viscosity (Pas)	Calculated Table 7	Harris et al. (2004)
δ	Brittle crust thickness (m)	Calculated Table 7	eqn (12)
ρ	Lava density (kg/m^3)	2591	
θ	Slope of underlying topography	Measured Table 6	

Parameter	Definition	Value	Source (Equation listed)
d	Flow depth (m)	Measured Table 6	
V	Flow velocity (m/s)	Calculated Table 7	

Table 4) Parameters used in estimating thermo-rheological properties of the Ring Creek lava flow. Data are organized by equation as referenced in the methods section. See Tables 4, 6, and 7 for calculated variables.

OBSERVATIONS OF THE RING CREEK LAVA FLOW

Field observations

Field examination has resulted in division of the Ring Creek lava flow into four zones (Figure 9). These zones, in keeping with Kilburn and Lopes (1991), are termed the proximal, transitional, medial-distal, and frontal zones. Kilburn and Lopes (1991) define these zones based on empirical observations of morphology, extrusion rate, and rheology of active lava flows of varying composition. These zones are applied to the Ring Creek lava flow based on morphological observations only, due to the pre-historic nature of the lava flow.

Proximal Zone

The proximal zone of the lava flow encompasses the area around Opal Cone and roughly 1 km of the total length of the Ring Creek lava flow (Figure 9). Investigations of Opal Cone revealed small amounts of explosive material; however, no pumice was observed (Figure 10). Specimens examined in the field exhibited plagioclase and amphibole as the two dominant phases. The material that comprises the plateau exhibited extensive maroon discoloration (Figure 11) and was often brittle and crumbled when touched. Analysis of hand samples from the plateau revealed plagioclase and amphibole to be the primary constituents, similar to samples from Opal Cone. Medial moraines were observed on the southern flank of Opal Cone indicating glacial scouring after eruption (Figure 7C). A plateau of material was observed east of Opal Cone, with ice from Lava Glacier obscuring the northern flow terminus. Glacial striations were also observed in all unbroken outcrops of material within the plateau (Figure 12).

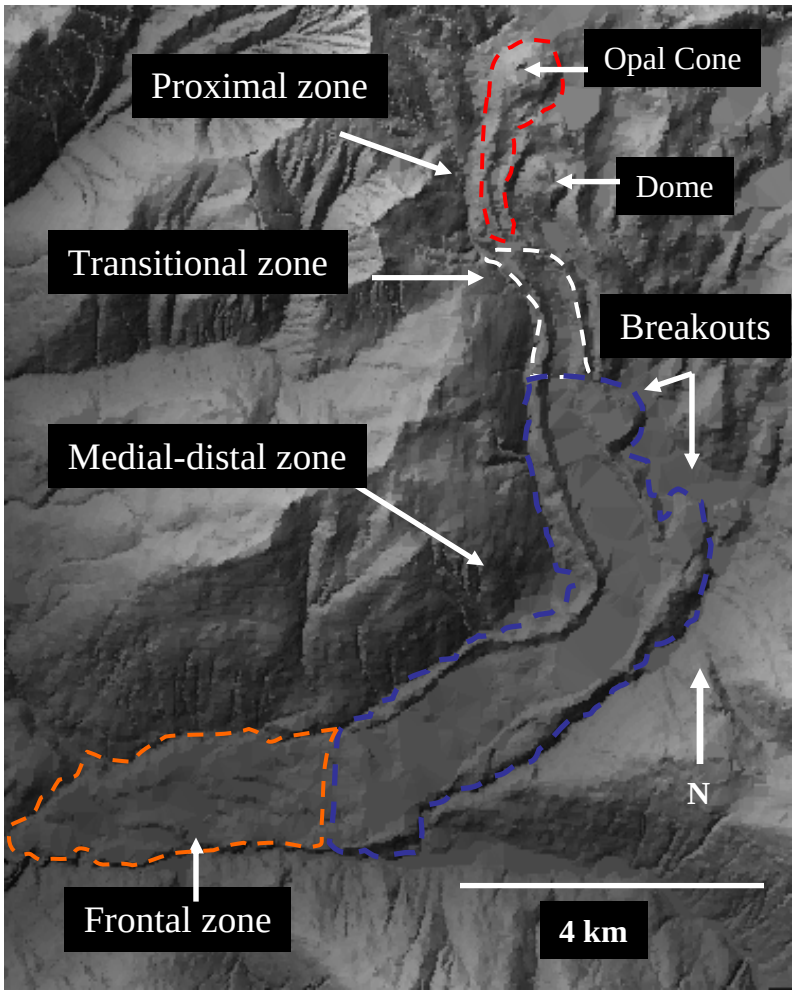

Figure 9) Zones of the Ring Creek lava flow following the descriptive methods of Kilburn and Lopes (1991).

Figure 10) Fragmented and explosive material with bread crust cooling found on the rim of Opal Cone. No explosive material was found beyond Opal Cone. Black dot in inset denotes location of photograph.

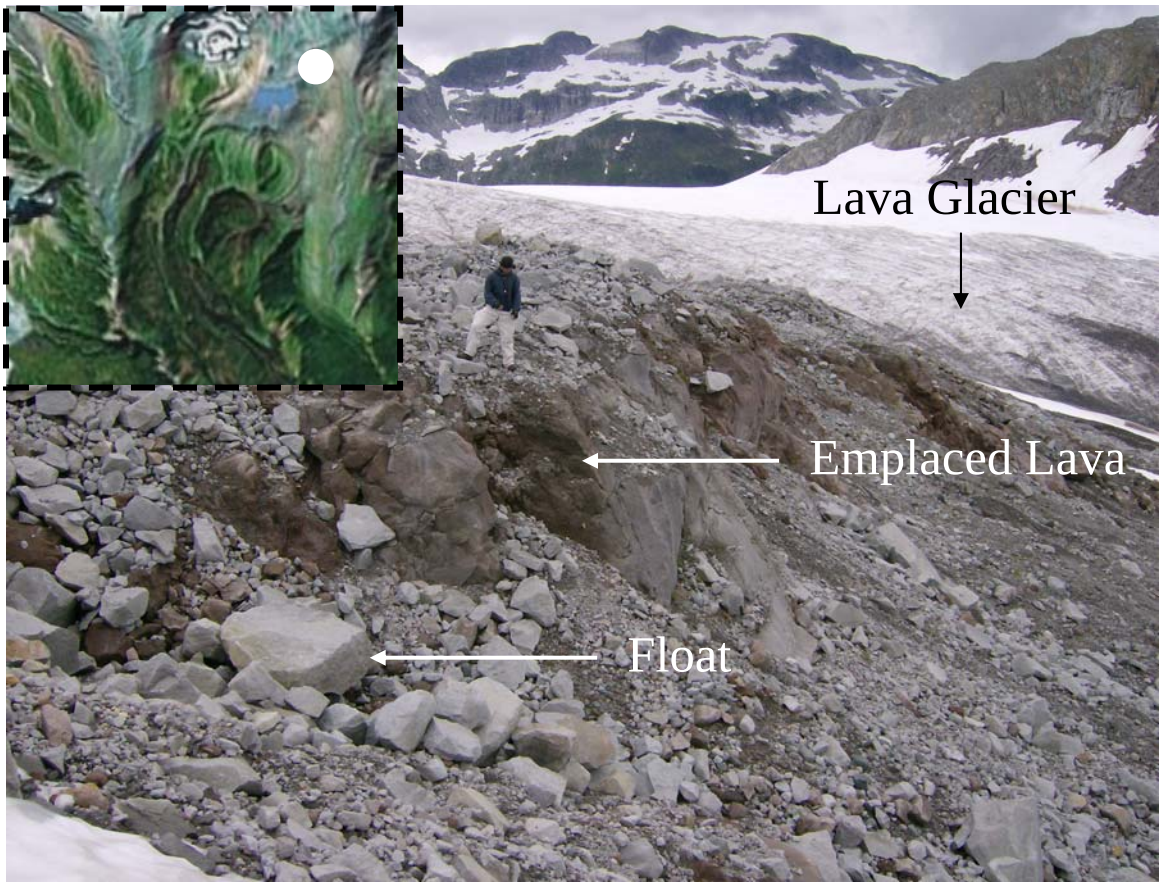

Figure 11) Light grey float deposited on top of emplaced maroon lava. Float deposited by Lava Glacier. Emplaced lava is associated with Opal Cone. White dot in inset shows the location of the photograph.

Figure 12) Glacial striations observed on the plateau of material south-east of Opal Cone. The location of striations and moraines (Figure 7C) indicate glacial thickness of at least 80 m. White dot in inset shows location of photograph.

Glacial striations within the proximal zone indicate glacial ice in the greater Opal Cone area persisted up to the Little Ice Age and may have had an important role in the eruption mechanism of Opal Cone. The presence of medial moraines on the southern flank of Opal Cone and terminal moraines south-east of Opal Cone show that the extent of Lava Glacier was further north prior to the emplacement of the Ring Creek lava flow and has since advanced (likely during the Little Ice Age) and retreated to its current extent. This suggests that Opal Cone did not erupt sub-glacially which is supported by the lack of ice-contact features throughout the rest of the Ring Creek lava flow. Previous workers have also suggested that the Ring Creek lava flow did not erupt sub-glacially (Mathews, 1958b; Powell, 2005). This indicates that the Ring Creek lava flow lacked an explosive phase due to sub-glacial eruption.

Approximately 500 m south of Opal Cone, a glacial outwash deposit was found (Figure 13). This deposit contained randomly oriented clasts of varied lithologies that ranged from 10 – 50 cm in diameter. Nearly 1 km south of Opal Cone, a dome structure was observed (Figure 7D; 14). Investigation of the structure revealed columnar jointed blocks that ranged from 15 – 50 cm in diameter and radiated outward from the topographic center. Blocks within the dome structure exhibited weathering similar to material from the plateau (and different from Opal Cone) with the exception of being consistently more brittle and exhibiting indentations and shallow gouges (not the result of glacial scouring). Also similar to Opal Cone and the plateau, samples from the dome structure exhibited plagioclase and amphibole as the two primary phases.

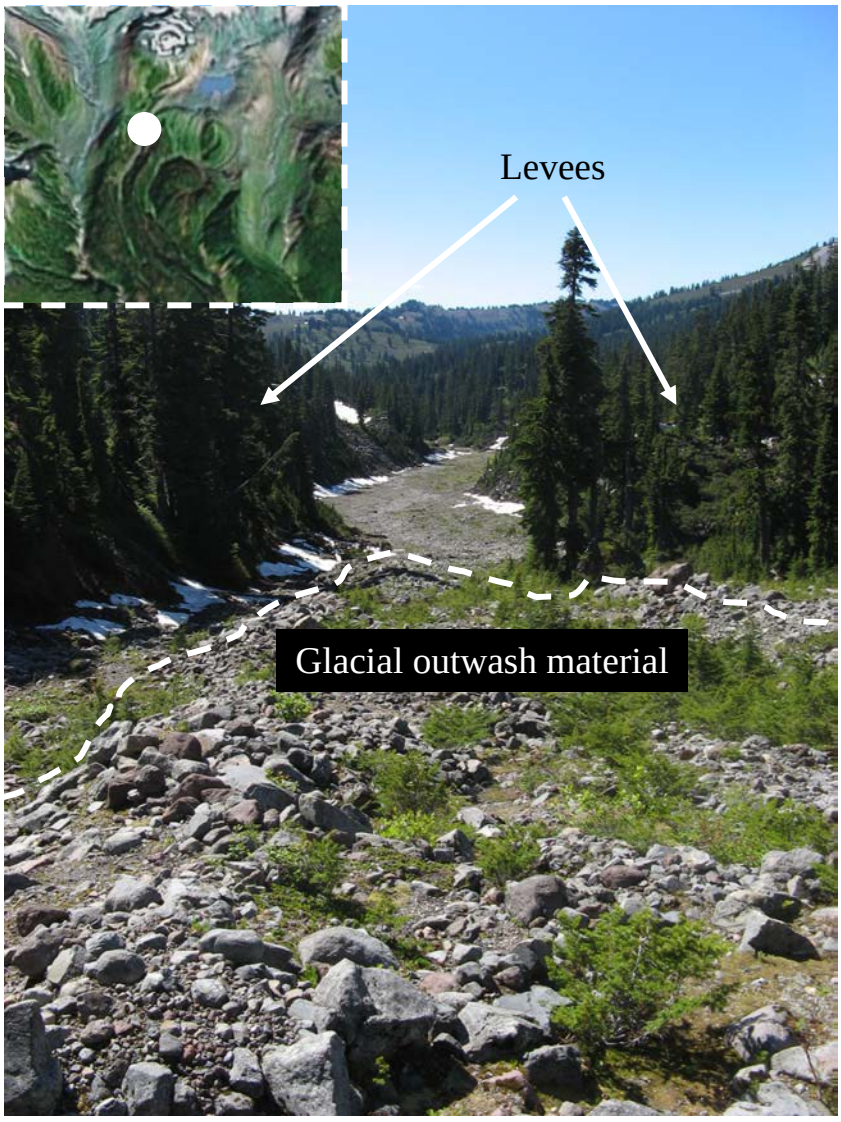

Figure 13) Glacial outwash observed in the channel proper of the Ring Creek lava flow. White dot in inset shows location of the photograph.

Figure 14) Jointed material exposed in a fracture along the left portion of the dome structure south east of Opal Cone. Columns are denoted by the light and dark arrows. Columns are roughly 15 – 50 cm in diameter. White dot in inset shows location of the photograph.

Because two distinct types of weathering were observed within the proximal zone of the Ring Creek lava flow, one in material associated with the main Ring Creek lava flow and the other in material from plateau and dome structure, it is possible that multiple events can be associated with the Ring Creek magma. The radial pattern of the columns from the dome structure, indicate a cooling pattern different from the flow direction of the Ring Creek lava flow. Cooling patterns observed at the dome structure, as well as the overall shape, suggest that it may be a torta (low lava dome). This also supports interpretations of multiple events derived from the Ring Creek magma. The similarity in observed phases from samples throughout the proximal zone (despite the difference in weathering observed in the plateau and dome structures) further suggests multiple events are linked to the same parent magma but occurred at different stages of magma evolution.

Transitional Zone

The transitional zone represents early stages of channel forming and is commonly identified by steep sided levees bounding a narrow well defined channel proper. This zone approximately 3.5 km of the total length of the Ring Creek lava flow (Figure 9). The transitional zone of the Ring Creek lava flow was observed remotely using aerial photography and digital analysis. Levee dimensions are consistently measured as roughly 100 m tall and 300 m wide (measured from the outer to inner boundary) and flow width remains constant at roughly 1100 m.

The development of a stable channel within the transitional zone potentially marks a change in the slope of underlying topography. Harris et al. (2004) discovered that

the transitional zone of the 2002 Santiaguito block flow developed at a break in the slope where a previous lava flow had leveled the topography. A similar break is slope is observed in the Ring Creek lava flow, at the beginning of the transitional zone, where an underlying bulge appears to have been overcome by the Ring Creek lava flow (Figure 9).

Medial-distal Zone

The medial-distal zone marks a transition where flow widening becomes a significant (if not dominant) growth pattern (Kilburn and Lopes, 1991). In the case of the Ring Creek lava flow the medial-distal is marked by an increase of flow thickness from approximately 100 m to 160 m and an increase in width from roughly 1 km to up to 2 km. For the Ring Creek lava flow, the medial-distal zone represents approximately 8 km of the total length of the lava flow (Figure 9).

Increased thickness and width within the medial-distal zone of the Ring Creek lava flow is initially counter-intuitive. Previous workers have observed that lava flows, of varying composition, typically decrease in flow thickness when significant widening occurs (Kilburn and Lopes, 1991). In the case of the Ring Creek lava flow it is not possible that the morphology of the Mamquam River Valley confined the lava flow (during the development of the medial-distal zone) allowing thickness to increase with width. Breakout features, as well as flow width (Figure 9), show that the Ring Creek lava flow did not fill the Mamquam River Valley, and therefore was not confined. It is possible that slow growth rate and viscosity account for the increase in thickness and width of the Ring Creek lava flow. If the Ring Creek lava flow advanced at a slow rate (typical of dacitic lavas) it follows that the thickness of the brittle surface crust (lava

armor) of the lava flow would need to be substantial to maintain temperature that would facilitate advance for a significant period of time. To develop thick lava armor, high yield strength is typically required (Harris et al., 2004). An alternate explanation for the increase in thickness and width of the Ring Creek lava flow within the medial-distal zone is a significant period of ponding. Long term ponding would also explain the occurrence of the two breakouts within the medial-distal zone (Figure 9), which are observed no where else throughout the length of the Ring Creek lava flow.

Frontal Zone

The frontal zone marks a rheological change where cooling is significant and subsequent lava armor is well developed (Kilburn and Lopes, 1991). In the case of the Ring Creek lava flow the frontal zone is approximately 5.5 km long (Figure 9). While several outcrops along the southern margin of the frontal zone were examined, data with the greatest value were obtained from outcrops at the EPCOR dam facility. Investigations at the EPCOR dam facility (Figure 5) revealed two joint defined units, a lens of material resembling flow bottom breccia, and a lack of defined levees. Fine columns ranging from 35 – 45 cm in diameter in a fan-like pattern were stratigraphically above more massive columns which were up to 50 -75 cm in diameter and 25 - 50 cm in length (Figure 15). A lens of brecciated material occupied the space between the dark colored smaller columns in the stratigraphic middle of the outcrop and the light colored columns at the base of the outcrop (Figure 15 C, D). Approximately 50 m down flow the brecciated material pinches out and a third set of large columns extend across the region where this brecciated layer would have appeared (Figure 16). The columns are approximately 18 m

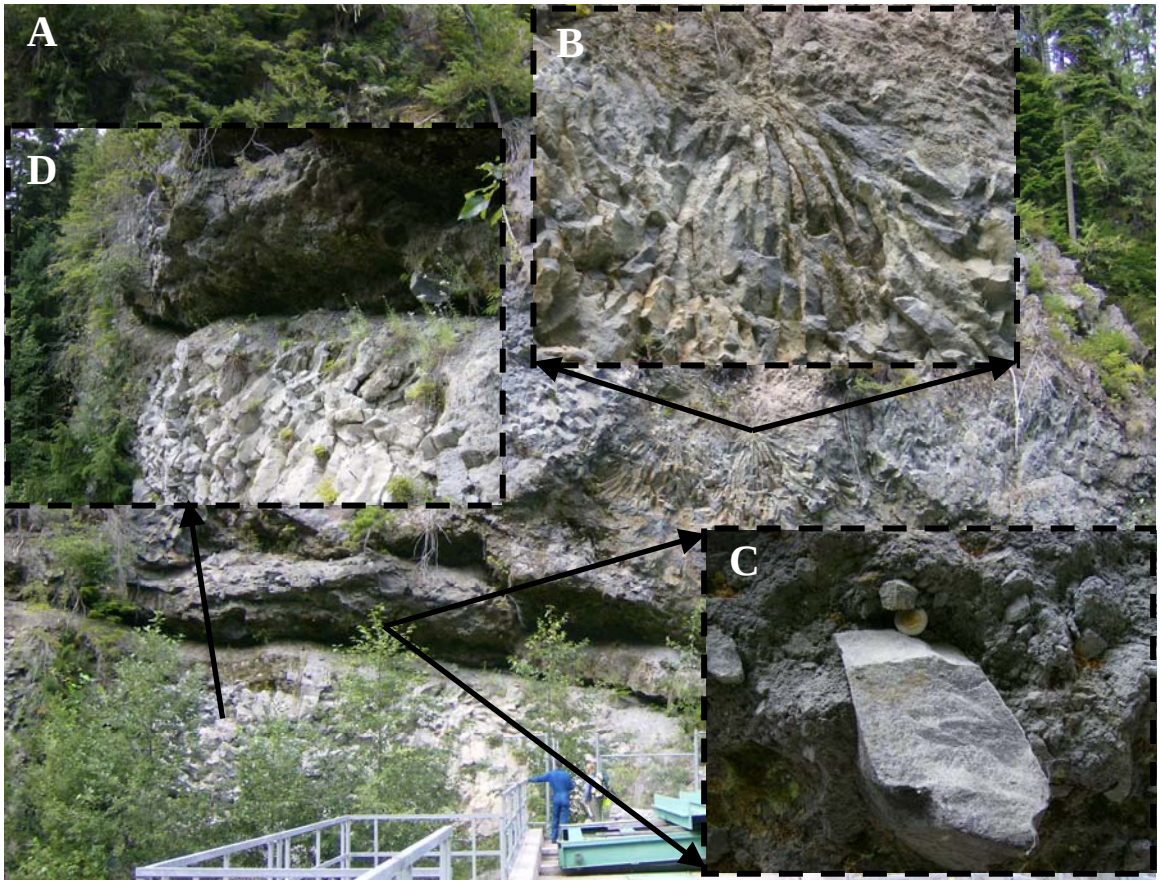

Figure 15) Outcrop at the EPCOR dam facility. Looking clockwise; (A) Outcrop exposed at the EPCOR Dam facility (Figure 5). (B) Close up of fine radial jointing. Columns are approximately 35-45 cm. (C) Brecciated material with entrained lava blocks, Canadian Twoney for scale. (D) West facing photograph of brecciated material and lower columns. Both sets are pentagonal and 25 – 50 cm long.

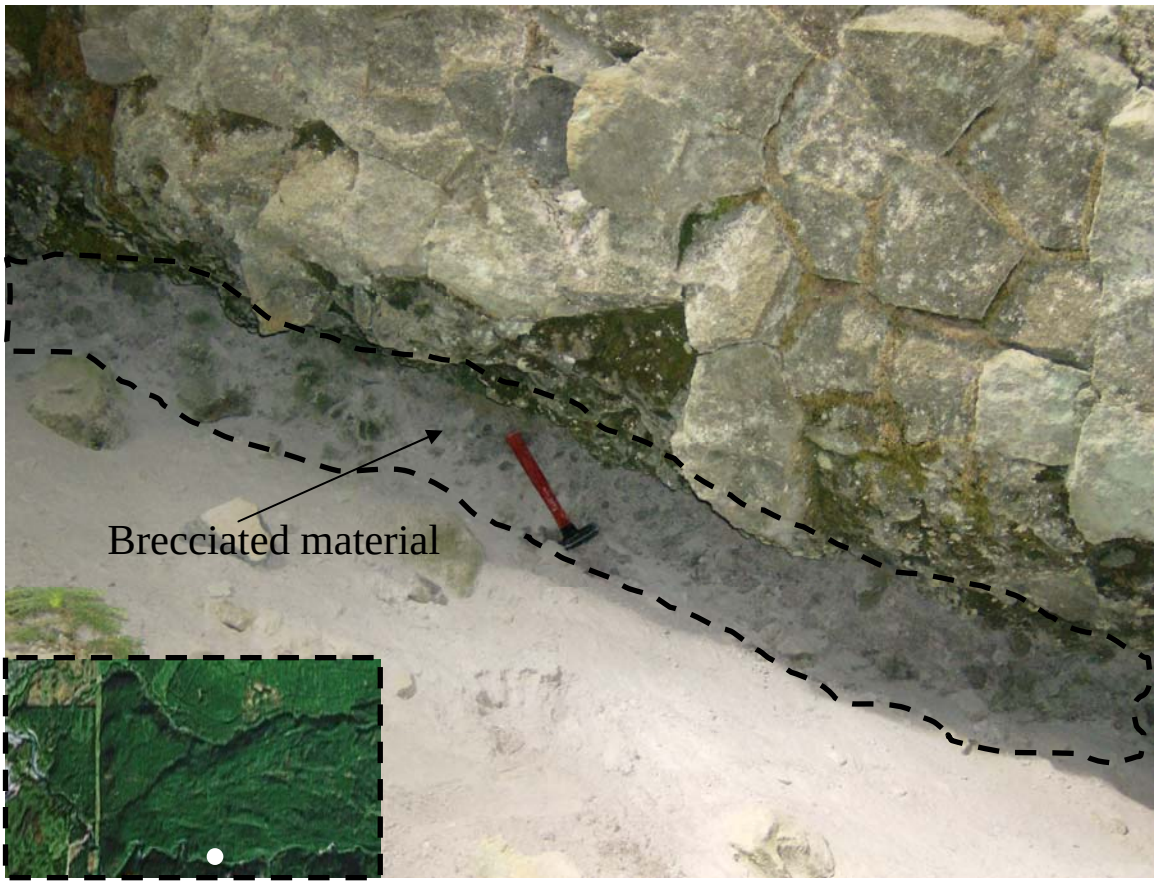

Figure 16) Approximately 50 m down flow from the EPCOR dam facility. The lens of brecciated material from Figure 15 is seen pinching out beneath a set of columnar jointed blocks. White dot in inset shows location of photograph.

tall and 1 m in diameter (Figure 17). Erosion of the Mamquam River has exposed the contact between the Ring Creek lava flow and the metamorphic basement rocks (Figure 18).

Cooling patterns observed at the EPCOR facility and other outcrops further up stream (east along the southern margin) indicate good insulation. This supports previous interpretations of thick lava armor (brittle surface crust) based on flow dimensions within the media-distal zone. The lens of brecciated material is interpreted to be the remains of a poorly defined levee that has since been eroded by the Mamquam River (Figure 19). Multiple flows at the EPCOR dam facility are not a likely explanation due to the intermittent nature of the brecciated material as well as the sudden appearance of the thick columns (Figures 16 and 17). Furthermore, if the joint sets represented two distinct flow units, each flow would be approximately 10 – 20 m thick. This thickness seems unrealistic given the length of the lava flow at the EPCOR dam facility (roughly 16 km).

Field observations of the toe of the lava flow revealed the two large triangular outcrops to be glacially deposited material overlying metamorphic basement rocks (Figure 20). The flow front of the Ring Creek lava flow is approximately 100 – 120 m thick and consists of loosely aggregated blocks, brecciated material, and soil (Figure 21). Material ranges from cobble to boulder size (0.5 - 1.5 m diameter) and shows signs of pock mark weathering and light discoloration. Observed xenoliths were dioritic and were 2 – 5 cm in length.

Due to the abutted nature of the contact between the Ring Creek lava flow and the two outcrops of basement material it is possible that the lava flow was dammed and could have continued slightly beyond 18 km. The sparse population of xenoliths in the flow

Figure 17) Large columns approximately 10 m down flow from Figure 18 within the frontal zone of the Ring Creek lava flow. Columns range in diameter from 1 – 2 m and are approximately 18 m in length. White dot in inset shows location of photograph.

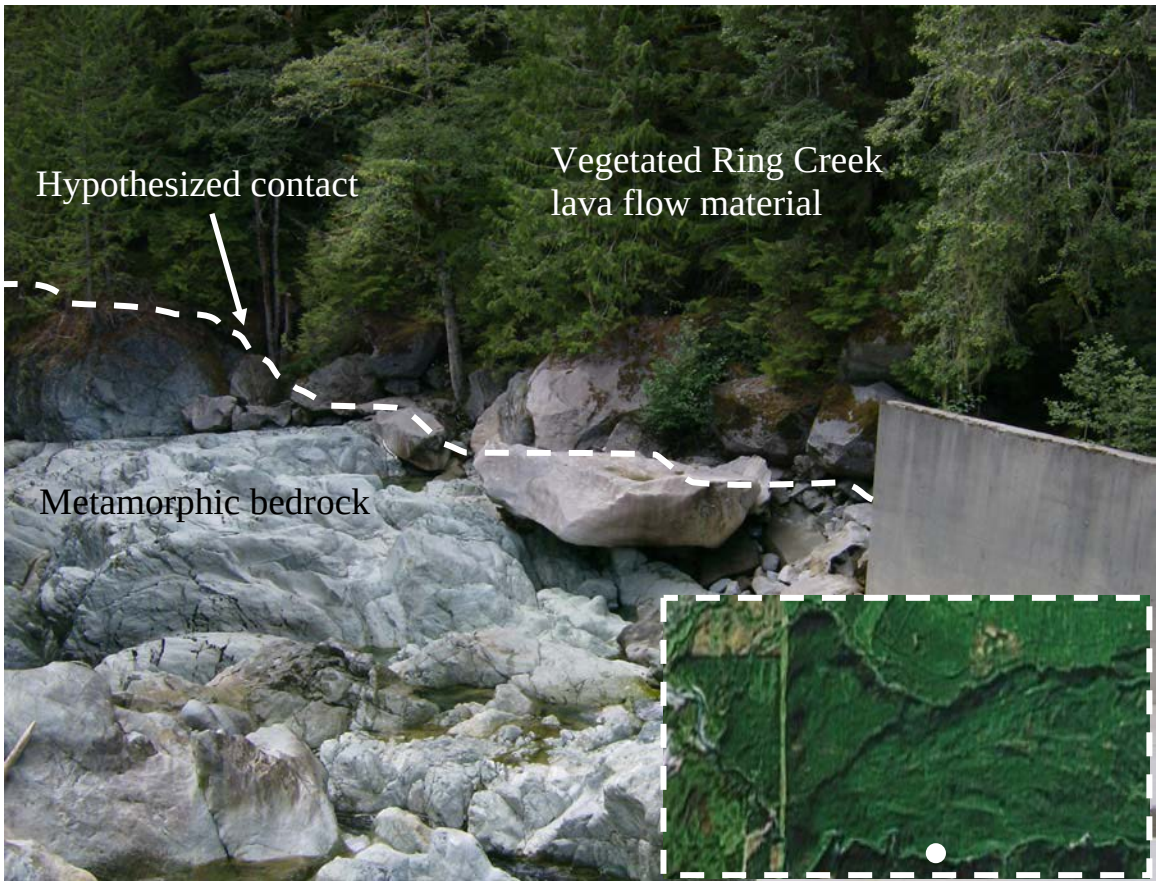

Figure 18) Metamorphic bedrock beneath the Ring Creek lava flow, with fallen blocks of the Ring Creek lava flow (maroon) on top. Beyond the trees lies a talus slope of eroded material from the Ring Creek lava flow. This places the contact between the lava flow and basement material roughly on the North side of the Mamquam River which is to the right of the image. The cement spillway from the EPCOR dam in the right portion of the image is ~ 3 m tall. White dot in inset shows location of photograph.

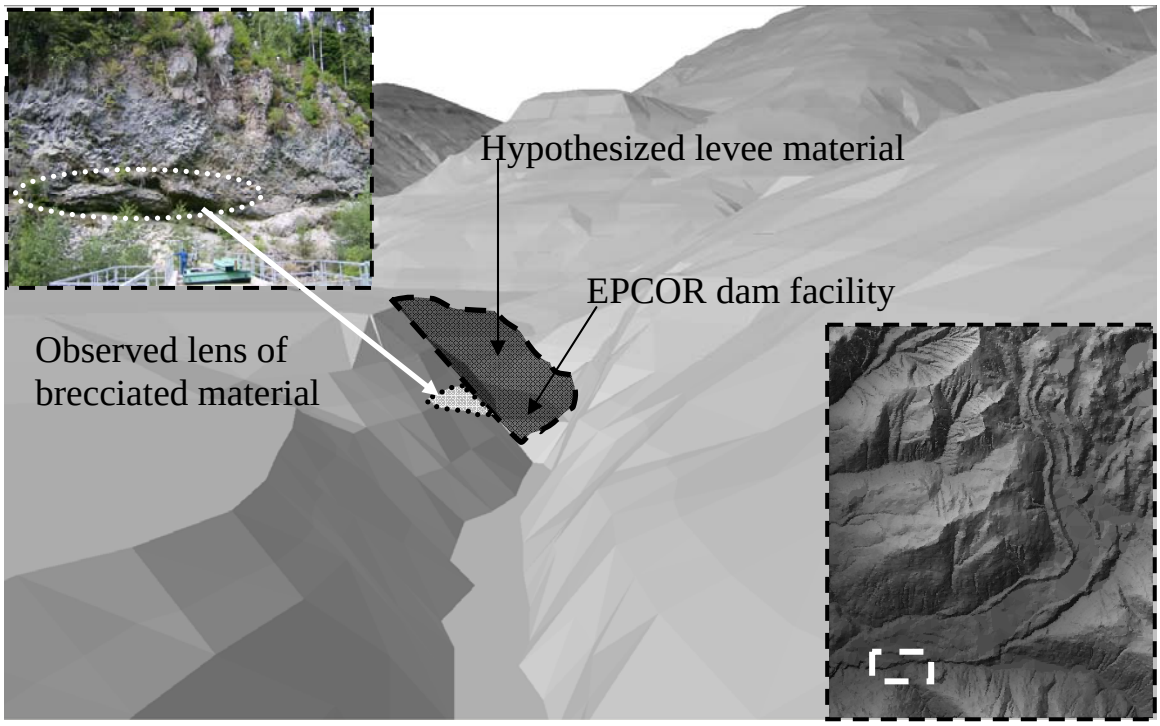

Figure 19) Oblique image of the lens of brecciated material at the EPCOR dam facility outcrop. Dark dashed polygon represents levee material that has since been eroded away by the Mamquam River and construction of the EPCOR dam. Light grey dashed polygon represents a three dimensional oblique view of the lens of brecciated material. White box in inset shows location of photograph.

Figure 20) Glacio-fluvial deposits with meta-sedimentary clasts found along the Northern margin of the lava flow. No volcanic material (Ring Creek float, pumice, or volcanic sand) was observed within the glacio-fluvial deposit. White dot in inset shows location of photograph.

Figure 21) Outcrop along the logging road near the top of the flow front. Material here has massive and brecciated sections with a fine powder that is a weathering byproduct. Also of note a thin (approximately 15 cm) stratum of rubble that is potentially a glacially derived stream deposit. White dot in inset shows location of photograph.

front (combined with their paucity throughout the rest of the lava flow) indicates that structural failure of the magma chamber did not occur (Rutherford and Devine, 1988).

Summary of Field Observations

Field investigations suggest the Ring Creek lava flow is not associated with a pyroclastic phase and that it developed thick lava armor during advance. The lack of a pyroclastic phase implies that substantial volatile buildup did not occur prior to eruption. The presence of thick lava armor suggests that yield strength, and viscosity, are high. With a viscous rheology, it follows that the Ring Creek lava flow would be well insulated. This would account for the anomalous length, with respect to the chemistry of the Ring Creek lava flow. Field investigations also suggest that there may have been precursory effusive events from the Opal Cone area prior to the eruption of the Ring Creek lava flow.

Mineralogy

Thin section analyses show a phase assemblage of plagioclase, hornblende, biotite, orthopyroxene, clinopyroxene, ülvospinel, olivine, and glass (Table 5). The most abundant phases are plagioclase and amphibole. Pyroxene is sparse; orthopyroxene has been observed in samples from Opal Cone only, and clinopyroxene has been seen in only one sample at the EPCOR dam facility. These phases were also observed by Powell (2005). Although phase assemblage remains constant through the lava flow, textural differences between several samples highlight variations between portions of the flow

sample number	12-4-1	13-6	14-4-2	15-1-1	14-4-1	*11-1	*39-1
Plagioclase	34	14	29	26	21.13	22.73	24.67
Amphibole	10	33	7	4.8	3.56	2.07	5.6
Biotite	2	4.2		1	<1	3.40	
Clino pyroxene	1				<1	<1	<1
Ortho pyroxene				2	<1	1.60	0.87
Olivine				1			
Fe-Ti oxide	1.8	2.5	1	3.2	4.97	1.2	1.53
Groundmass	51	48	63	62	69.31	68.53	67.33

Table 5) Modal analyses of samples gathered throughout the Ring Creek lava flow. See Figure 5 for sample locations. Data reflect 100-225 points counted using a grid draped over scanned images of thin sections of the samples. Samples with an asterisk were taken from Powell (2005).

(Figure 22). Material collected from Opal Cone (e.g., sample 12-4-1) contains amphibole with reacted or vermicular textures (Figure 22 A). Samples gathered from the dome structure (e.g., sample 13-6) exhibit acicular and bladed amphibole that appears to be in equilibrium with the surrounding melt, though oxidized (Figure 22 B). Sample 13-6 also exhibits the highest concentration of amphibole with 33% (Table 5). Sample 14-4-1, from the base of the outer edge of the east levee contains two populations of amphibole, one with reaction rims and the other nearly completely reacted away (Figure 22 C).

Amphibole in sample 14-4-1 exhibit reaction rims similar to samples from Opal Cone and the outcrop at the EPCOR dam facility (Table 5). Examination of sample 15-1-3 from the outcrop at the EPCOR dam facility shows amphibole in complete disequilibrium with several grains showing reaction textures next to plagioclase grains (Figure 22 D). Plagioclase grains within sample 15-1-3 exhibit clot like textures as well as complex zoning, complete with thin (1 – 2 μm) equilibrium-growth rims surrounding the grain. This complex texture of plagioclase has been observed in samples 12-4-1(Opal Cone), 11-4-1 (from the west levee), and 5-4-B3 (from the toe), however no such texture was observed for samples 13-2-1 (plateau structure) and 13-6 (dome structure). Modal analysis of sample 15-1-3 is similar to sample 14-4-1 (Table 5).

Textural analysis of samples 13-6 and 14-4-1 compared to other samples such as 12-4-1 and 15-1-3 provides many qualitative answers about the evolution of the Ring Creek magma. Firstly because phase assemblage remains constant between the older dome structure and the younger Ring Creek lava flow (evidenced by samples 13-6 and 15-1-3) magma mixing unlikely. Secondly, mineralogical investigations compositional homogeneity throughout the Ring Creek lava flow. This is supported by whole rock

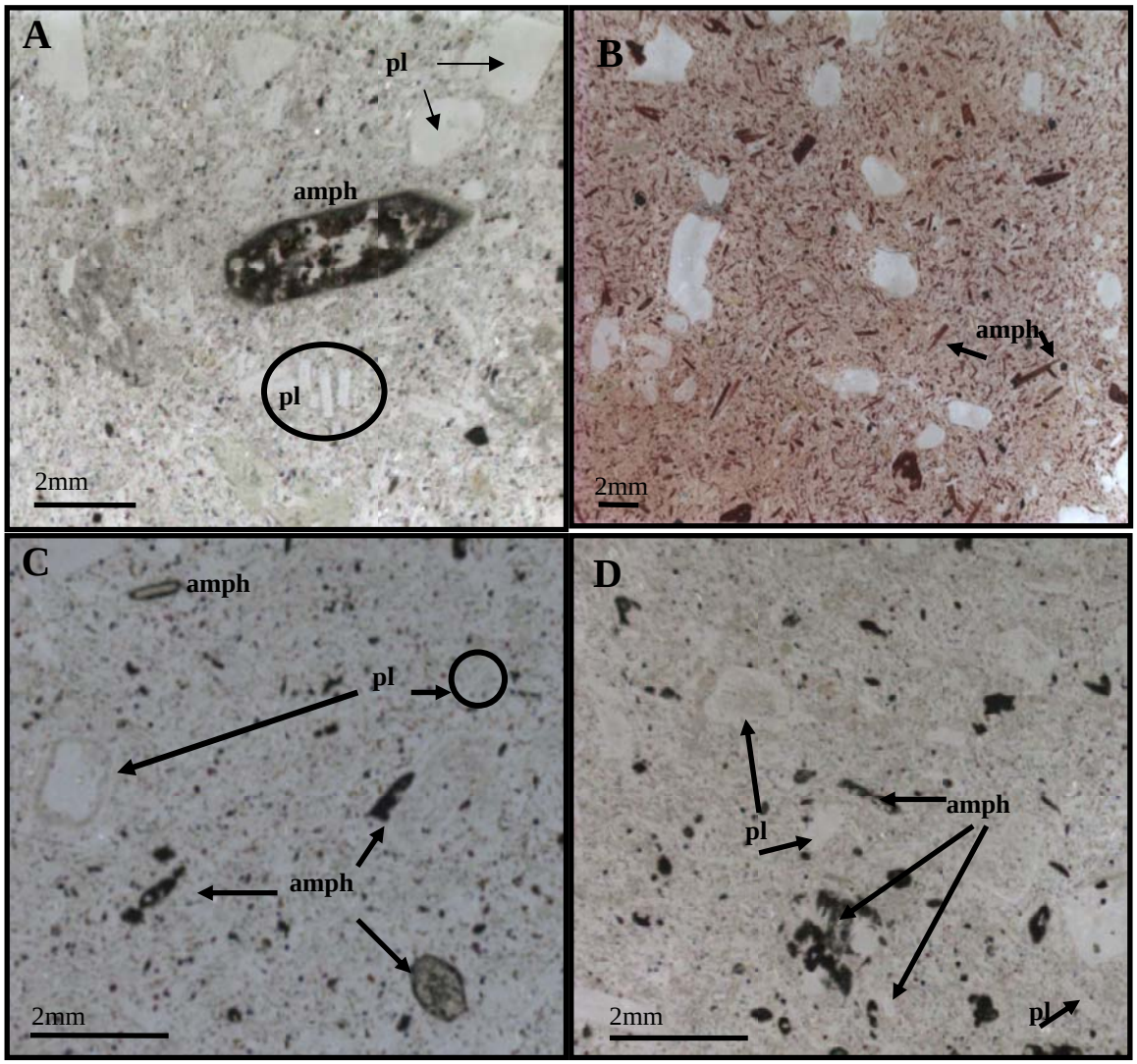

Figure 22) Photomicrographs of amphibole from samples throughout the Ring Creek lava flow. (A) Sample 12-4-3 from Opal Cone, (B) Sample 13-6 from the dome structure, (C) Sample 14-4-1 from the southern margin of the proximal zone, and (D) Sample 15-1-3 from the EPCOR dam facility outcrop. Note the increased disequilibrium from (B; in equilibrium despite oxidization) to (C; some replaced some with rims) and (A) and (D) where all amphibole present is replaced by Fe-Ti oxides.

chemistry. Analysis of sample 14-4-1, in conjunction with sample 12-4-1, 13-6, and 15-1-3, shows an intermediate stage of amphibole breakdown which suggests that the Ring Creek magma likely erupted in at least three events defined as: flow unit 1 (the dome structure), flow unit 2 (the plateau structure and underlying flow within the proximal zone of the Ring Creek lava flow), and flow unit 3 (the Ring Creek lava flow). These events are distinguished by severity of amphibole breakdown and are collectively classified (by this study) as the Ring Creek Complex. This new evidence suggests that the Ring Creek magma did not erupt in one single event after stalling.

Summary of Mineralogical Observations

Mineralogical investigations confirm interpretations from chemical and field data that composition throughout the Ring Creek magma was homogenous. Three classes of amphibole degradation texture supports interpretations that magma stalled beneath Opal Cone for some time; however it suggests that several extrusions occurred prior to the formation of the Ring Creek lava flow. Furthermore there is no data to support injection of fresh material as an eruption mechanism for Opal Cone.

Chemistry

Whole rock data of the Ring Creek samples, collected during field investigations, are comparable to data from Powell (2005) and confirm the original classification of the Ring Creek lava flow as a low-silica dacite (Mathews, 1958b;Table 1). Although chemistry of the Ring Creek lava flow is comparable to the Mount St. Helens and Santiaguito dacites, several samples plot as andesite (Figure 23; Rutherford, 1985; Harris

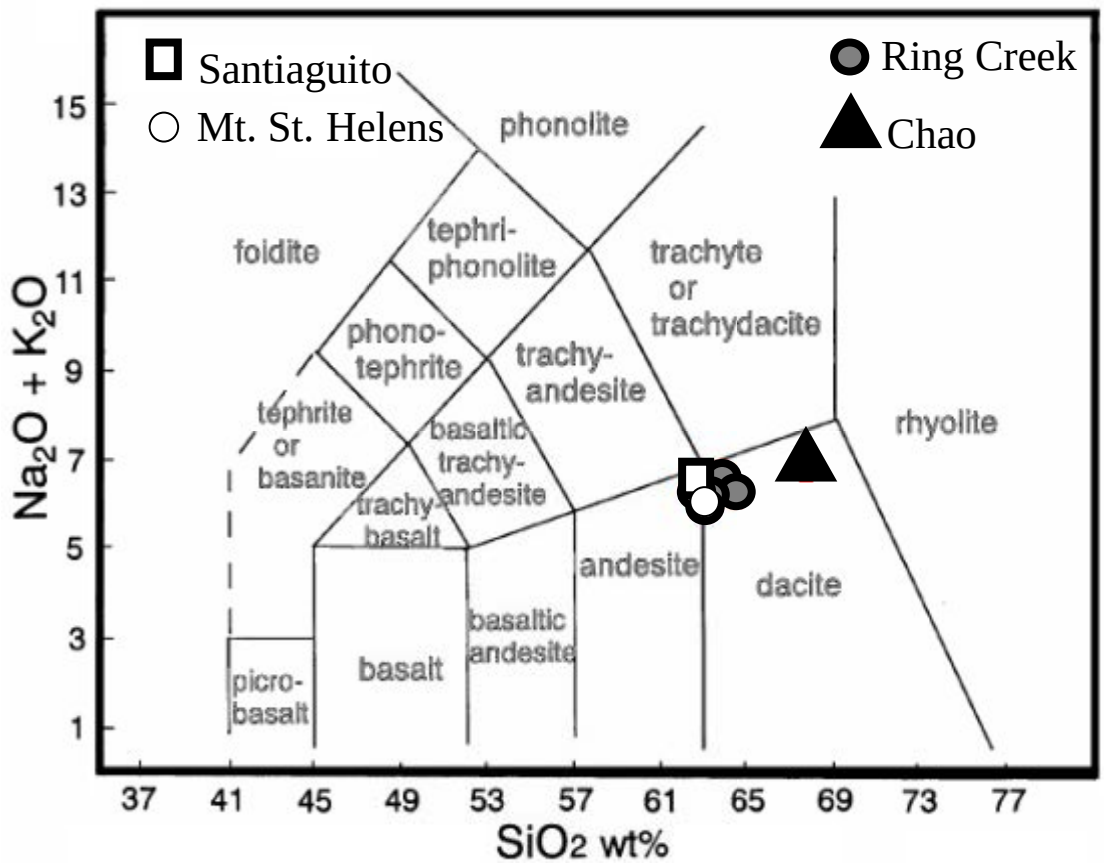

Figure 23) Total Alkali-Silica content plot of the Ring Creek lava flow and three analogous dacites. Data for the analogous dacites were obtained from Rutherford, (1985; Mt. St. Helens), deSilva et al., (1994; Chao), and Harris et al., (2002; Santiaguito).

et al., 2002, Harris et al., 2003, Harris et al., 2004). The difference in chemistry between the Ring Creek and Chao dacite is roughly 3 wt% SiO_2. Analysis of whole rock data does not show any compositional anomalies throughout the Ring Creek lava flow.

Similarity of the chemistry between the Ring Creek and Mount St. Helens lavas suggests that low silica (for a dacite), is not the primary reason for the lack of a significant explosive phase during the eruption of Opal Cone. Furthermore similar chemistry between the Ring Creek and Santiaguito lavas is crucial for the application of rheological equations proposed by Harris et al. (2002), Harris et al. (2003) and Harris et al. (2004) to the Ring Creek lava flow, as chemistry often impacts rheology. The compositional homogeneity throughout the Ring Creek lava flow suggests that magma mixing did not occur during storage beneath Opal Cone. Paucity of magma mingling textures in hand sample and thin section also supports the rejection of magma mixing. This excludes injection of fresh material, into the Ring Creek magma as an eruption mechanism for Opal Cone. Chemistry from samples 13-2-1, 13-6, and 14-4-2 (Figure 5; Table 1) support previous hypotheses, based on field examinations within the proximal zone, that the plateau of material and dome structure are derived from the same magma as the Ring Creek lava flow.

Compositional data of plagioclase grains in samples gathered by this study, agree well with both rim and interior positions analyzed by Powell (2005) (Table 2). While totals for plagioclase data were frequently 99-100%, glass analyses produced totals between 95 and 98 (Table 2). This is likely the result of lack of consideration for the phase apatite within the melt. During microprobe analysis of thin sections, apatite grains were infrequently observed in the groundmass, however the apatite phase was not

included in the calibration, prior to analysis. No significant change in composition was observed when comparing phenocryst rims and lath cores (Table 2).

Little to no variation from rim to interior positions within plagioclase grains is observed. If the Ring Creek magma evolved during crustal stagnation, normal zoning would be observed within plagioclase grains. Conversely, if fresh (mafic) material was injected into the Ring Creek magma, reverse zoning (or anomalous calcic zones) would be observed. Because plagioclase grains within the Ring Creek lava flow are consistently calcic ($An^{55} – An^{60}$) it is likely that fresh calcium was being incorporated from reacting amphibole or the melt within the Ring Creek magma. Calcium from decaying amphibole could also explain the presence of apatite within the melt.

Summary of Chemistry Observations

Both whole rock and microprobe analyses of samples indicate homogeneity of the Ring Creek magma. Chemical (and mineral) homogeneity provides valuable insight into the eruption mechanism of Opal Cone. If the magma beneath Opal Cone did not experience injection of fresh material, then some external change (e.g., faulting, or some mechanism that would decrease lithostatic pressure) must be responsible for triggering the eruption of Opal Cone.

Digital Analysis of Lava Flow Morphology

Using ArcGIS the Ring Creek lava flow was estimated to cover 24 km^2 and have a total volume of 2.4 km^3. The volume of Opal Cone was estimated to be less than 0.1 km^3. These data as well as other physical parameters can be seen in Table 6. Flow

Length (m)	18000 ± 500 m
Mean flow width (m)	1375 ± 192 m
Mean levee width (m)	155 ± 20 m
Mean depth (m)	110 ± 20 m
Total flow area (km^2)	24.7 ± 4 km^2
Volume of lava (km^3)	2.4 ± 0.54 km^3
Volume of Opal Cone (km^3)	0.083
Slope of underlying topography	
Proximal zone	8.7
Transitional zone	7.6
Medial-distal zone	1.43
Frontal zone	4.44

Table 6) Morphometric parameters of Opal Cone and the Ring Creek lava flow. Values for slope reflect mean estimates. All volumetric values apply only to the Ring Creek lava flow (flow unit 3).

thickness was estimated to be 80 m in the proximal and transitional zones, 160 m in the medial-distal zone, and 100 m in the frontal zone. This resulted in an average thickness of approximately 110 m. Topographic profiles taken along the axis of the Ring Creek lava flow reveal several varying slopes. These slopes were quantified in the pre-emplacement DEM and can be seen in Table 6.

Proximal Zone

Cross sectional profiles of the proximal zone of the Ring Creek lava flow revealed an underlying lava flow and shed light on the dome structure south-east of Opal Cone (Figure 24). The presence of this underlying flow was also supported by an oblique image taken using Google Earth (Figure 25). From Figure 26 the underlying flow is estimated to be roughly 1.2 km wide and 100 m thick. The Ring Creek lava flow is estimated to be approximately 500 m wide and 80 m thick.

Digital analysis of the proximal zone has revealed that sample 14-4-1 was collected at the east levee (near the flow front) of this underlying flow. The presence of a separate underlying flow would explain the different populations of amphibole within the Ring Creek lava flow (Figure 22)**.** Moreover, an underlying flow provides an intermediate stage of amphibole texture between sample 13-6 (oxidized yet stable amphibole) and 15-1-3 (replaced and unstable amphibole; Figure 22). Finally the underlying flow suggests at least three units, defined as flow unit 1 (dome structure), flow unit 2 (underlying flow) and flow unit 3 (the Ring Creek lava flow) are associated with the Opal Cone area. This is significant as the three flow units support field based and

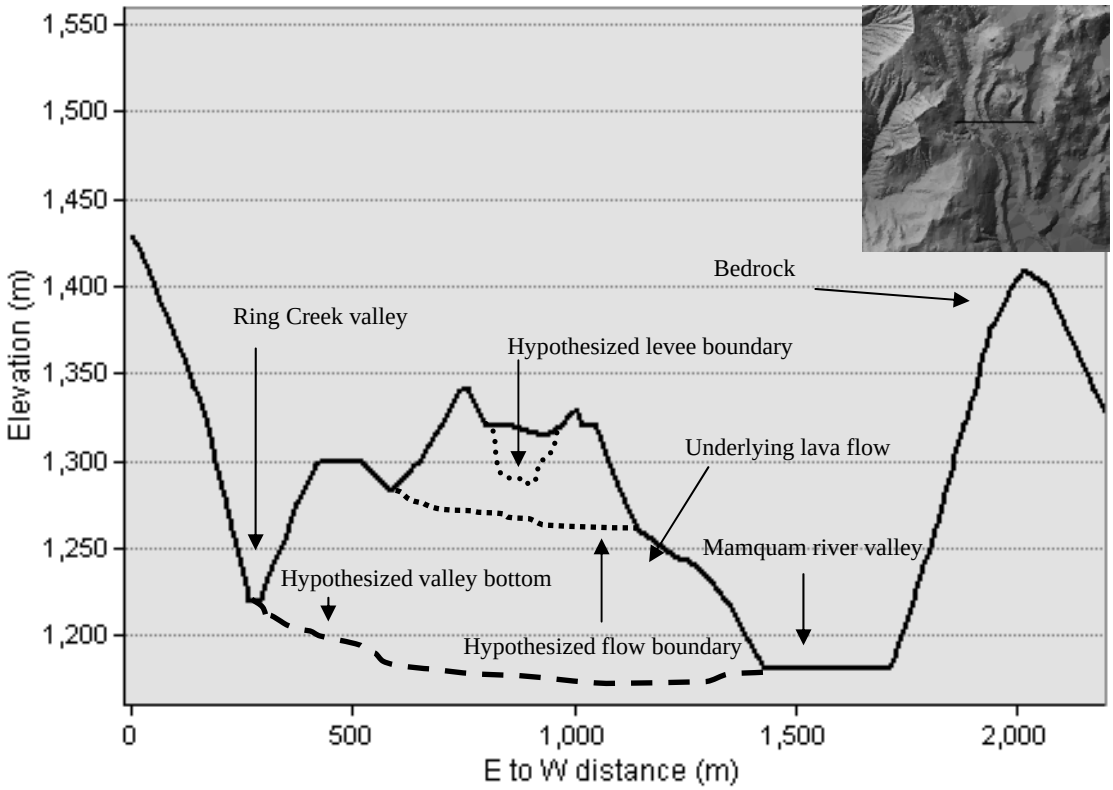

Figure 24) Cross sectional profile of the proximal zone of the Ring Creek lava flow. The line labeled hypothesized flow boundary marks the boundary between the first event from Opal Cone overlain by the modern Ring Creek lava flow. The black line in the inset image shows the location of the cross section within the proximal zone. Approximately six times vertical exaggeration.

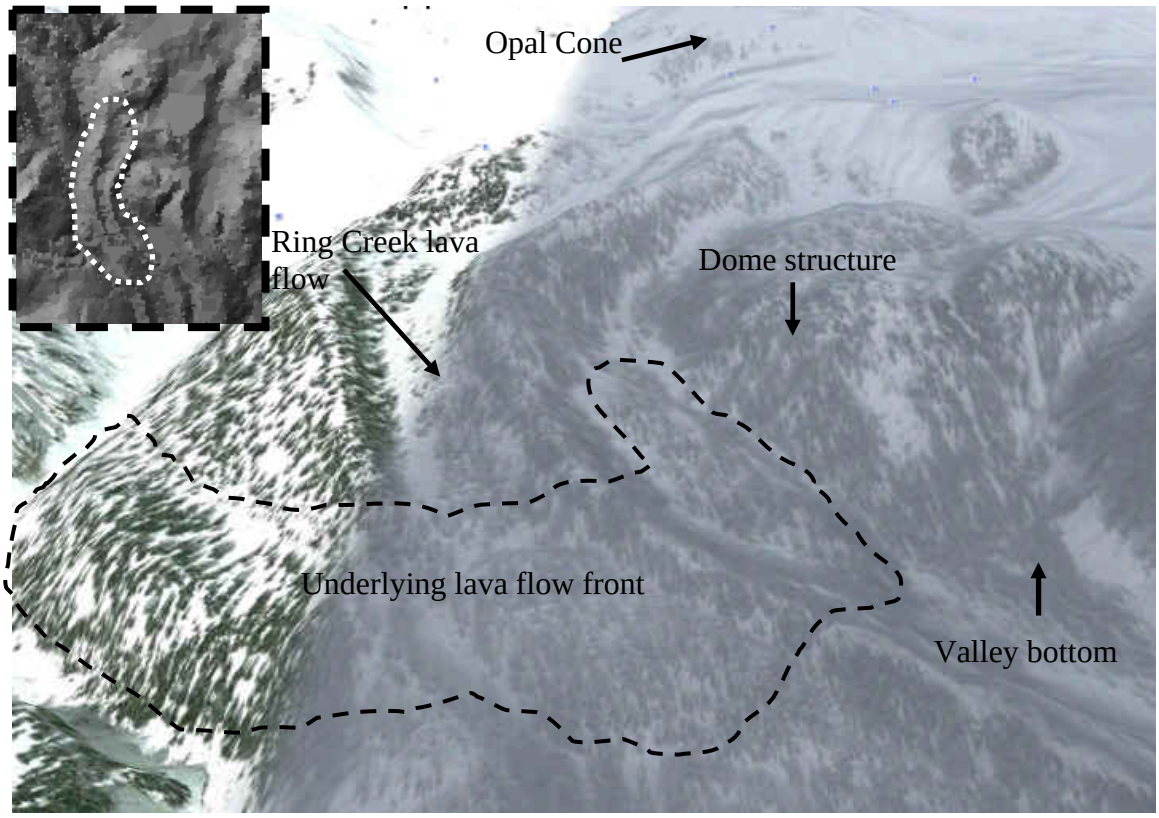

Figure 25) Oblique view of the proximal zone of the Ring Creek lava flow. The feature outlined in black is the lobe of an older flow overlain by the modern Ring Creek lava flow. Note that both flows still do not fill the valley. Outlined feature in inset denotes the location of the underlying lava flow. Image collected using Google Earth.

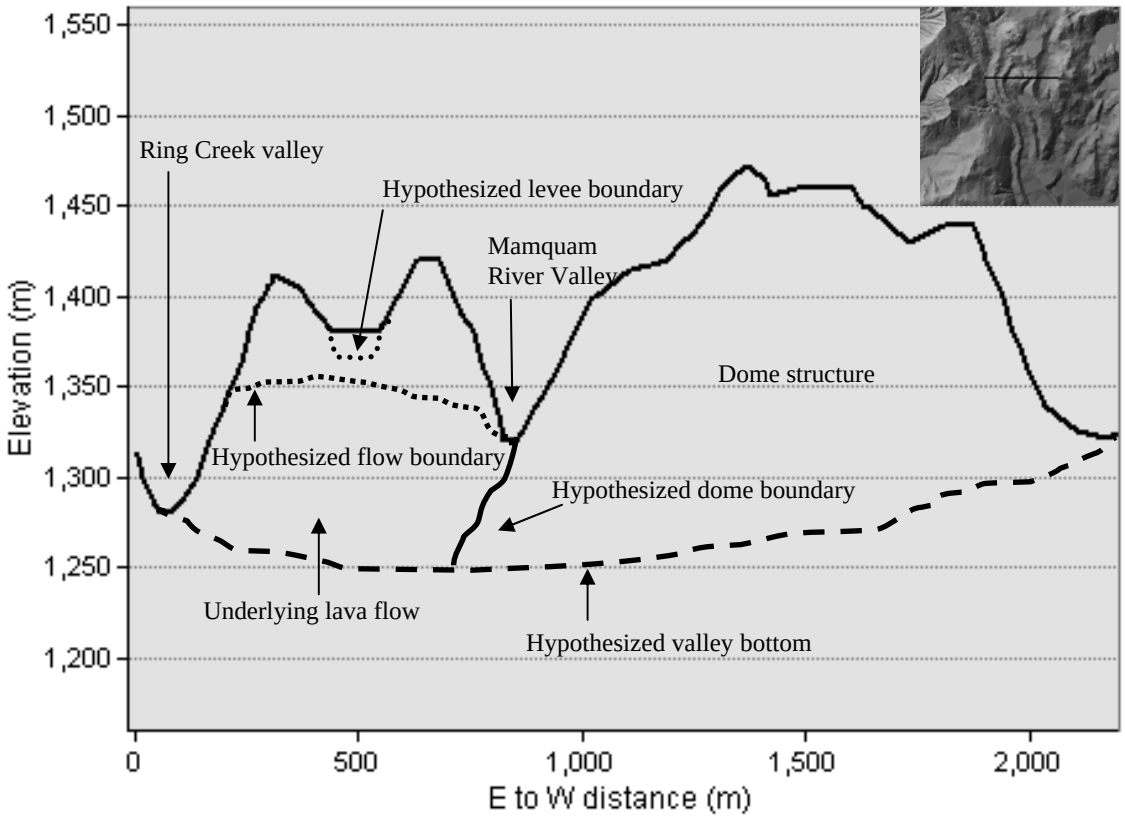

Figure 26) Cross sectional profile of the Ring Creek lava flow next to the dome structure. The hypothesized flow boundary line marks a previous event erupted from Opal Cone that was subsequently overlain by the modern Ring Creek lava flow. The line labeled hypothesized dome boundary represents the assumed original shape of the dome structure. The black line in the inset image shows the location of the cross section within the proximal zone. Approximately six times vertical exaggeration.

mineralogical data that suggest multiple eruptive events originated from the Ring Creek magma.

Transitional Zone

A cross section of the transitional channel of the Ring Creek lava flow marks the disappearance of the underlying flow unit seen in the proximal zone (Figure 27). In the transitional zone, the Ring Creek lava flow appears to be roughly 1 km wide. Projection of topography underneath the lava flow (original Mamquam River Valley bottom topography) resulted in a thickness estimate of roughly 120 m. The levees appear to be steep and well defined, with some asymmetry observed in the west levee (Figure 27). It is also apparent that the Ring Creek lava flow now fills the Mamquam River Valley.

The morphology of the Ring Creek lava flow in Figure 27 is typical of the transitional zone. Steep sided levees likely mark a break in slope in the down flow direction, which would accommodate the construction of larger, steeply sloped levees. Harris et al. (2004) directly observed this at the 2002 Santiaguito flow approximately 1.2 – 2.4 km away from the El Caliente vent (the source of the 2000, 2001, and 2002 Santiaguito lava flows). At this point in the 2002 Santiaguito block flow, the morphology consisted of a main narrow channel that was only partially filled and bounded by steep sided levees.

Medial-distal Zone

The medial-distal zone of the Ring Creek lava flow shows significant widening and thickening in cross section compared to the proximal and transitional sections of the lava

flow (Figure 28). The cross section also shows that the lava once again does not fill the Mamquam River Valley despite a wider flood plain into which the flow could have expanded. This is likely due to the substantial increase in width of the valley from 1.3 km in the transitional zone to 2.7 km in the medial-distal zone. There is also an apparent asymmetry in the levees. The west levee is approximately 500 m wide while the east levee is roughly 300 m wide. Two breakout features were located within the medial-distal zone. The first breakout is roughly 4km south of Opal Cone and the second is at approximately 7km south of Opal Cone (Figure 29). Overall thickness of the lava flow is estimated to be approximately 160 m (Figure 28).

The substantial thickening combined with widening with the medial-distal zone of the Ring Creek lava flow are indicative of a change in the rheology of the Ring Creek lava flow. Lava flows do not typically thicken as they disperse unless they have high yield strength and viscosity values or a slow advance rate (Kilburn and Lopes, 1991; Harris et al., 2004). High viscosity and yield strength would also lend themselves to the development of thick lava armor, which would serve to insulate the Newtonian core of the lava flow. This could explain how the Ring Creek lava flow was able to maintain temperatures hot enough to accommodate advance despite the formation of two significant breakouts (Figure 8). During the formation of these the Ring Creek lava flow may not have significantly lengthened. These breakouts could therefore represent flow widening during a period of ponding which can lead to cooling limitation of slow moving

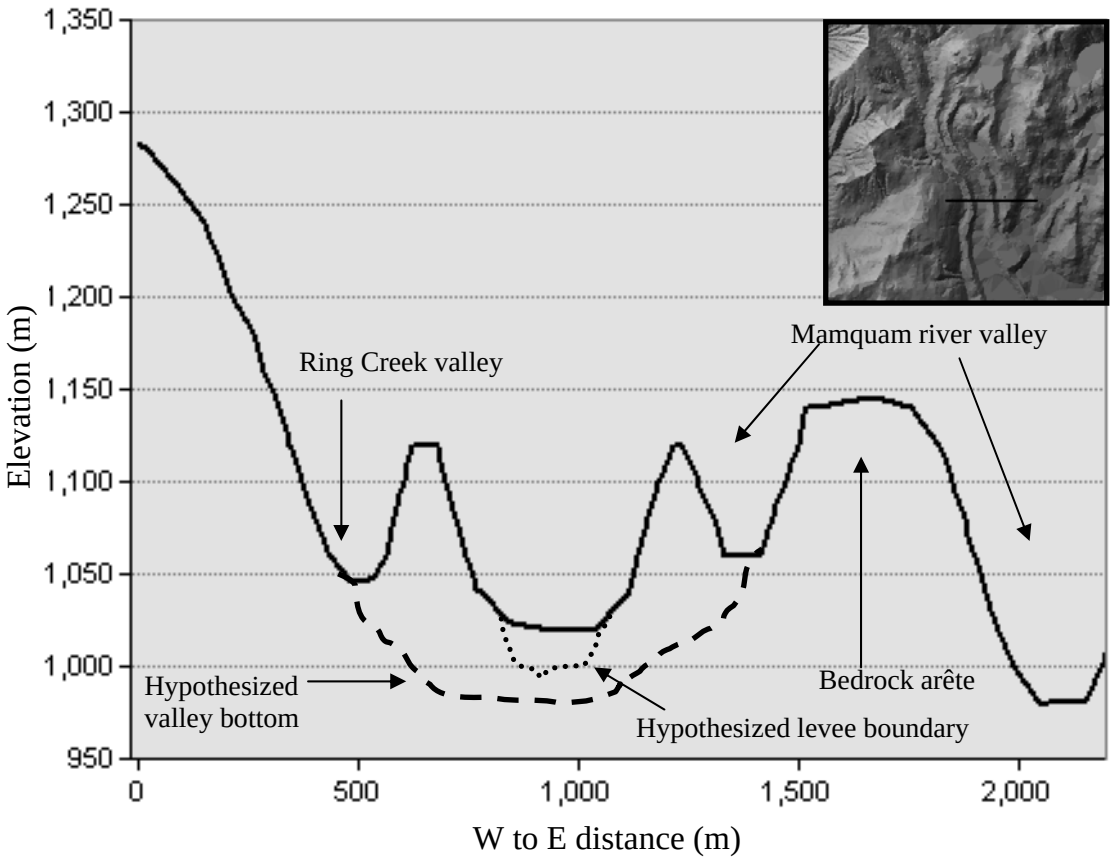

Figure 27) Cross sectional profile of the transitional zone of the Ring Creek lava flow. The black line in the inset image shows the location of the cross section within the proximal zone. Five times vertical exaggeration.

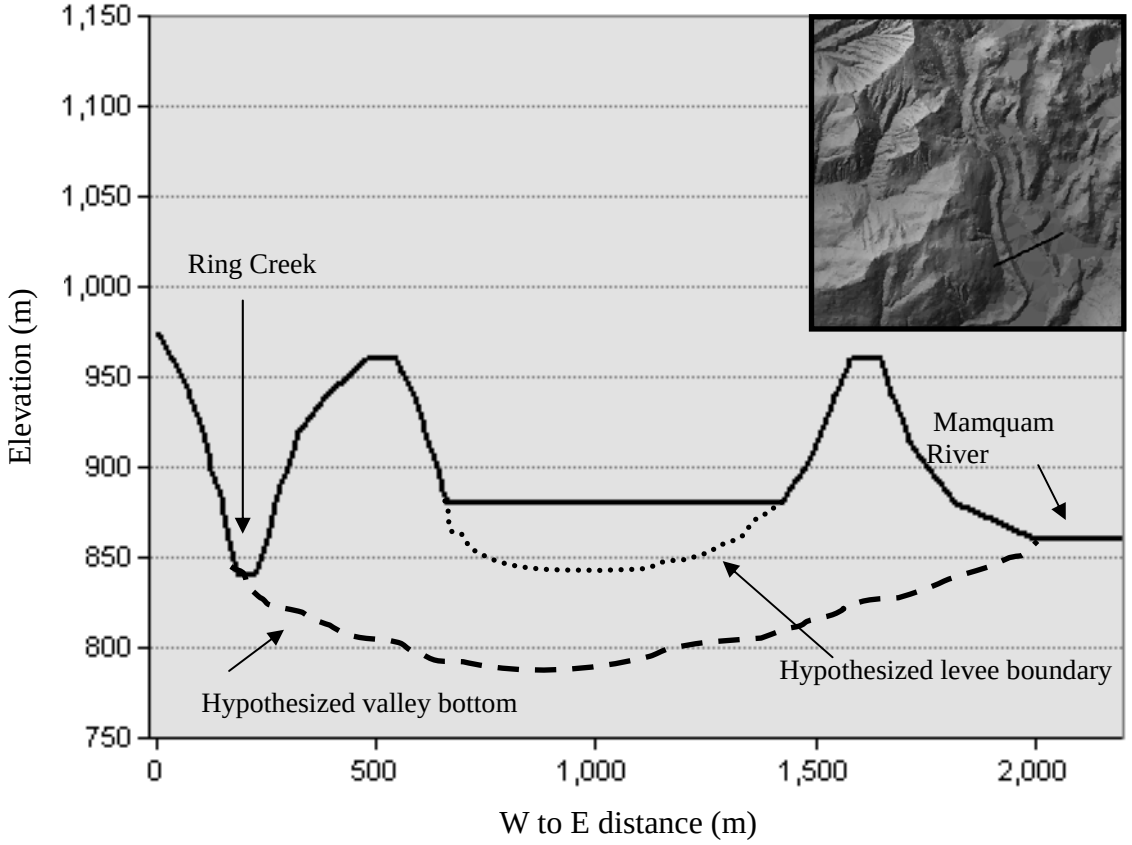

Figure 28) Cross sectional profile of the medial-distal zone of the Ring Creek lava flow. The black line in the inset image shows the location of the cross section within the proximal zone. Five times vertical exaggeration.

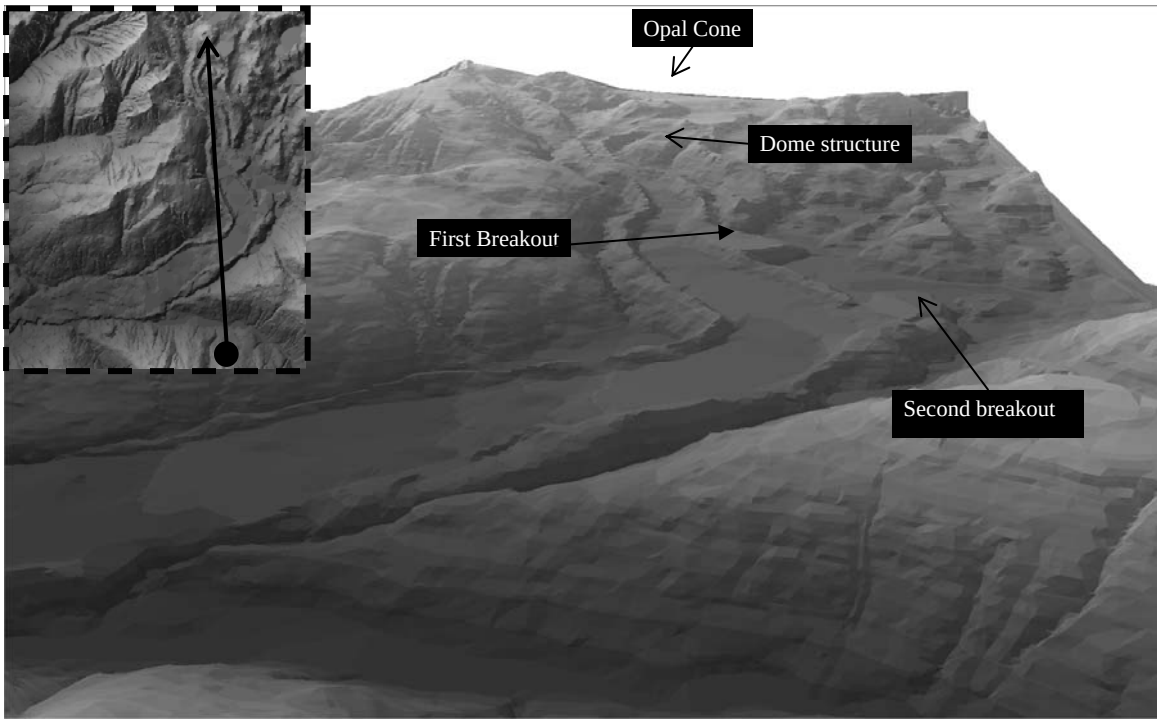

Figure 29) Oblique view of the medial-distal zone of the Ring Creek lava flow. Image taken from the vantage point of the dot within the inset facing in the direction of the arrow within the inset. Image captured using Arc GIS.

lavas. The fact that the Ring Creek lava flow was not limited by cooling despite these breakout features strongly suggests thick lava armor was present.

Frontal Zone

In contrast to the other flow zones, the Ring Creek lava flow fills the Mamquam River Valley throughout the frontal zone (Figure 30). Although field evidence and the cross section shows no defined levees, an oblique view of the frontal zone shows two broad raised levee-like structures (Figure 31). The borders of this channel are correlated to lineations observed in map view (Figure 9). Lineations such as those shown in Figures 31 and 32 are often indications of shear stress from levee building. Shear based lineations develop as the bulk of the flow begins to solidify and approximates Bingham rheology (Kilburn and Lopes, 1991). As the lava becomes more viscous, buildup of shear stress (along the base of the levees within the channel proper) results in material being rafted upward, forming ridges (Kilburn and Lopes, 1991; Harris et al., 2004). An example of this was observed by Harris et al. (2004) in the Santiaguito lava flow (Figure 32). Lineations observed in oblique images of the frontal zone of the Ring Creek lava flow are likely a product of this phenomenon.

Summary of Digital Analysis

Morphological values in Table 6 apply only to flow unit 3. Volume calculations of 2.4 km^3 do not include either flow units 1 or 2. Cross section analysis supports hypotheses of multiple events suggested by mineralogical, and field based data (Figure 33). Flow units 1, 2, and 3 are collectively referred to as the Ring Creek Complex. While

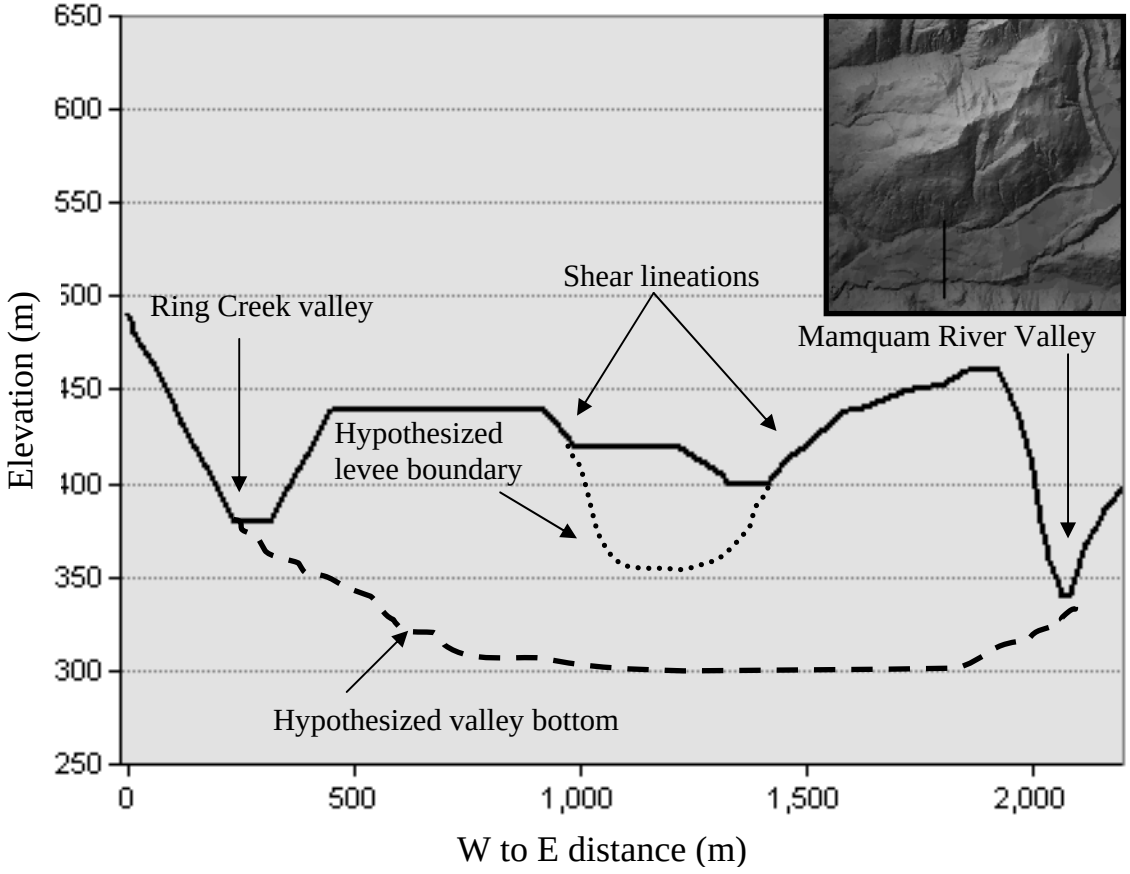

Figure 30) Cross sectional profile of the frontal zone of the lava flow. The shear lineations bound the sunken channel or channel proper of the lava flow. Inset image shows the location of the cross section within the frontal zone. Five times vertical exaggeration.

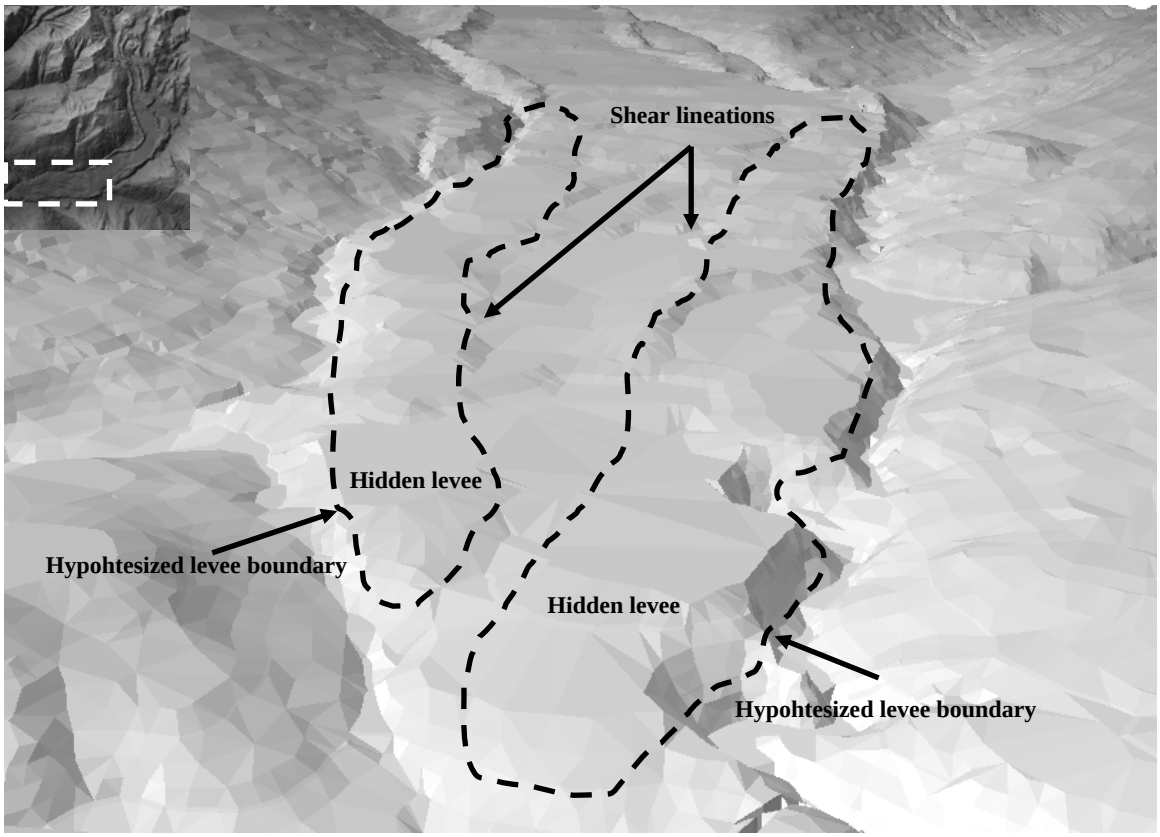

Figure 31) Oblique view (up flow) of the frontal zone of the Ring Creek lava flow. Dashed polygons represent the hypothesized location of the levees within the filled channel. The arrows labeled shear lineations indicate where sections of the flow have been forced upward during advance as can be seen in Figure 32. White box in inset gives an overview of the area examined by the oblique image.

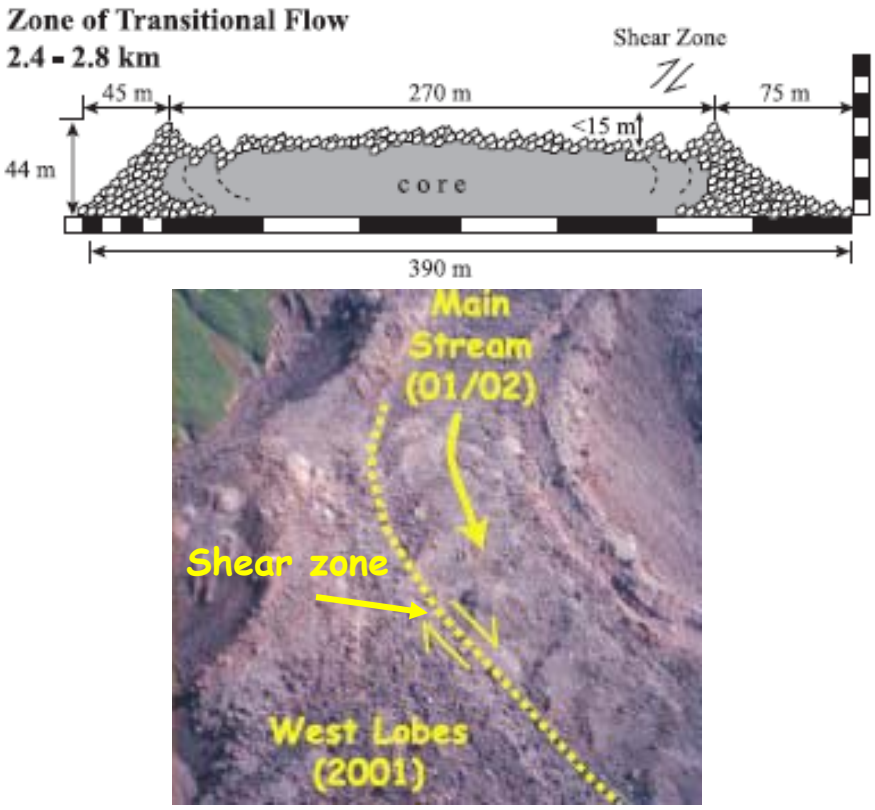

Figure 32) Shear zones observed in the transitional zone of the 2001 Santiaguito flow. The dotted line in the bottom image denotes the ridge that is formed in the above image (labeled shear zone) as a result of shearing within the channel proper. Figure modified from Harris et al., (2004).

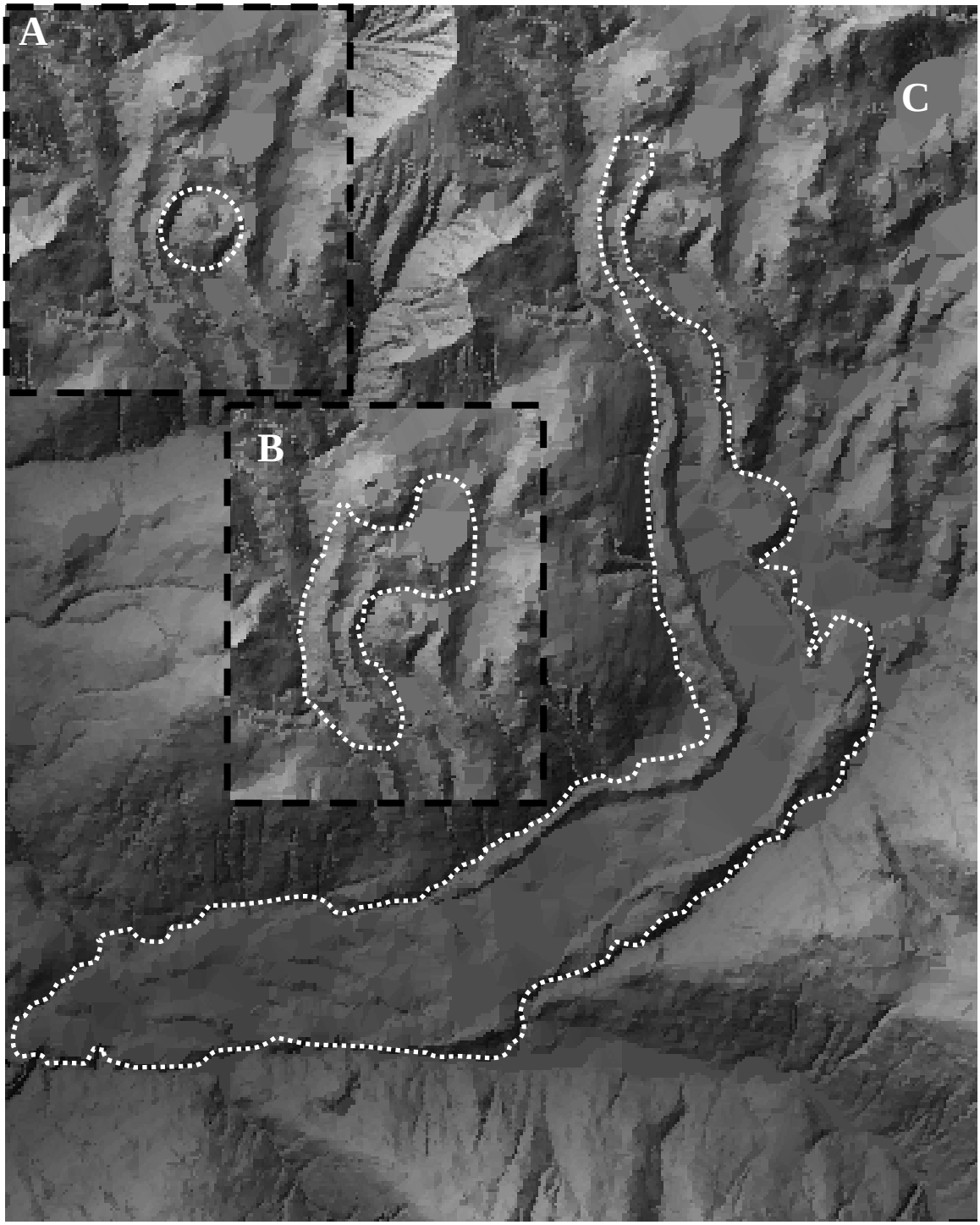

Figure 33) Progression of flow units 1, 2, and 3. (A) flow unit 1, the dome structure. (B) flow unit 2, the plateau and underlying lava flow within the proximal zone of the Ring Creek lava flow. (C) flow unit 3, the Ring Creek lava flow.

it is likely that the flow unit 1 (the dome structure) did not erupt from Opal Cone, the identical phase assemblage and similar bulk chemistry strongly suggests that the dome structure and Opal Cone are derived from the same parent magma. Contrary to flow unit 1, flow unit 2 (the underlying flow within the proximal zone, and potentially the plateau) likely originated from Opal Cone. Analysis of oblique and cross sectional profiles of the frontal zone strongly suggests the presence of hidden levees that have been obscured by inflation of the lava flow at the toe.

DETERMINATION OF INTENSIVE PARAMETERS

Temperature and Pressure

Expected error estimates for equations (1) – (3), as reported by Putirka (2005), are 28^{o} C, 2.2 kbar, and 1.4 wt% H_2O respectively. Simultaneous solving of Putirka's (2005) equations (1 & 2) produced the temperature range of 818 – 868^{o} C for the Ring Creek magma (Table 3). Higher temperatures were associated with cone samples while lower temperatures were estimated for frontal zone samples. Standard deviation of the data from equations (1 & 2) (48 ^{o}C) combined with the 28^{o} C reported by Putirka (2005) results in a mean temperature estimate of 843 ± 76 ^{o}C.

When compositional data from Rutherford's (1988) study of the Mt. St. Helens dacite was input into equations 1 – 3, equation (1) was found to consistently overestimate temperature (Figure 34). It appears that equation (1) yields significantly poorer results when applied to dacite as opposed to basaltic rocks examined by Putirka (2005). This is a common problem found in plagioclase based thermometers as temperature, pressure, and water content of the magma effect plagioclase growth (Putirka, 2005).

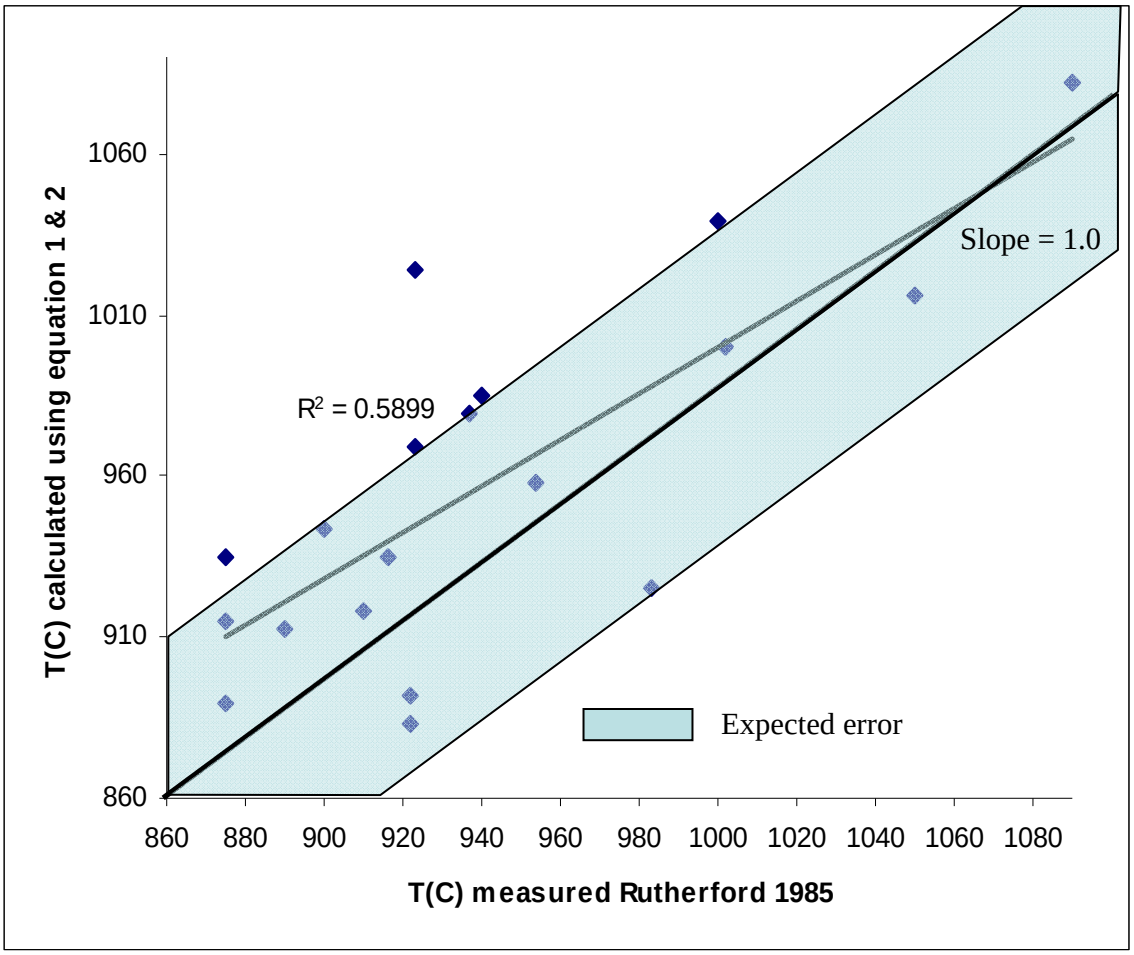

Figure 34) Correlation of temperature measured by Rutherford (1985) and calculated by this study (using equation 1 and 2) for Mt. St. Helens dacite. The shaded region represents positive and negative expected error of 48 ^{o}C.

Temperature estimates from (equation 1) were input into equation (2) to produce a pressure estimate of 3.1 kbar. Standard deviation of data from equations (2) and (1) was 0.6 kbar. Combined with the standard deviation, reported by Putirka (2005), of 2.3 kbar the error associated with the 3.1 kbar estimate is ± 2.9. Pressure values ranging from 2.3 – 4.9 kbar correspond to a depth of 7 – 14 km for the Ring Creek magma. During application of the Putirka (2005) plagioclase barometer (equations 1 and 2), pressure estimates were consistently negative. This was reported as a relatively common occurrence (Putirka 2005) and so the absolute values of pressure data were reported.

The pressure estimates obtained using Putirka's (2005) barometer, are significantly greater than expected. Because the amphibole grains within the Ring Creek lava flow exhibit severe disequilibrium a pressure estimate of 1 – 2 kbar was expected. Because analyses of mineral rims and melt locations near grain boundaries were analyzed, it is expected that near eruptive conditions should be reproduced. Testing of Putirka's (2005) barometer on Rutherford's (1985) Mt. St. Helens data set produced significant variation and the correlation coefficient (R^2) was 0.012 (Figure 35). This suggests that barometric estimates are subject to the same limitations as thermometric calculations. Depth estimates, from pressure values, are somewhat larger than expected due to the degraded nature of amphibole. Because amphibole is in disequilibrium, depth estimates of 3 – 6 km were expected as these values reflect pressures of 1 – 2 kbar, which is out of amphibole stability range.

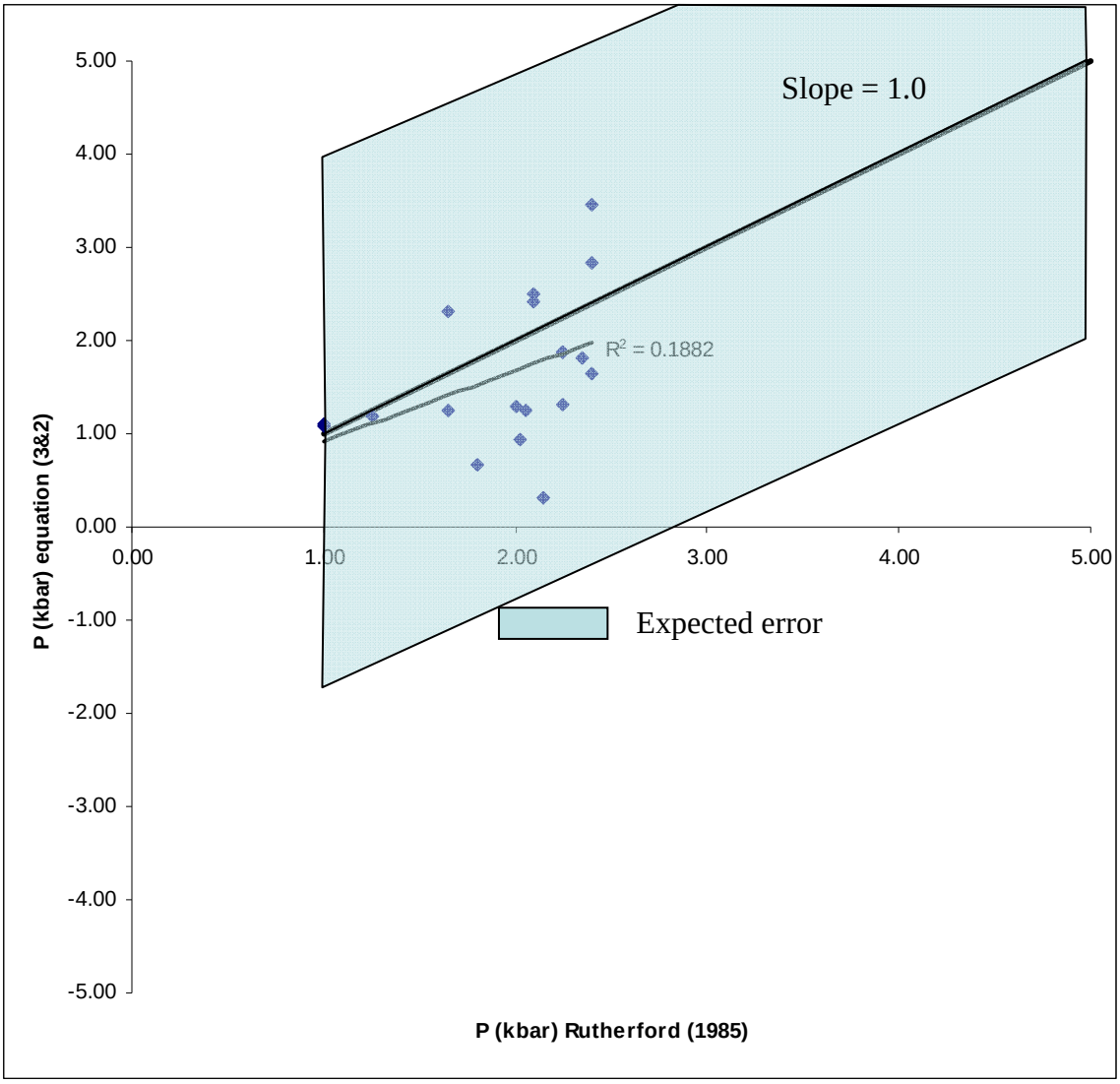

Figure 35) Correlation of pressure estimates (for the Mt. St. Helens dacite) obtained using equations (2) and (3), to pressure measured by Rutherford (1985). Shaded region represents positive and negative expected error of 2.3 kbar.

Water Content

Water content of the Ring Creek magma, estimated using equation 3, showed significant spread ranging from 0.2 wt% - 2 wt%, with a mean value of 0.6 wt%. Data exhibited standard deviation of 0.42 for equations (3&1). Combined with the reported standard deviation of 1.2 a total error of ± 1.6 is assumed.

Application of Putirka's (2005) hygrometer (equation 3) to Rutherford's (1985) data produced results with correlation problems similar to equation (1) (Figure 36). During the application of Putirka's equations 1 – 3 to Rutherford's (1985) data set, as well as the Ring Creek lava flow, a trend was observed with respect to the slope of an ideal data set (Figure 36). This is attributed to increased error associated with lower temperature and more hydrous material (Putirka, 2005). Water content estimates for the Ring Creek magma are 1 – 2 wt% lower than the Mount St. Helens estimates (Rutherford, 1985) resulting in the pattern seen in Figure 36. The discrepancy between the Ring Creek and Mount St. Helens water content estimates is attributed to the difference in Mg (weight percent as determined using microprobe analysis) in the liquid (0.86 for Mount St. Helens and 0.09 for the Ring Creek lava flow).

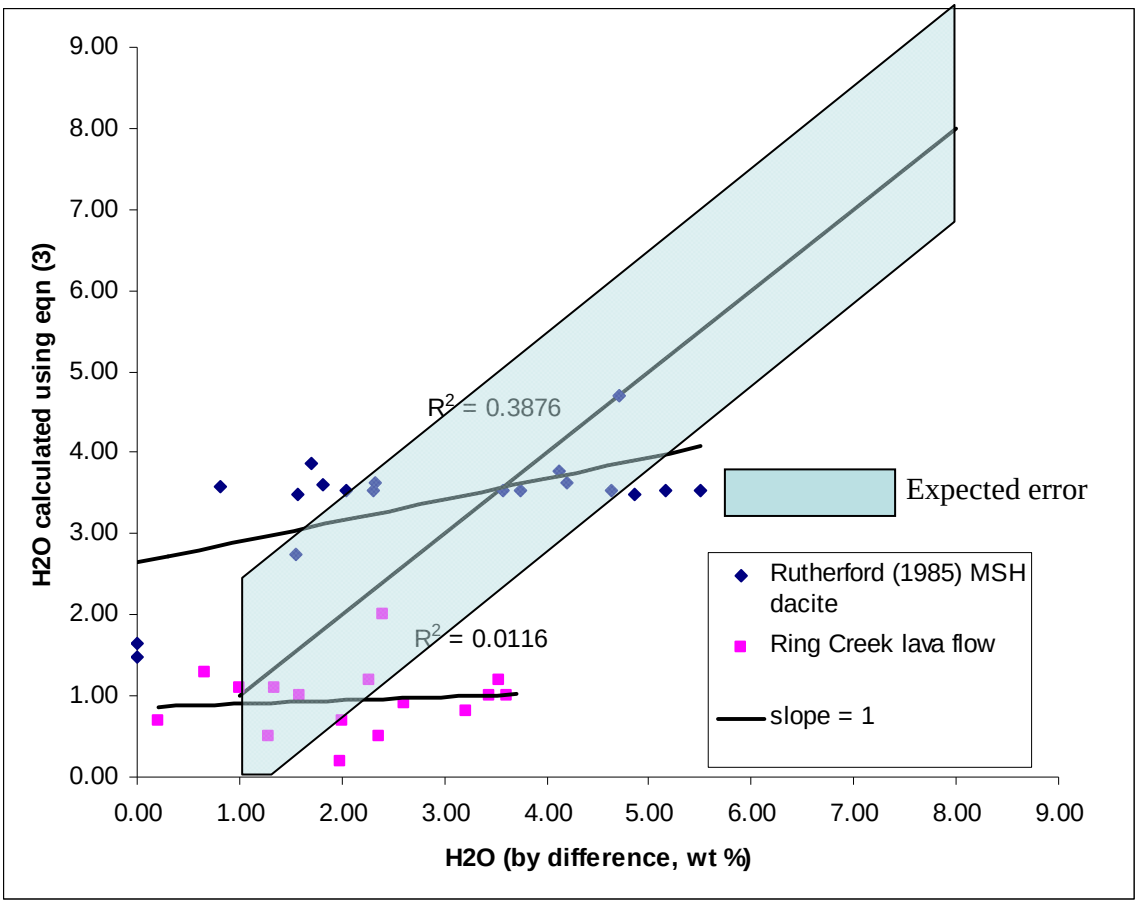

Figure 36) Correlation of water content estimates obtained using volatile by difference and simultaneous solution of equations (1) and (3) for Mt. St. Helens dacite. Chemical data used to estimate water content using volatile by difference was taken from Rutherford (1985). Shaded region represents positive and negative expected error of 1.6 wt%.

Viscosity

Viscosity estimates are sensitive to temperature and water content, and given the expected error of temperature estimates derived from the preceding models, the resultant viscosity estimates are limited in terms of reliability. Pre-eruptive viscosity estimates for the Ring Creek magma, using Putirka's (2005) igneous plagioclase thermometer (equations 1 and 2), ranged from $10^7 – 10^8$ Pas (Table 3). Standard deviation for viscosity data was 0.42 log units. Combined with the reported standard deviation of 0.16 log units (Whittington, 2009) the total error associated with viscosity estimates, for the Ring Creek magma, is ± 0.58 log units.

Viscosity estimates for the Ring Creek magma are slightly elevated compared to Mt. St. Helens, Chao, and the Santiaguito estimates (Rutherford and Devine, 1988; deSilva et al., 1994; Harris et al., 2004). The difference in viscosity suggests a dryer magma which is supported by estimates of water content. It is important to note that the viscosity estimates obtained using Whittington's (2009) viscosity model (equation 4) are mostly correlated with plagioclase rim compositions and therefore should represent near-eruptive conditions of the magma. This could also explain the higher viscosity calculated for the Ring Creek lava flow compared to other known dacites.

Summary of Intensive Parameters

Temperature and pressure data for the Ring Creek magma correspond to storage depths of 7-14 km. This depth is relatively similar to that of the Mt. St. Helens magma (8-10 km) determined by Rutherford and Hill (1993). At these conditions roughly 4.2 wt% water is required to maintain stability of amphibole (Rutherford, 1985). In the case of the

Ring Creek magma storage conditions are deeper and hotter yet the magma contains less wt% water. This suggests that the magma was too dry to maintain amphibole stability, a hypothesis that is supported by viscosity estimates and textural observations of amphibole in cone (12-4-1, 12-4-2, and 12-4-3) and EPCOR facility (15-1-1 and 15-1-3) samples.

CALCULATION OF FLOW PROPERTIES

One of the most difficult aspects of investigating pre-historic lava flows is the inability to directly measure thermal (e.g. flow surface temperature) and time dependent (e.g. extrusion rate, advance rate, and viscosity) parameters. Previous workers have devised several models that relate morphometric parameters (e.g. flow width and thickness, levee width, and slope of underlying topography) to determine time dependent variables in an attempt to overcome this problem (Moore et al., 1978; Kilburn and Lopes, 1991; deSilva et al., 1994; Harris et al., 2004; Parfitt and Wilson, 2008). In this section the methods developed by these previous workers are applied to the Ring Creek lava flow. Values discussed in the following sections apply only to the Ring Creek lava flow (flow unit 3 within the Ring Creek Complex). It is important to note that during the application of equations (5) – (12) to the Ring Creek lava flow, propagation of error was traced and the values reported in this section (Table 7 at the end of this section) represent mean values. Table 7 also contains the range in values for all parameters to show the result of propagating error.

Eruption Duration and Extrusion Rate

Equation (5), a thermodynamically based approach, calculated extrusion rate to be 23 m^3/s for the Ring Creek lava flow. This translates to eruption duration of $1.2x10^3$ days. To test the accuracy of equation (6), eruption duration was calculated for the Santiaguito block flow and compared to the value determined by Harris et al. (2004) using field based and satellite observation. The value produced from equation (6) of 633 days compares relatively well to the 473 day observation from Harris et al. (2004). Equation (6), which calculates eruption duration and subsequent extrusion rate, yields a mean value of eruption duration of $4.03x10^3$ days (11 years) for the Ring Creek flow. This eruption duration translates to an extrusion rate (given 2.4 km^3 volume) of roughly 7 m^3/s. Equation (7) produced a mean value for extrusion rate of 46.5 m^3/s which corresponds to an eruption duration estimate of 574 days (~19 months) for Opal Cone.

Models proposed by Harris et al. (2000), Harris et al. (2002), and Harris et al. (2004) concerning the Santiaguito block flow provide the first active analogue to the Ring Creek lava flow. As one of the most significant pitfalls of modeling previously emplaced lavas is the lack of thermal data, the Santiaguito block flow provides an excellent initial proxy for these values. Although both lavas are similar in composition and flow mechanics it is likely that these assumptions have increased error associated with the extrusion rate and subsequent eruption duration calculated for the Ring Creek lava flow. However, despite these limitations, the incorporation of thermal and time dependent variables allows equation (5) to more completely account for extrusion rate in real time, as opposed to using end morphology to back calculate extrusion rate. While this makes equation (5) a powerful tool, it is still limited in its application to the Ring

Creek lava flow (as well as any other pre-historic lava flow) where these parameters cannot be directly measured.

There are several limitations to equation (6) that Kilburn and Lopes (1991) and deSilva et al. (1994) suggest cause the overestimation of eruption duration. One of these limitations is the error associated with the flow thickness H. Both Kilburn and Lopes (1991) and deSilva et al. (1994) found that there was approximately 70% error associated with flow thickness measurements which was a significant contributor to the error in eruption duration estimates. In the case of the Ring Creek flow, digital imaging (using ArcGIS) of pre-eruptive topography has minimized the error (± 20 m) associated with lava flow depth estimates.

Another limitation of equation (6) is the slope parameter α. Equation (6) assumes that lava is erupted onto a continuous uniform slope which is not true for this study. In the case of the Mamquam River Valley four separate valley conditions (slope and width each unique to the four zones previously described) define the topography onto which the Ring Creek lava flow was erupted. This is significant as previous workers have determined that slope of underlying topography typically affects surface morphology (e.g. shallow slopes produce wide flows while steep slopes produce steep levees and narrow flows; Moore et al.,, 1978; Kilburn and Lopes, 1991). To account for this variation, eruption duration estimates were calculated using slope and dimensional (flow thickness and width) values pertaining to each of the four zones of the Ring Creek lava flow. These values were then summed to produce the best estimate of 4.03×10^3 day (roughly 11 years) as seen in Table 7.

Equation (7) employed by deSilva et al. (1994) to determine the extrusion rate and subsequent eruption duration of the Chao also has significant limitations. Extrusion rate values of approximately 20 m^3/s, applying equation (7) to the 2002 Santiaguito block flow, did not agree well with the 1.61 m^3/s estimated by Harris et al. (2004) study. The eruption duration of 38 days, estimated using the 20 m^3/s value, also compares poorly to the 473 day estimate made by Harris et al. (2002). This is likely due to assumptions of steady state eruption conditions required by equation (7) (deSilva et a., 1994). Similar to equation (6) the flow thickness (H) is a key parameter which is often associated with the most error. Flow thickness is typically a difficult parameter to estimate as flow bottoms are often obscured (either by other flows, bedrock, or debris). This problem was encountered by deSilva et al. (1994) while studying the Chao dacite, where error in thickness estimates resulted in eruption duration estimates (calculated from the extrusion rate obtained from equation 7) ranging from 20 – 250 years. In the case of the Ring Creek lava flow, with an uncertainty of ± 20 m for flow thickness, resultant eruption duration (from extrusion rate using equation 7) ranges from 1 – 19 years. The other limitation of equation (7) is the Grätz number. First, the Grätz number assumes continuous steady state eruption conditions, which ignores changes in vent size and changes in extrusion rate (deSilva et al., 1994). Previous workers have directly observed sharp changes in extrusion rate from of 2 to 26 m^3/s at Mt. St. Helens and from 0.48 to 1.61 m^3/s at El Caliente vent (the source of the Santiaguito block flow), both over two year periods (Swanson et al., 1987; Harris et al., 2004). In short, equation (6) and (7) are limited in that post emplacement values are used to assume pre emplacement conditions (extrusion rate, eruption duration, and local topography) which cannot be directly correlated due to

the dynamic nature of eruption mechanics (e.g. change in extrusion rate, conduit diameter, and topography).

Emplacement Duration and Flow Front Velocity

Emplacement duration differs from eruption duration in that eruption duration represents the time elapsed during the extrusion of a certain volume of lava, while emplacement duration represents the amount of time it takes to advance, cool and emplace. It is important to note that upon extrusion, lava is being emplaced. Therefore the full eruption duration is part of emplacement duration. By assuming the Grätz number to be 320 and inputting average channel dimensions for the Ring Creek lava flow, the parameter t (time in seconds) in equation (11) was solved for and an emplacement duration estimate of $1.9x10^{3}$ days (~5 years) was obtained (Table 7). Testing of equation (11) on the Santiaguito block flow yielded a value of approximately 289 days, which was within the 161 – 328 days range calculated by Harris et al. (2003) using satellite imagery to examine changes in flow front shape and temperature. From emplacement duration, a constant flow front velocity of $1.0x10^{-4}$ m/s was estimated (Table 7). This velocity is comparable to observed velocity (using satellite imagery) for the Santiaguito block flow ($2.31x10^{-5}$ – $1.50x10^{-4}$ m/s) made by Harris et al. (2004). Flow front velocity obtained from emplacement duration (equation 11), as an input parameter for equation (12), produced a post-eruptive viscosity estimate of $7.4x10^{10}$ Pas. This estimate is approximately two orders of magnitude higher than magmatic viscosity estimates from equation (4). Post-eruptive viscosity of the Ring Creek lava flow is roughly one order of magnitude higher than bulk viscosity of the Santiaguito lava (Harris et al., 2004) and

much less viscous than estimates for the Chao (10^{15} – 10^{24} Pas; deSilva et al., 1994; Table 8).

Although Kilburn and Guest (1993) found that calculating emplacement duration via conductive cooling typically overestimates actual values, equation (11) better defines the Grätz number which compensates for these limitations. By combining the Grätz number and channel dimensions (defined by the parameter d_e), a relationship is developed that estimates the time it takes for an open channel flow to stop advancing based on the time needed for conductive cooling to penetrate the surface and basal zones of the flow. The good agreement between equation (11) and values from Harris et al. (2004) suggests that the limitations of the Grätz number observed by deSilva et al. (1994; equation 7) do not impact values calculated using the Grätz number to estimate emplacement duration (equation 11).

The primary limitation of calculating flow velocity (and subsequent emplacement duration) using equation (11) is the assumption of constant conditions. For example changes in extrusion rate may result in fluctuations of flow velocity. By estimating flow velocity from emplacement duration only, changes in topography (which may slow or speed the advance of the flow front) is not accounted for. In the case of the Ring Creek lava flow changes in the dimensions of the Mamquam River Valley likely affected the speed at which the flow front advanced, and so the flow front velocity likely underestimates the true value. The limitation of this assumption is further propagated in equation (12), potentially resulting in an inflated post-eruptive viscosity estimate.

Yield Strength

Testing of equation (8) on the 2002 Santiaguito block flow produced yield strength estimates of $1.26x10^5$ Pa which compare favorably to the $1.3 x10^5$ Pa estimated by Harris et al. (2004) using equation (8). Testing of equation (9) on the 2002 Santiaguito block flow yielded an estimate of $3.2 x 10^5$ Pa which agreed somewhat with the value of $1.3 x 10^5$ Pa proposed by Harris et al. (2004). Yield strength estimates for the Ring Creek lava flow, from both equation (8) and (9), range from $4.8x10^4$ Pa – $2.2x10^5$ Pa. Yield strength estimates for the Ring Creek lava flow, using equations (8) and (9) range from $4.8x10^4 – 2.2x10^5$ Pa (Table 7). The lower bound was calculated following the methods of Moore et al. (1978) in equation (8) and the upper bound was calculated using equation (9) developed by Moore et al. (1970) and presented by Parfitt and Wilson (2008). Yield strength estimates for Ring Creek lava flow compare well those presented by Harris et al. (2004) for the Santiaguito block flow ($7x10^4 – 3.7x10^5$ Pa) but are significantly lower than the yield strength estimated by deSilva et al. (1994) for the Chao ($8x10^5$ Pa). The discrepancy between values for the Ring Creek and Chao dacites is expected due to the difference in silica content (62 – 64 wt% for the Ring Creek and 68 wt% for the Chao), and the difference in flow thickness (110 m for the Ring Creek and 500 m for the Chao). The similarity of the estimates for the Ring Creek lava flow to the Santiaguito block flow indicates that equation (8) is appropriate for the Ring Creek lava flow, and that the morphological input data used for the calculation is trustworthy.

While the range of yield strength values produced from equations (8) and (9) is acceptable both models present important limitations with respect to the Ring Creek lava flow. During application of equations (8) and (9) to the Ring Creek lava flow, change in

the topographic slope parameter did not appear to significantly impact yield strength calculations. Changes in parameters such as levee width and flow thickness, however, resulted in yield strength estimates ranging from 10^2 Pa – 10^6 Pa. It is therefore apparent that the primary limitation of equation (8) and equation (9) is the assumption of continuous dimensions. To correct for this mean values of slope, depth, and levee width were used to produce bulk yield strength. This approach was also done by deSilva et al. (1994) and Harris et al. (2004) for the Chao and Santiaguito lavas respectively.

Core cooling and cooling limitation

Core cooling for the Ring Creek lava flow ranges from $9.1x10^{-4\,o}$ C/m – $1.5x10^{-2\,o}$ C/m (Table 7). These values are approximately one order of magnitude lower than those calculated for the Santiaguito block flow ($5.7x10^{-2o}$ C/m – 0.1^{o} C/m; Harris et al., 2002). The difference in values, between the Ring Creek and Santiaguito lavas, is likely due to the difference in flow thickness (110 m for the Ring Creek lava flow and roughly 30 m for the Santiaguito lava; Table 8) as all other parameters are taken from Harris et al. (2002), Harris et al. (2003), and Harris et al. (2004). By assuming the ΔT is approximately 200^{o} C (following Harris et al., (2002) for the Santiaguito based on similar chemistry, morphology, and phase assemblage), cooling limited duration of the Ring Creek lava flow ranged from $1.0x10^3$ days – $1.7x10^4$ days.

Equation (10) is trusted as cooling limited length is known and the liquidus solidus difference is safely assumed to be 175 – 200^{o} C. This leaves only one core cooling to solve for. The cooling limited duration (flow emplacement) obtained from equation (10) translates to a flow velocity of approximately 8 m/day ($9.3x10^{-5}$ m/s), which is

within range of the $2.7x10^{-5} – 4.3x10^{-4}$ m/s produced using equation (11) from Harris et al. (2004). This further supports the validity of core cooling estimated, for the Ring Creek lava flow, from equation (10).

Summary of Flow Properties

The most obvious limitation of equations used during calculation of flow properties is the assumption of continuous or constant conditions. In the case of the Ring Creek lava flow morphology and topography vary significantly and the lack of sensitivity to these changes has likely increased error associated with some properties (e.g. extrusion rate, yield strength, and emplacement duration). Despite similarities between the Ring Creek and Santiaguito lavas, it is likely that assumed values from Harris et al. (2002), Harris et al. (2003), and Harris et al. (2004) resulted in increased error in extrusion rate, core cooling, and subsequent emplacement duration. Because of these limitations, the data obtained in this section represent a bracket of reasonable minimums and maximums that reflect a thick, slow moving, well insulated lava.

Thermo-Rheological and time dependent parameters

Parameter	Value	Source
Eruption Duration (day)	$4.0x10^3$ ±844	Kilburn & Lopez (1991) eqn (6)
	$1.2x10^3$ ± 225	Harris et al. (2004) eqn (5)
	574 (396 – $1.0x10^3$)	deSilva et al (1994) eqn (7)
Extrusion rate (m^3/s)	7.2 ± 1.5 m^3/s	Kilburn & Lopez (1991) eqn (6)
	23 ± 4.0 m^3/s	Harris et al. (2004) eqn (5)
	46.5 ± 22 m^3/s	deSilva et al (1994) eqn (7)
Yield strength (Pa)	$4.8x10^4$ ($1.6x10^3$ – $3.6x10^5$)	Moore et al. (1978) eqn (8)
	$2.2x10^5$ ($5.6x10^4$ – $5.2x10^5$)	Parfitt & Wilson (2009) eqn (9)
Core cooling ($^oC/m$)	$9.7x10^{-3}$ ($9.4x10^{-3}$ – $1.0x10^{-2}$)	Harris et al. (2002, 2004) eqn (10)
Flow velocity (m/s)	$1.0x10^{-4}$ ($2.7x10^{-5}$ – $4.3x10^{-4}$)	Parfitt & Wilson (2008) eqn (11)
Post-eruptive viscosity (Pas)	$7.4x10^{10}$ ($3.3x10^{10}$ – $1.5x10^{11}$)	Harris et al (2004) eqn (12)
Core cooling rate ($^oC/hr$)	$3.5x10^{-3}$ ($9.1x10^{-4}$ – $1.5x10^{-2}$)	$(\delta T/\delta x)$ x (V) from eqn (10)
Q_{conv} (W/m^2)	10.5	Harris et al. (2004) Appendix
Q_{rad} (W/m^2)	609	Harris et al. (2004) Appendix
Q_{base} (W/m^2)	32.7	Harris et al. (2004) Appendix
Q_{cond} (W/m^2)	620	Harris et al. (2004) Appendix
Q_{tot} (W/m^2)	665	Harris et al. (2004) Appendix
Emplacement duration (day)	$1.9x10^3$ (478 – $7.6x10^3$)	Parfitt & Wilson (2009) eqn (11)
Cooling duration (day)	$4.4x10^3$ ($1.0x10^3$ - $1.7x10^4$)	Harris et al. (2002, 2004)

Table 7) Time dependent and thermo-rheological parameters for the Ring Creek lava flow. Values reported outside parentheses reflect mean values while parenthetical values reflect the minimum to maximum range. Values for heat loss parameters do not exhibit significant variation. Eqn (#) refers to equation as listed in the text. All values apply only to the Ring Creek lava flow (flow unit 3).

ERUPTION HISTORY OF THE RING CREEK LAVA FLOW

Evolution of the Ring Creek Magma

Size and number of amphibole phenocrysts (Table 5) suggests deep crystallization of hydrous magma for a significant period of time. Slightly reacted amphibole textures indicate shallow storage conditions for the Ring Creek magma prior to eruption. Rutherford and Hill's (1993) study of Mt. St. Helens dacite, suggests an amphibole reaction rim of 14 – 60 μm would develop after approximately 8 - 25 days. Amphibole grains within the Ring Creek magma, which are 1 – 2 cm diameter, would completely react over 220 – 440 days. However, because amphibole grains within sample 13-6 do not show reaction (Figure 22 B), it is likely that the Ring Creek magma did not experience shallow (below the minimum stability field of amphibole, roughly 2.5 kbar; Figure 37) stagnation prior to the first flow unit (dome structure). Because amphibole in sample 14-4-1 (Figure 22 C) show rims of thickness similar to Mount St. Helens amphibole (14 – 60 μm), the Ring Creek magma potentially stagnated for only 8 – 25 days before producing the second flow unit (the plateau and underlying flow). Amphibole texture in sample 15-1-3 (Figure 22 D) suggests substantial stagnation (approximately 440 days) occurred after flow unit (2) and prior to flow unit (3) (the Ring Creek lava flow). While the estimate of stagnation between flow units (2) and (3) is substantiated by the discrepancy in weathering and hand sample texture (as well as amphibole texture), the period of stagnation between flow units (1) (the dome structure) and (2) is difficult to support. This is due to identical weathering in flow units (1) and (2), after the emplacement of flow unit (3), and because the underlying flow is only exposed at the eastern levee, which exhibits similar weathering to flow unit (1).

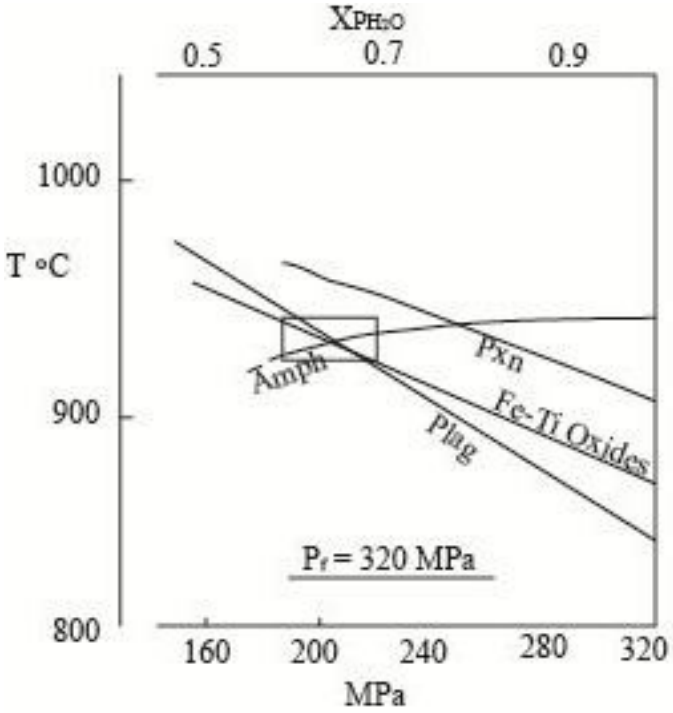

Figure 37) Amphibole + plagioclase stability conditions for the Mt. St. Helens dacite. The lower region of the box represents stability conditions for the observed phase assemblage; amph + plag + pxn + Fe-Ti oxides. In this diagram fluid pressure (P_f) is equal to total pressure. The values along the top axis reflect the ratio of P_{H2O} to P_{fluid}. Figure modified from Rutherford (1985).

Paucity of significant compositional variation within plagioclase grains suggests the textures observed (ragged zones, sieve textures, and subhedral - euhedral rims; Figure 38A, 38B, 38C) record changes equilibrium conditions of the Ring Creek magma. These changes likely occurred during the transition from deep to shallow storage and stagnation (Figure 39). Sieve and ragged textures within the interior and core sections of plagioclase grains of the Ring Creek lava flow suggest deep crystallization of a hydrous (4 – 6 wt% H_2O; Whittington, 2009) magma, as water is known to suppress plagioclase growth (Putirka, 2005). During this time, amphibole would be crystallizing and plagioclase would be suppressed by amphibole crystallization and remaining water content of the magma (Figure 38 C). Conversely subhedral –euhedral rims of plagioclase grains (Figure 38D) are indicative of a shift in equilibrium conditions from amphibole to plagioclase. This could be the result of a decrease in water content, possibly from degassing during ascent and stagnation. The drop in partial pressure of water would favor plagioclase growth, at least in part associated with amphibole breakdown from such a change (Rutherford and Devine, 2003).

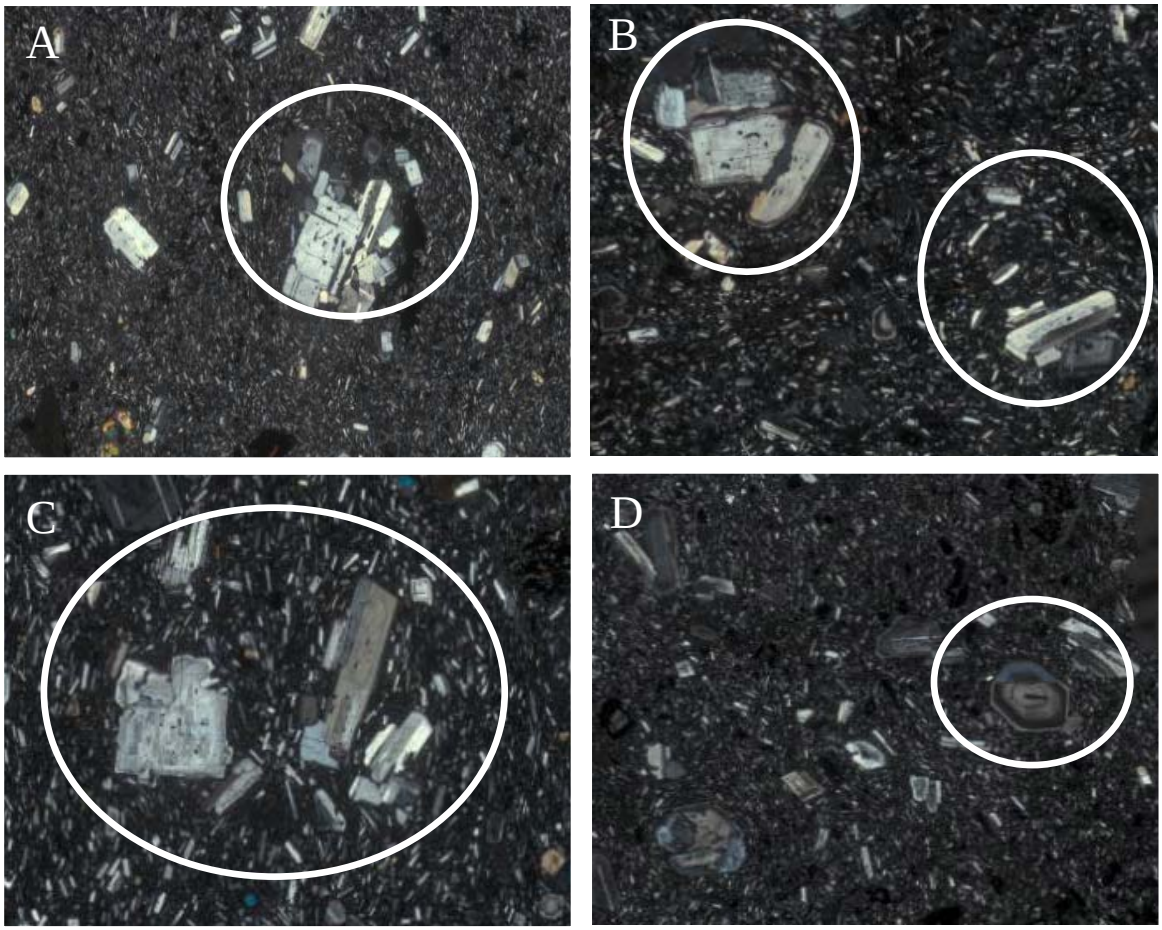

Figure 38) Zonation of plagioclase grains throughout the Ring Creek lava flow. (A) Sample 12-4-1 from Opal Cone. (B) Sample 13-2-1 from the plateau of material near Opal Cone. (C) Sample 11-4-1 from the west levee. (D) Sample 15-1-3 from the EPCOR dam facility.

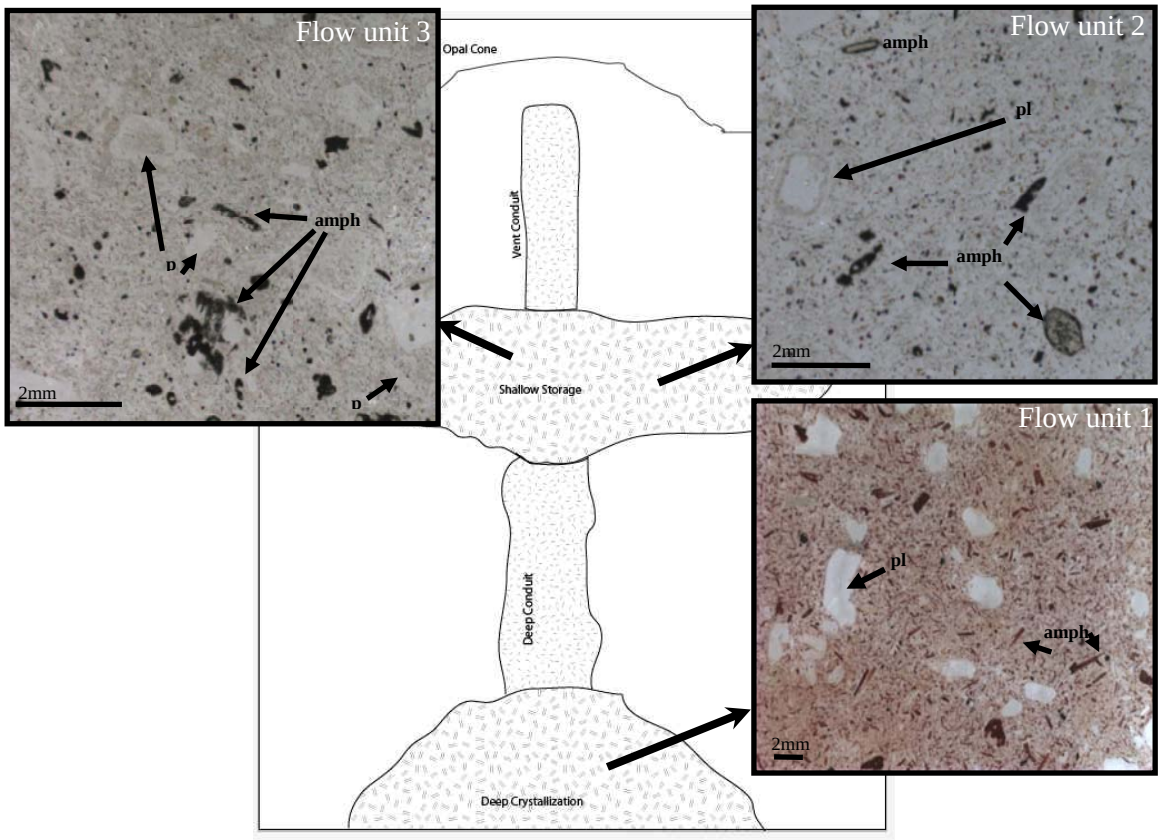

Figure 39) Hypothesized evolution of the Ring Creek magma. The original deep crystallization event, representing initial crystallization, is in the bottom portion of the figure followed by a series of feeder dikes and shallow ponding. Drawing not to scale. The total depth of the sketch is 15 km to the base of Opal Cone. Shallow storage conditions are thought to be roughly 3.3 kbars and approximately 836^{o} C.

Eruption Mechanism of Opal Cone

During chemical and mineralogical investigations no evidence for injection of new material (of a different composition) was found. Therefore, the eruption mechanism for Opal Cone would need to either reduce confining pressure (via tectonic or structural processes such as faulting or major landslide) or increase pressure within the magma chamber. The lack of a large scale explosive phase indicates classic vapor phase over-pressurization did not occur within the magma chamber. Without evidence for magma mixing or structural or tectonic events, reduction in confining pressure is a likely cause for the magma to erupt. Therefore to induce or accommodate an eruption, relief of said pressure is required.

A likely candidate for the reduction of confining pressure is removal of cryostatic pressure caused by wholesale removal of glacial ice. As discovered by Mathews (1958b) and Green et al. (1988) extensive glaciation has occurred throughout the Mt. Garibaldi area to include the Mamquam River Valley. Glacial ice was present in the Mamquam River Valley until 11.8 ka (Figure 3). In accordance with radio carbon dates (10.6 ka – 9.3 ka; Brooks and Friele, 1992) that bracket the age of the Ring Creek lava flow, deglaciation had already occurred in full by (and just prior to) the time the lava flow erupted (Figures 2, 3). Figure 2 shows deglaciation of Opal Cone and the Mamquam River Valley occurred over approximately 900 years (from 12.7 ka – 11.8 ka). This rapid deglaciation corresponds to the removal of roughly 500 m of ice and a relief of 4.5 MPa (0.045 kbar; Clague Personal Comm., 2010). The decrease of cryostatic pressure would facilitate devolatilization of the Ring Creek magma during stagnation, and potentially depressurize the magma chamber enough to erupt (Figure 40).

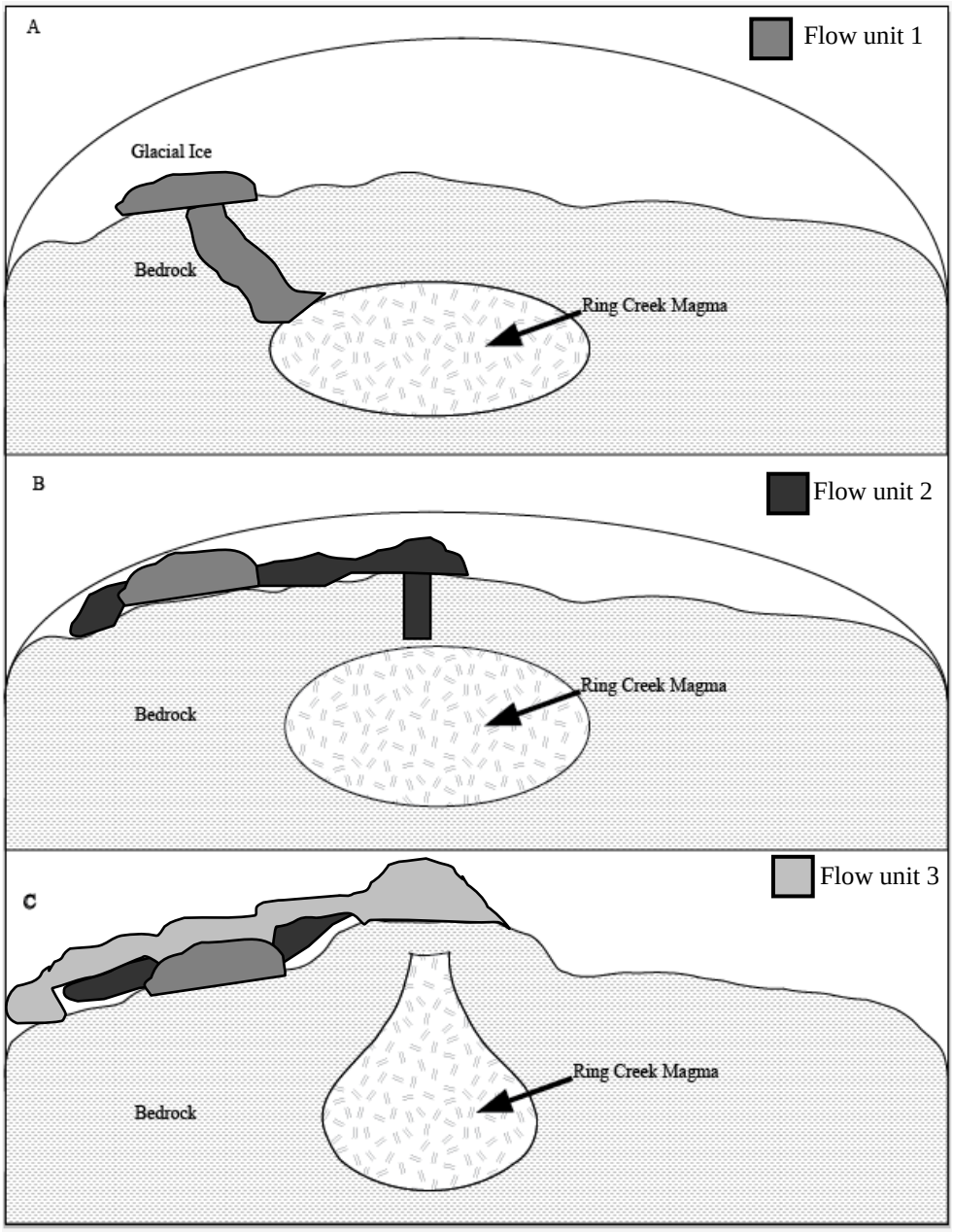

Figure 40) Rapid deglaciation and subsequent ascent of the Ring Creek magma. (A) Magma is stagnated beneath 500 m of ice and flow unit 1 erupts through a shallow conduit. (B) As glacial ice retreats cryostatic pressure begins to relax and flow unit 2 erupts as magma is drawn upwards. (C) Finally, when the ice is gone flow unit 3 (the Ring Creek lava flow erupts. Drawing not to scale.

In the case of Opal Cone, deglaciation could explain the first two phases of the eruption (the formation of the dome, plateau, and underlying lava flow) as well as the subglacial nature of some of these features (e.g. the dome). As glacial ice receded from the Mamquam River Valley it is likely that cryostatic pressure was gradually and periodically overcome, resulting in both sub and post glacial events. This would account for the textural gradation (yet compositional homogeneity) observed in samples from flow units 1, 2, and 3 (samples 13-6, 14-4-1, and 15-1-3 respectively), as well as the sub=glacial textures observed in the dome and the increased weathering observed in rocks of these early flow units.

Emplacement of the Ring Creek lava flow

Extrusion rates ranging from 7.2 – 46.5 m^3/s indicate that Opal Cone was active for 1.5 – 10 years. Compared to the estimates for the Santiaguito (1 year) and the Chao (120 years) lavas, the values for the Ring Creek lava flow mark a middle member. It is expected that extrusion rate and eruption duration estimates for the Ring Creek lava flow fall between the Santiaguito and Chao lavas as the volume of the Ring Creek lava flow is also between the Santiaguito and Chao lavas. Due to the nature of the Grätz number, and its use in equation (7), it is likely that extrusion rate estimates of 46.5 m^3/s ±22 m^3/s represent peak values or values during initial stages of eruption. deSilva et al. (1994) state that initial extrusion rate, for intermediate – silicic lavas, is typically high and drastically increases for a short time, before sharply falling to a lower rate. Once extrusion rate slows, it typically maintains at that rate until equilibrium within the magma chamber and conduit is achieved, and eruption halts. The decrease of extrusion rate of the 2000 and

2002 Santiaguito events from El Caliente dome was observed by Harris et al. (2002) and Harris et al. (2004).

Rheology of the Ring Creek lava flow is similar to the Santiaguito flow which was decidedly well insulated by thick lava armor (Harris et al., 2002; Harris et al., 2003; Harris et al., 2004). This has been referred to as "thermal stealth" by Harris et al. (2002) due to the near invisibility of the lava flow using thermal satellite imagery during advance (Figure 41). Values for core cooling of the Ring Creek lava flow ($9.4x10^{-3}$ – $1.0x10^{-2}$ ^{o}C/m), support thick lava armor which would result in thermal stealth. Therefore it is likely that the anomalous length of the Ring Creek lava flow was obtained due to significant insulation, which allowed the lava flow to maintain temperatures hot enough to accommodate advance.

Results from emplacement and cooling duration calculations support previous hypotheses, proposed by this study, that thickness of the lava armor has affected the growth of the Ring Creek lava flow. Assuming eruptive temperature for the Ring Creek lava flow was approximately 836^{o} C (Table 3), cooling and emplacement duration suggest that 5 – 12 years was the time necessary for the lava core to reach a temperature (~500^{o} C; Harris et al., 2002) cool enough to halt advancement. Emplacement duration estimates of $1.9x10^{3}$ days (5 years, based on morphometric parameters) and $4.4x10^{3}$ days (12 years, based on core cooling rate), potentially overestimate the true emplacement duration of the Ring Creek lava flow. Continuous advance, of the Ring Creek lava flow, for up to 12 years is anomalous even for well insulated viscous lava. This is evidenced by the Santiaguito lava flow which was associated with emplacement duration estimates ranging from 161 – 328 days, despite thick lava armor.

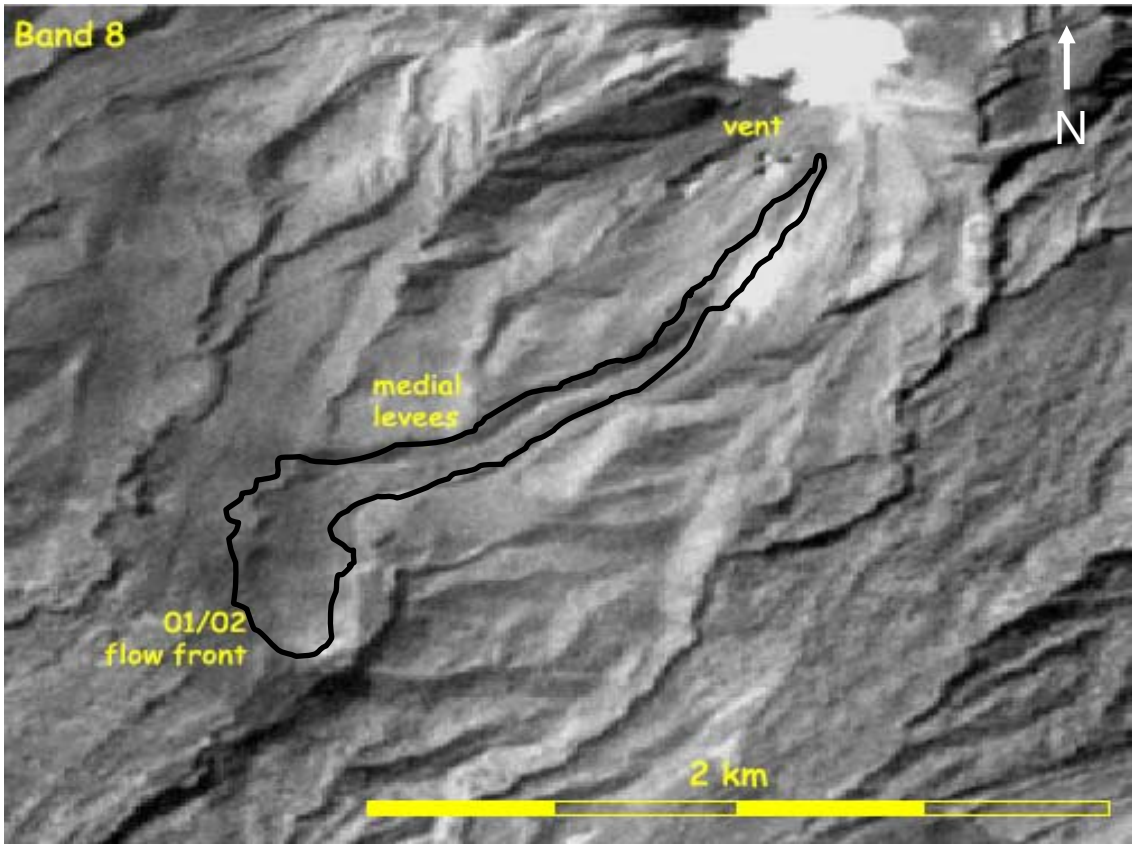

Figure 41) Satellite thermal imagery from the Santiaguito block flow in Guatemala. Shades in DEM are correlated to heat produced via radiation at the surface of the lava flow. Note the lightest shades are seen at the vent and within the proximal zone where a rock fall has exposed the inner lava. Image taken from Harris and others (2004).

CONCLUSIONS

The eruptive history of the Ring Creek lava flow is more complex than previously thought. The Ring Creek lava flow is in fact only one of three extrusions of a complex, classified by this study as the Ring Creek Complex. Lack of ice-contact features of the Ring Creek lava flow and the sub-glacial features of flow units 1 and 2 indicate that deglaciation may be the mechanism that triggered the eruption of Opal Cone, to produce the Ring Creek lava flow. Deglaciation as the eruption mechanism is also supported by chemical homogeneity of the Ring Creek lava flow, and lack of chemical variation between flow units 1, 2, and 3. Although the Ring Creek lava flow is anomalously long, flow evolution is typical of other dacites such as the Chao and Santiaguito. Thermal insulation allowed the lava flow to advance as far as it did despite its high viscosity, low water content, low velocity, and breakout features within the medial distal zone.

While a semi-quantitative history for Opal Cone and the Ring Creek lava flow can be determined, quantitative results are best described as ranges due to propagation of error. To adequately determine a quantitative history for the Ring Creek lava flow, several intrinsic thermo-rheological parameters are required that simply can not be measured post-emplacement. Due to the prehistoric nature of the Ring Creek lava flow, and the lack of necessary phases (e.g. Fe-Ti oxide pairs), a loosely defined data set is all that is currently attainable.

Future work on the Ring Creek lava flow would be most valuable if focused on experimental petrology. Similar to the experiments of Rutherford and Hill (1993), samples of Ring Creek material could be melted and exposed to various pressure and temperature environments to determine the necessary time for complete amphibole

decay. This experimentation would also reveal how the Ring Creek magma rose from deep to shallow crystallization zones (e.g. isothermal decompression or adiabatic decompression). Experimental petrology would also provide more accurate pre-eruptive water content estimates. Physical experiments involving a parallel plate viscometer, following the methods of Whittington (2009), would provide more accurate viscosity estimates. Better defined viscosity could be used in equation (12) to produce a more accurate flow velocity and subsequent emplacement duration. Data obtained through empirical experimentation would also provide a valuable cross check for values proposed by this study using equations (1) – (12).

To better understand pre-historic lavas future work could alternatively be focused on observing and modeling more active block flows such as the Santiaguito. For the purpose of this study, Harris et al. (2002) and Harris et al. (2004) provided the most comprehensive and accurate methods to determine the evolution of thick, moderately–silicic and anomalously long flows. Only with a deeper understanding of such active flows can the limitations of modeling pre-historic lava flows be overcome.

References

Björk, S., Walker, M.J.C., Cwynar, L.C., Johnsen, S., Knudsen, K.-L., Lowe, J.J., Wohlfarth, B., INTIMATE members, 1998. An event stratigraphy for the Last Termination in the North Atlantic region: a proposal by the INTIMATE group. Journ. Quat. Sci., 13, 283 – 292.

Borgia, A., Linneman S.R., 1990. On the mechanisms of lava flow emplacement and volcano growth: Arenal, Costa Rica. In: Fink, J.H. (Eds.), Lava flows and domes. Springer-Verlag, Berlin, pp. 208-243.

Brooks, G.R., Friele, P.A., 1992. Bracketing Ages for the Formation of the Ring Creek Lava Flow, Mount Garibaldi Volcanic Field, Southwestern British Columbia. Ca. J. Earth Sci. 29, 2425-2428.

Carrasco-Nunez, G., 1997. Lava flow growth inferred from morphometric parameters: a case study of Citlaltepetl volcano, Mexico. Geol. Magazine. 134, 151-162.

Clague, J., 2010. Personal Communication.

Francis, P., Oppenheimer, C. Volcanoes, 2004. Oxford University Press, London pp 536.

Friele, P.A., Clague, J.J., 2002. Younger Dryas readvance in Squamish River valley, southern Coast mountains, British Columbia. Quat. Sci. Rev. 21, 1925 – 1933.

Green, N.L., 1981. Geology and petrology of Quaternary volcanic rocks, Garibaldi Lake area, southwestern British Columbia: Summary. Geol. Soc. Am. Bull. 92, 697-702.

Green, N.L., Armstrong, R.L., Harakal, J., Souther, J.G., and Read, P. B., 1988. Eruptive history and K-Ar geochronology of the Garibaldi Volcanic Belt, southwestern British Columbia/ Geol. Soc. Am. Bull. 100, 563-579.

Harris, A.J.L., Flynn, L.P., Matias, O., Rose, W.I., 2002. The thermal stealth flows of Santiaguito dome, Guatemala: Implications for the cooling and emplacement of dacitic block-lava flows. Geol. Soc. Am. Bull. 114, 533-546.

Harris, A.J.L., Rose, W.I., Flynn, L.P., 2003. Temporal trends in lava dome extrusion at Santiaguito 1922-2000. Bull. Volcanol. 65, 77-89.

Harris, A.J.L., Flynn, L.P., Otoniel, M., Rose, W.I., Comejo, J., 2004. The evolution of an active silicic lava flow field: an ETM+ perspective. J. Volcanol. Geotherm. Res. 135, 147-168.

Hausback, B.P., 1987. An extensive, hot, vapor-charged rhyodacite flow, Baja California, Mexico. Geol. Soc. Am. Bull. Special Paper 212, 116-118.

Hiroaki, S., Setsuya, N., Toshitsugu, F., Michihiko, N., Keiko, S., 1999. Groundmass pargasite in the 1991 – 1995 dacite of Unzen volcano: phase stability experiments and volcanological implications. J. Volcanol. Geotherm. Res. 89, 197-212.

Holman, J.P. Heat transfer, 1992. McGraw Hill, London, pp 713.

Hulme, G., Fielder, G., 1977. Effusion rates and rheology of lunar lavas. Philos. Trans. R. Soc. London. 285, 227-234.

Kays W.M., Crawford, M.E. Convective heat and mass transfer, 1980. McGraw-Hill, New York, pp 420.

Kelman, M. C., Russell, J. K., Hickson, C. J., 2002. Effusive intermediate glaciovolcanism in the Garibaldi Volcanic Belt, southwestern British Columbia, Canada. Geol. Soc. London. Special Publications, 202, 195-211

Kilburn, C.R.J., Lopes, R., 1991. General patterns of flow field growth: Aa and blocky lavas. Journal of Geophysical Research. 96, 19721-19732.

Kilburn, C.R.J., Guest, J.E., 1993. Aa lavas of Mount Etna, Sicily. In: Kilburn, C. (Eds.), Active Lavas. pp. 73-106.

Mathews, W.H., 1958a. Geology of the Mount Garibaldi map-area, southwestern British Columbia, Canada, Part I: Igneous and metamorphic rocks. Geol. Soc. Am. Bull. 69, 161-178.

Mathews, W.H., 1958b. Geology of the Mount Garibaldi map-area, southwestern British Columbia, Canada, Part II: Geomorphology and Quaternary Volcanic Rocks. Geol. Soc. Am. Bull. 69, 179-198.

Moore, H.J., Arthur, D.W.G., Schaber, G.G., 1978. Yield strengths of flows on Earth, Mars, and Moon. Proc. Lunar Planet. Sci. Conf. 9th. 3351 – 3378.

Nicholls, I.A., Harris, K.L., 1980. Experimental rare earth element partition coefficients for garnet, clinopyroxene and amphibole coexisting with andesitic and basaltic liquids. Geochimica et Cosmochimica Acta. 34, 331-340.

Parfitt, E.A., Wilson, L. Fundamental of Physical Volcanology, 2008. Blackwell Publishing, Malden, MA, pp 126-141.

Powell, J.Jr., 2005, Quaternary magmas of the Raffuse Creek-Mamquam River

Area, Southwest British Columbia. Masters Thesis, Univ. of Alabama. Tuscaloosa, Alabama

Price, R.A., Monger, J.W.H., 2003. A transect of the southern Canadian Cordillera from Calgary to Vancouver. Geol. Ass. Canada, Cordilleran Section. pp. 1 - 161

Putirka, K.D., 2005. Igneous thermometers and barometers based on plagioclase + liquid equilibria: Tests of some existing models and new calibrations. Am. Min. 90, 336-346.

Rutherford, M.J., Sigurdsson, H., Carey, S., Davis, A., 1985. The May 18, 1980 Eruption of Mount St. Helens Melt composition and Experimental Phase Equilibria. J. Geophys. Res. 90, 2929-2947.

Rutherford, M. J., Devine, J. D., 1988. The May 18, 1980, eruption of Mount St. Helens, III. Stability and chemistry of amphibole in the magma chamber. J. Geophys. Res. 93, 11949-11959.

Rutherford, M.J., Hill, P.M., 1993. Magma Ascent Rates From Amphibole Breakdown: An Experimental Study Applied to the 1980-1986 Mount St. Helens Eruptions. J. Geophys. Res. 98, 19667-19685.

Rutherford, M.J., Devine, J., 2003. Magmatic Conditions and Magma Ascent as Indicated by Hornblende Phase Equilibria and Reactions in the 1995-2002 Soufriere Hills Magma. J. Petrol. 44, 1433-1454.

de Silva, S. L., Self, S., Francis, P.W., Drake, R.E., Ramirez, C.R., 1994. Effusive silicic volcanism in the Central Andes: The Chao dacite and other young lavas of the Altiplano-Puna Volcanic Complex. J. Geophys. Res. 99, 17805-17825.

Swanson, D.A., Dzurisin, D., Holcomb, R.T., Iwatsubo, E.Y., Chadwick, J.J.Jr., Casadevall, T.J., Ewert, J.W., Heliker, C.C., 1987. Growth of the lava dome at Mount St Helens, Washington, (USA), 1981 – 1983. Geol. Soc. Am. Bull. Special Paper. 212, 119-145.

Whittington, A.G., Hellwig, B.M., Behrens, H., Joachim, B., Stechern, A., Vetere, F. 2009. The viscosity of hydrous dacitic liquids: implications for the rheology of evolving silicic magmas. Bull. Volcanol. 71, 185-199.

Wilson, L., Head, J.W., 1983. A comparison of volcanic eruption processes on Earth, Moon, Mars, Io and Venus. Nature, 302, 663-669.

APPENDIX I: Sample Locations

Sample	Latitude (Degrees)	Longitude (Degrees)	Elevation (Meters)
5-4-B3	49.71969	-123.082202	238.5
15-1-1	49.715865	-123.053596	NA
15-1-3	49.715865	-123.053596	NA
11-4-1	49.738399	-123.0013	570
14-4-1	49.805107	-122.978055	1372.3
14-4-2	49.80579	-122.97588	1264.9
13-6	49.808637	-122.966977	1391.2
12-5	49.821015	-122.974298	1694.8
12-4-1	49.82263	-122.975662	1685.3
12-4-2	49.82263	-122.975662	1685.3
12-4-3	49.82263	-122.975662	1685.3
12-3	49.82395	-122.970507	1687.6
13-2-1	49.823407	-122.96023	1516

Note: Sample locations and elevation taken with hand held GPS device and should be considered accurate within 7 meters. NA = elevation not taken or unreal.

APPENDIX II: Trace Element Chemistry (ppm)

Sample	5-15-B3	11-4-1	12-3	12-5	13-2-1	14-4-1	14-4-2	15-1-1	15-1-3	13-6
Trace element										
Rb	16.3	19.8	19.3	19.7	15.3	15.8	15.4	18.8	18.2	26.7
Ba	500.7	560.2	599.9	658	459	467.7	417.7	522.1	499.9	692.8
Th	1.54	1.27	1.74	1.72	1.64	1.73	1.44	1.72	1.49	3.68
U	0.81	0.86	0.83	0.85	0.76	0.75	0.82	0.82	0.8	1.68
Nb	4.04	4.31	4.14	4.16	4.19	3.98	4.3	4.22	4.31	4.68
Ta	0.3	0.3	0.3	0.3	0.3	0.3	0.3	0.3	0.2	0.3
La	10.9	9.57	13.26	13.12	11.29	12.42	11.51	12.43	11.17	23.19
Ce	23.9	21.2	29.2	29.2	25.1	28	25.6	27.3	24.7	51.7
Sr	978	1180	1087	1176	1024	1029	1030	941	938	1385
Nd	13.28	12.43	16.92	17.28	14.25	15.78	14.44	15.13	13.53	26.91
Sm	2.56	2.39	3.2	3.32	2.81	3.07	2.77	2.93	2.59	4.45
Zr	118	131	126	128	108	112	109	121	123	181
Hf	3.1	3.41	3.28	3.41	2.96	2.98	2.83	3.07	3.05	4.88
Eu	0.762	0.694	0.928	0.96	0.834	0.901	0.826	0.857	0.776	1.148
Tb	0.305	0.259	0.358	0.359	0.336	0.355	0.311	0.354	0.31	0.39
Ho	0.339	0.268	0.376	0.368	0.356	0.385	0.321	0.383	0.336	0.336
Yb	0.908	0.76	1.045	1.02	0.981	1.062	0.834	1.011	0.904	0.818
Lu	0.141	0.115	0.163	0.156	0.154	0.165	0.136	0.161	0.142	0.127
Y	9.63	8.05	11.11	10.83	10.07	10.88	9.32	11.08	10.08	9.76
Be	1.16	1.41	1.28	1.26	1.04	1.05	1.13	1.2	1.28	1.66
Bi	0.037	0.039	0.014	0.019	0.011	0.055	0.075	0.026	0.023	0.036
Cd	0.05	0.05	0.05	0.05	0.04	0.04	0.04	0.05	0.05	0.05
Co	11.8	11.9	11.4	11.7	12	11.8	11.2	11.2	11.9	11
Cr	26	27	25	24	27	<24	<24	24	27	<24
Cs	0.368	0.448	0.435	0.452	0.29	0.352	0.365	0.444	0.44	0.241
Cu	21	17	23	24	27	16	21	19	21	30
Dy	1.7	1.4	1.9	2	1.8	2	1.6	1.9	1.6	1.8
Er	0.87	0.72	0.99	0.99	0.97	1	0.85	1.02	0.88	0.86
Ga	17.91	18.76	17.99	17.81	17.94	17.86	17.87	18.48	18.29	19.42
Gd	2.1	1.82	2.53	2.55	2.26	2.48	2.27	2.5	2.17	3.11
Li	9.7	10.9	11.7	11.3	7	9.9	11.1	11.8	12.6	9.8
Mo	0.96	1.08	0.96	1	0.83	0.88	0.93	0.96	1.08	0.36
Ni	26	24	23	23	25	24	21	24	34	16
Pb	6.4	8.9	7.7	8.5	7.8	6.1	5.9	6.6	6.5	8.5

Sample	5-15-B3	11-4-1	12-3	12-5	13-2-1	14-4-1	14-4-2	15-1-1	15-1-3	13-6
Trace element										
Pr	3.12	2.86	3.99	3.99	3.35	3.72	3.41	3.58	3.22	6.59
Sb	0.07	0.07	0.06	0.07	0.05	0.06	0.06	0.07	0.08	0.1
Sc	7.2	6.1	7.4	6.9	6.9	7.6	6.5	7.6	7.2	6.6
Sn	0.68	0.76	0.72	0.76	2.49	0.67	0.68	0.68	0.72	1.18
Ti	2678	2934	2780	2839	2878	2706	2752	2704	2784	3539
Tl	0.101	0.123	0.071	0.122	0.048	0.072	0.089	0.104	0.061	0.112
Tm	0.139	0.113	0.161	0.155	0.157	0.158	0.136	0.157	0.14	0.132
V	81	84	79	79	86	74	71	77	78	60
W	<0.5	<0.5	<0.5	<0.5	<0.5	<0.5	<0.5	<0.5	<0.5	<0.5
Zn	57	64	60	62	60	58	57	61	62	64

Note: All values reported are in parts per million (ppm).

APPENDIX III: Plagioclase Analyses

Sample	Position	SiO_2	Al_2O_3	FeO	MgO	CaO	Na_2O	K_2O	Total
12-4-1	rim	53.62	29.14	0.6994	0.061	11.43	4.57	0.2239	99.75
12-4-1	rim	55.02	28.28	0.6966	0.0687	11.03	4.95	0.2157	100.25
12-4-1	rim	57.18	27.02	0.5785	0.0211	9.4	5.83	0.287	100.32
12-4-1	rim	58.69	25.64	0.73	0.0417	8.03	6.38	0.5264	100.04
12-4-1	rim	55.14	28.69	0.549	0.0513	11.01	4.87	0.1509	100.46
12-4-1	rim	55.61	27.95	0.6336	0.0456	10.61	5.15	0.2358	100.23
12-4-1	rim	54.7	28.58	0.6623	0.0653	11.27	4.67	0.2221	100.17
12-4-1	rim	57.63	27.16	0.263	0.0291	9.02	6.14	0.216	100.46
12-4-1	rim	54.6	28.59	0.7161	0.067	11.57	4.65	0.1844	100.37
12-4-1	lath	54.19	2.8037	14.49	23.51	2.9261	0.3275	0.205	98.46
12-4-1	lath	59.85	4.23	10.69	17.92	3.48	0.9267	1.2299	98.32
12-4-1	lath	61.14	4.91	10.26	16.27	2.4407	1.2122	1.5757	97.82
12-4-1	lath	62.94	4.63	10.43	17.55	1.5763	1.1713	1.5392	99.84
12-4-1	lath	55.31	1.1986	14.41	26.32	1.7171	0.0586	0.0425	99.05
12-4-1	lath	67.68	12.33	4.82	6.01	2.4888	3.84	2.08	99.25
12-4-1	lath	55.28	1.8751	14.91	25.95	1.6314	0.0882	0.0984	99.84
12-4-1	lath	64.65	8.17	6.2	9.38	6.17	2.3279	1.869	98.76
12-4-1	lath	54.74	2.4283	14.64	25.47	2.1861	0.1562	0.0328	99.66
12-4-1	lath	63.96	5.01	10.57	16.41	1.8502	1.1447	1.6081	100.55
12-4-2	rim	54.97	28.51	0.8318	0.0701	11.37	4.93	0.1629	100.85
12-4-2	rim	55.14	28.26	0.8086	0.0787	10.86	5	0.2032	100.35
12-4-2	rim	56.47	27.49	0.7484	0.0647	10.05	5.7	0.2779	100.8
12-4-2	rim	54.1	28.73	0.6979	0.0626	12.01	4.62	0.2053	100.43
12-4-2	rim	54.31	29.32	0.6341	0.0853	11.97	4.48	0.1317	100.93
12-4-2	lath	54.24	28.55	0.7058	0.0803	11.6	4.61	0.1872	99.98
12-4-2	lath	55.6	27.8	0.7082	0.1039	10.92	5.27	0.1783	100.58
12-4-2	lath	56.88	26.76	0.9387	0.0824	10.77	4.58	0.478	100.5
12-4-2	lath	55.52	27.9	0.7432	0.0978	10.83	5.35	0.2142	100.65
12-4-2	lath	56.43	26.98	0.7289	0.0421	10.02	5.74	0.2838	100.22
12-4-3	rim	55.1	28.73	0.678	0.1068	11.47	4.71	0.1782	100.98
12-4-3	rim	55.49	28.72	0.6872	0.0775	11.34	4.77	0.2078	101.29
12-4-3	rim	66.42	20.77	0.9751	0.0504	6.27	4.94	1.3509	100.77
12-4-3	rim	82.02	10.49	1.237	0.0893	0.3745	1.1612	3.31	98.67
12-4-3	rim	53.69	29.18	0.652	0.0854	12.36	4.37	0.1364	100.47
12-4-3	lath	56.41	27.75	0.7561	0.0657	10.73	5.32	0.2313	101.27
12-4-3	lath	55.77	27.59	0.7692	0.0885	10.93	5.07	0.2046	100.42
12-4-3	lath	54.76	28.61	0.6923	0.0793	11.58	4.74	0.1712	100.64
12-4-3	lath	54.57	28.77	0.7383	0.0828	11.69	4.67	0.1704	100.68
12-4-3	lath	54.82	27.7	0.6967	0.1019	10.89	4.73	0.2826	99.23

Sample	Position	SiO_2	Al_2O_3	FeO	MgO	CaO	Na_2O	K_2O	Total
15-1-1	rim	53.86	29.45	0.6493	0.0326	12.53	4.39	0.2033	101.12
15-1-1	rim	54.7	28.82	0.6297	0.0351	11.75	4.7	0.2113	100.85
15-1-1	rim	55.32	27.69	0.6983	0.0625	10.74	5.2	0.2991	100.01
15-1-1	rim	55.43	28.55	0.6305	0.0449	11.29	4.84	0.2149	101
15-1-1	rim	54.77	29.12	0.7946	0.0535	11.65	4.57	0.2607	101.22
15-1-1	lath	54.52	28.15	0.6765	0.0339	11.13	4.88	0.2688	99.66
15-1-1	lath	55.91	27.99	0.7064	0.0489	10.97	5.08	0.2608	100.96
15-1-1	lath	55.91	28.24	0.7553	0.0465	10.9	5.12	0.3054	101.27
15-1-1	lath	56.15	28.06	0.5524	0.0443	10.62	5.23	0.2764	100.93
15-1-1	lath	55.76	28.14	0.7384	0.0464	10.94	5.11	0.271	101.01
15-1-3	rim	52.43	30.04	0.6326	0.0514	12.94	4.2	0.1835	100.48
15-1-3	rim	53.28	29.55	0.6555	0.0478	12.01	4.52	0.2131	100.28
15-1-3	rim	54.8	28.69	0.5682	0.0381	11.4	5.19	0.3118	101.01
15-1-3	rim	54.07	29.37	0.6154	0.0388	12.2	4.71	0.189	101.19
15-1-3	rim	52.95	29.47	0.5859	0.0422	12.27	4.42	0.1618	99.91
15-1-3	rim	53	29.99	0.6217	0.0374	12.79	4.21	0.1916	100.86
15-1-3	lath	54.35	28.86	0.5397	0.0306	11.49	4.91	0.2811	100.45
15-1-3	lath	54.17	29.05	0.6374	0.0461	11.6	4.73	0.2442	100.47
15-1-3	lath	54.97	28.6	0.6524	0.042	11.59	4.85	0.2954	101
15-1-3	lath	55.36	28.01	0.7003	0.046	10.84	5.06	0.3183	100.34
15-1-3	lath	54.53	28.57	0.7116	0.0455	11.06	4.88	0.2846	100.08

Note: Values reported are in oxide weight percent. Lath position reflects microphenocrysts suspended in the glass near the rim of the phenocryst analyzed.

APPENDIX III Continued: Glass Analyses

Sample	SiO_2	TiO_2	Al_2O_3	FeO	MgO	CaO	Na_2O	K_2O	Total
12-4-1	77.25	0.5646	10.55	1.4728	0.0822	0.2555	1.4324	4.11	95.72
12-4-1	79.17	0.7255	10.3	1.5779	0.0863	0.2335	1.7255	4.17	97.99
12-4-1	78.61	0.6605	10.5	1.3841	0.0825	0.2499	1.1959	3.51	96.19
12-4-1	79.54	0.6571	10.89	1.1339	0.0612	0.1883	1.377	3.78	97.63
12-4-2	76.27	0.5043	11.35	1.5637	0.1362	0.7052	2.9388	4.13	97.6
12-4-2	77.05	0.5238	10.63	1.4964	0.1188	0.2216	2.0945	4.66	96.8
12-4-2	76.52	0.4874	10.86	1.3713	0.0848	0.2691	2.159	4.55	96.29
12-4-2	77.58	0.6211	10.64	1.4417	0.0865	0.2664	2.7738	4.66	98.07
12-4-2	75.5	0.6212	11.47	1.2502	0.0628	0.4915	2.8278	4.24	96.47
12-4-3	77.33	0.6241	10.71	1.6659	0.116	0.2461	2.6296	4.7	98.02
12-4-3	76.37	0.5527	11.25	1.2808	0.0801	0.5123	3.26	4.47	97.77
12-4-3	78.63	0.6177	11.12	1.2734	0.0659	0.2429	2.918	4.93	99.8
12-4-3	76.56	0.6828	10.77	1.2531	0.0641	0.2891	2.5031	4.59	96.72
12-4-3	77.55	0.558	10.84	1.3201	0.113	0.2939	3.09	4.73	98.49
12-4-3	78.91	0.5489	11.08	1.3959	0.0953	0.3428	3.09	4.77	100.23
15-1-1	75.42	0.5498	11.44	1.4073	0.1085	0.5291	2.7019	5.24	97.39
15-1-1	76.84	0.3341	12.08	1.1605	0.0531	1.3305	3.61	2.9984	98.41
15-1-1	70.78	0.4934	15.02	1.2402	0.0645	1.6165	4.04	3.95	97.21
15-1-3	72.06	0.64	14.2	1.25	0.1304	1.7877	4.05	3.62	97.74
15-1-3	75.79	0.5938	11.43	1.4855	0.127	0.2892	1.6365	5.04	96.39
15-1-3	74.17	0.6353	11.89	1.3221	0.102	0.509	2.9877	4.94	96.56
15-1-3	70.24	0.5454	15.55	1.3588	0.1616	2.2185	5.09	3.5	98.67
15-1-3	70.61	0.6075	14.61	1.2073	0.107	1.7791	4.61	3.74	97.27

Note: Point analyses are of glass between lath and phenocryst rims. Values reported are in oxide weight percent.

APPENDIX IV: Calculation of Heat Loss Parameters

Based on Enhanced Thematic Mapper (ETM) image analysis and field work, Harris et al. (2002), Harris et al. (2003), and Harris et al. (2004) derive the following equation to describe extrusion rate of an actively flowing dacitic lava:

$$E_r = \frac{Q_{tot}}{\rho_{lava} \cdot \left(C_p \cdot \Delta T + c_L \cdot \Delta\phi \right)}$$

Where C_p is the specific heat, ΔT is the liquidus – solidus temperature difference (^{o} K), c_L is the latent heat of crystallization, $\Delta\phi$ is the post eruptive crystallinity, Q_{tot} is the total heat lost, and ρ_{lava} is the lava density. Q_{tot} is derived as follows:

$$Q_{tot} = Q_{rad} + Q_{conv} + Q_{base}$$

Each Q or heat loss parameter is described by Harris et al (2004) as:

$$Q_{rad} = \sigma \cdot \varepsilon \cdot A_{lava} \cdot T_{crust}^{\ 4}$$

$$Q_{conv} = h_c \cdot \left(T_{surf} - T_{air} \right)$$

$$Q_{base} = A_{lava} \cdot k_{lava} \cdot \left(\frac{T_{erupt} - T_{base}}{h_{base}} \right)$$

$$Q_{cond} = Q_{rad} + Q_{conv}$$

Variables for these equations are defined as follows; for Q_{rad} σ is the Stefan Boltzman, ε is the emissivity of lava surface, A_{lava} is the area of the lava flow, and T_{crust} is temperature of the surface crust of the lava. For Q_{conv} the variables h_c is the convective heat transfer coefficient, T_{surf} is the effective temperature of the surface of the lava flow above the channel, and T_{air} is the ambient air temperature. For Q_{base} the variables k_{lava} is the thermal conductivity of the lava flow, and h_{base} is the thickness of the base of the lava flow. Firstly, Q_{rad} is described as follows:

$$Q_{rad} = \sigma_{RC} \cdot \varepsilon_{RC} \cdot A_{RClava} \cdot T_{crustRC}^{\ 4}$$

In this calculation (and subsequent parameters) the subscript RC refers to the Ring Creek lava flow. For example, A_{RClava} defines the area of the Ring Creek lava flow. Furthermore, subscripts of min, mean, and max denote the minimum, average, and maximum values calculated based on variation of flow morphology. These values are reported to show the effect of compound error throughout the calculation process.

$\sigma_{RC} := 5.67 \cdot 10^{-8} \frac{W}{m^2 \cdot K^4}$

$\varepsilon_{RC} := 1$

$T_{crustRC} := 49K + 273K$

$A_{RClavamin} := 17500m \cdot (1375m - 192m)$

$A_{RClava} := 18000m \cdot 1375m$

$A_{RClavamax} := 18500m \cdot (1375m + 192m)$

Note: Temperature of the surface crust of the Ring Creek lava flow was assumed to be approximately that of the Santiaguito lava flow as measured by Harris et al. (2002). With each of the parameters defined Q_{rad} is calculated as:

$Q_{radRCmin} := \sigma_{RC} \cdot \varepsilon_{RC} \cdot A_{RClavamin} \cdot T_{crustRC}^4 = 1.262 \times 10^{10} W$

$Q_{radRC} := \sigma_{RC} \cdot \varepsilon_{RC} \cdot A_{RClava} \cdot T_{crustRC}^4 = 1.509 \times 10^{10} W$

$Q_{radRCmax} := \sigma_{RC} \cdot \varepsilon_{RC} \cdot A_{RClavamax} \cdot T_{crustRC}^4 = 1.767 \times 10^{10} W$

Per area, for the Ring Creek lava flow, Q_{rad} becomes:

$$\frac{Q_{radRC}}{A_{RClava}} = 609.546 \frac{W}{m^2}$$

Next, Q_{conv} is defined as:

$$Q_{conv} = h_c \cdot (T_{surf} - T_{air})$$

Q_{conv} for the Ring Creek lava flow cannot be calculated until an estimate of crustal thickness is made. Using Borgia and Linneman (1993) crustal thickness (H_{RC}, without the flow plug) is estimated to be 24m.

$Nu = 260$

$k_{air} = 0.026 \frac{W}{m \cdot K}$

$T_{airRC} := \frac{(T_{surf} + 293K)}{2}$

$T_{airRC} = 331K$

$T_{surfRC} := 96K + 273K$

$H_{RCmin} := 9.5m$

$H_{RC} := 24.m$

$H_{RCmax} := 46m$

$$h_{cRCmin} := \frac{Nu \cdot k_{air}}{H_{RCmax}} = 0.145 \frac{kg}{s^3 \cdot K} \qquad h_{cRC} := \frac{Nu \cdot k_{air}}{H_{RC}} = 0.278 \frac{kg}{s^3 \cdot K}$$

$$h_{cRCmax} := \frac{Nu \cdot k_{air}}{H_{RCmin}} = 0.701 \frac{kg}{s^3 \cdot K}$$

Q_{conv} can then be calculated as:

$$Q_{convRCmin} := A_{RClavamin} \cdot h_{cRCmin} \cdot \left(T_{surfRC} - T_{airRC}\right) = 1.14 \times 10^8 \, W$$

$$Q_{convRC} := A_{RClava} \cdot h_{cRC} \cdot \left(T_{surfRC} - T_{airRC}\right) = 2.611 \times 10^8 \, W$$

$$Q_{convRCmax} := A_{RClavamax} \cdot h_{cRCmax} \cdot \left(T_{surfRC} - T_{airRC}\right) = 7.727 \times 10^8 \, W$$

Per unit area, for the Ring Creek lava flow, Q_{conv} becomes:

$$\frac{Q_{convRC}}{A_{RClava}} = 10.551 \frac{W}{m^2}$$

Q_{cond} for the surface is then:

$$Q_{condRCmin} := Q_{radRCmin} + Q_{convRCmin} = 1.273 \times 10^{10} \, W$$

$$Q_{condRC} := Q_{radRC} + Q_{convRC} = 1.535 \times 10^{10} \, W$$

$$Q_{condRCmax} := Q_{radRCmax} + Q_{convRCmax} = 1.844 \times 10^{10} \, W$$

Per unit area, for the Ring Creek lava flow, Q_{cond} becomes:

$$\frac{Q_{condRC}}{A_{RClava}} = 620.097 \frac{W}{m^2}$$

When calculating Q_{base} for the R.C.F. it is assumed that the same temperature properties of the Santiaguito flow apply to the Ring Creek lava flow. This means the same values (from Harris et al., 2002) will be used for T_{base} and k_{lava} for the Ring Creek lava flow:

$$Q_{base} = A_{lava} \cdot k_{lava} \cdot \left(\frac{T_{erupt} - T_{base}}{h_{base}} \right)$$

$A_{RClava} = 2.475 \times 10^{7}\ m^2$ $\quad h_{RCbasemin} := 9.5\,m$ $\quad T_{erupt} := 898\,K + 273\,K$

$h_{RCbase} := 24.28\,m$ $\quad T_{base} := 500\,K + 273\,K$

$k_{lava} := 2 \frac{W}{m \cdot K}$ $\quad h_{RCbasemax} := 46\,m$

$$Q_{baseRCmin} := A_{RClavamin} \left[k_{lava} \cdot \left(\frac{T_{erupt} - T_{base}}{h_{RCbasemax}} \right) \right] = 3.582 \times 10^{8}\,W$$

$$Q_{baseRC} := A_{RClava} \cdot k_{lava} \cdot \left(\frac{T_{erupt} - T_{base}}{h_{RCbase}} \right) = 8.114 \times 10^{8}\,W$$

$$Q_{baseRCmax} := A_{RClavamax} \cdot k_{lava} \cdot \left(\frac{T_{erupt} - T_{base}}{h_{RCbasemin}} \right) = 2.429 \times 10^{9}\,W$$

Per unit area, for the Ring Creek lava flow, the mean value of Q_{base} becomes:

$$\frac{Q_{baseRC}}{A_{RClava}} = 32.784 \frac{W}{m^2}$$

With Q_{rad}, Q_{conv}, Q_{cond}, and Q_{base} defined, Q_{tot} is calculated as follows:

$$Q_{totRCmin} := Q_{radRCmin} + Q_{convRCmin} + Q_{condRCmin} + Q_{baseRCmin} = 2.582 \times 10^{10}\,W$$

$$Q_{totRC} := Q_{radRC} + Q_{convRC} + Q_{condRC} + Q_{baseRC} = 3.151 \times 10^{10}\,W$$

$$Q_{totRCmax} := Q_{radRCmax} + Q_{convRCmax} + Q_{condRCmax} + Q_{baseRCmax} = 3.932 \times 10^{10}\,W$$

With Q_{tot} defined, extrusion rate is calculated as follows:

$$E_r = \frac{Q_{tot}}{\rho_{lava} \cdot \left(C_p \cdot \Delta T + c_L \cdot \Delta \phi \right)}$$

$\rho_{lavaRCmin} := 2.556 \times 10^3 \frac{kg}{m^3}$ $C_{pRC} := 1150 \frac{J}{kg \cdot K}$ $c_{LRC} := 3.5 \cdot 10^{-5} \frac{J}{kg}$ $\Delta\phi_{RC} := 0.40$

$\rho_{lavaRC} := 2591 \frac{kg}{m^3}$ $\Delta T_{RC} := (200 + 273) \cdot K$

$\rho_{lavaRCmax} := 2.706 \cdot 10^3 \frac{kg}{m^3}$

$$E_{rRCmin} := \frac{Q_{totRCmin}}{\rho_{lavaRCmin} \cdot \left(C_{pRC} \cdot \Delta T_{RC} + c_{LRC} \Delta\phi_{RC}\right)} = 18.574 \frac{m^3}{s}$$

$$E_{rRC} := \frac{Q_{totRC}}{\rho_{lavaRC} \cdot \left(C_{pRC} \cdot \Delta T_{RC} + c_{LRC} \Delta\phi_{RC}\right)} = 22.355 \frac{m^3}{s}$$

$$E_{rRCmax} := \frac{Q_{totRCmax}}{\rho_{lavaRCmax} \cdot \left(C_{pRC} \cdot \Delta T_{RC} + c_{LRC} \Delta\phi_{RC}\right)} = 26.71 \frac{m^3}{s}$$